Universidade de Aveiro
2021

Rita Alexandra Silva Moreira

Nanopartículas de conversão ascendente para terapia fototérmica e entrega de fármacos em células de melanoma

Upconversion nanoparticles for photothermal therapy and drug delivery in melanoma cells

Universidade de Aveiro
2021

Rita Alexandra Silva Moreira

Nanopartículas de conversão ascendente para terapia fototérmica e entrega de fármacos em células de melanoma

Upconversion nanoparticles for photothermal therapy and drug delivery in melanoma cells

Dissertação apresentada à Universidade de Aveiro para cumprimento dos requisitos necessários à obtenção do grau de Mestre em Biologia Molecular e Celular, realizada sob a orientação científica da Doutora Helena Cristina Correia de Oliveira, Investigadora Auxiliar do Departamento de Biologia e do Centro de Estudos do Ambiente e do Mar da Universidade de Aveiro e da Doutora Verónica Isabel Correia Bastos, Investigadora do Departamento de Biologia e do Centro de Estudos do Ambiente e do Mar da Universidade de Aveiro.

This work was developed within the project POCI-01-0145-FEDER-031794, financially supported funded by FEDER, through COMPETE2020 - Programa Operacional Competitividade e Internacionalização (POCI), and by national funds (OE), through FCT/MCTES (PTDC/BTMMAT/31794/2017).

“Success is walking from failure to failure with no loss of enthusiasm.”
Winston Churchill

o júri

Presidente	Doutora Clara Lúcia Ferreira Rodrigues Investigadora Auxiliar em Regime Laboral, CESAM & Departamento de Biologia, Universidade de Aveiro
Arguente	Doutora Ana Luísa Daniel da Silva Investigadora Auxiliar em Regime Laboral, CICECO & Departamento de Química, Universidade de Aveiro
Orientadora	Doutora Helena Cristina Correia de Oliveira Investigadora Auxiliar em Regime Laboral, CESAM & Departamento de Biologia, Universidade de Aveiro

agradecimentos

Muitas foram as pessoas que, direta ou indiretamente, me ajudaram na execução deste trabalho e a quem, por isso, muito agradeço.

Gostaria de agradecer, em primeiro lugar, às minhas orientadoras. À Doutora Helena Oliveira e à Doutora Verónica Bastos por todo o apoio e ajuda ao longo deste último ano. À Doutora Helena agradeço por me orientar sabiamente e por todos os ensinamentos transmitidos. À Doutora Verónica, um enorme obrigada pela atenção, paciência e orientação técnica e científica. Agradeço-lhes também toda a simpatia, amizade e disponibilidade ao longo deste percurso.

Agradeço aos meus pais, Joaquim e Graça, por todo o amor, carinho, compreensão e apoio ao longo deste percurso e ao longo da minha vida. Às minhas irmãs, Ana e Inês, por todo o apoio e positivismo para entrar nesta aventura, por toda a ajuda que me deram e por acreditarem em mim.

Agradeço ao João, por ser o meu pilar, por me apoiar incondicionalmente e por ser um companheiro de todas as aventuras. A ele agradeço também a enorme paciência que teve e continua a ter para mim, todo o amor e carinho, todas as repreensões e exigência no trabalho e toda a sua energia para me animar nos momentos mais difíceis.

Agradeço às minhas amigas Diana Martins e Mariana Vassal por serem as melhores ao longo destes dois anos, por todas as gargalhadas e por toda a ajuda. Por tornarem os momentos mais difíceis em coisas mais simples.

Agradeço aos membros do grupo 3 C's pelo companheirismo, incentivo e ajuda, em especial à Ana Calçona, Marlene Soares, Susana Soares, Diana Salvador e Simone Pascoal pelo apoio que me deram durante este ano.

Agradeço ao Fernando Maturi do grupo Phantom-G por toda a disponibilidade e paciência que teve para mim e por toda a ajuda que me deu na realização dos ensaios de otimização das condições de irradiação para a terapia fototérmica.

Agradeço à Doutora Ana Luísa Daniel, ao João Nogueira e à Maria António, do departamento de Química da Universidade de Aveiro, pela ajuda na funcionalização das nanopartículas com ouro, bem como pelo auxílio no processo de loading de doxorrubicina nas nanopartículas e respetivos ensaios de libertação deste fármaco.

Obrigada a todos.

palavras-chave Melanoma, Nanopartículas de conversão ascendente, Terapia Fototérmica, Entrega de fármacos

resumo

O melanoma é o tipo mais agressivo de cancro da pele apresentando elevadas taxas de mortalidade. É muito importante que seja detetado numa fase inicial pois pode ser removido cirurgicamente com uma taxa de sobrevivência elevada. Embora as terapias existentes e a cirurgia tenham obtido um grande progresso nos últimos anos, o melanoma continua a ter uma alta resistência às terapias e, se for descoberto num estado avançado, as opções de tratamento são escassas e de baixa eficácia.

As nanopartículas de conversão ascendente (UCNPs) têm atraído atenção neste campo devido às suas excelentes propriedades, nomeadamente a capacidade de converter fotões na região do infravermelho próximo, de baixa energia, em radiação de alta energia que varia desde o ultravioleta até à região do visível. Estas nanopartículas apresentam geralmente baixa citotoxicidade e possuem alta estabilidade luminescente, não exibem fotobranqueamento e têm capacidade de penetrar profundamente nos tecidos.

A terapia fototérmica, que utiliza radiação para criar um efeito de aquecimento localizado apenas nas áreas-alvo, é uma solução promissora para o tratamento do melanoma. Esta terapia usa agentes fototérmicos, que normalmente são nanopartículas de conversão ascendente, que por absorverem na região do infravermelho próximo não causam danos aos tecidos biológicos (nessa região, a absorção de radiação dos tecidos biológicos é mínima). A radiação laser intensa pode causar danos aos tecidos e às próprias nanopartículas. Por isso, é essencial determinar as condições de irradiação ideais (tempo e densidade de potência) para gerar o aquecimento localizado nos tecidos tumorais, mantendo os tecidos normais e as nanopartículas intactos, de maneira a alcançar os resultados fototerapêuticos ideais. Outra estratégia para tratar apenas as áreas afetadas pela doença, evitando o aparecimento de efeitos colaterais noutras partes do corpo, é a entrega direcionada de fármacos. Na entrega de fármacos usando nanopartículas, o medicamento é carregado na nanopartícula e transportado para o local de destino onde será libertado. As nanopartículas de conversão ascendente são candidatas ideais para esta entrega sendo frequentemente ativadas por luz ou pelo pH.

Este trabalho teve como objetivo avaliar o potencial de diferentes tipos de UCNPs para o tratamento do melanoma humano. Focou-se, ainda, na otimização das condições de irradiação para aplicação da terapia fototérmica e no estudo do carregamento e libertação mediada por pH do fármaco doxorrubicina. Para tal, foi feita a avaliação da biocompatibilidade de UCNPs com diferentes composições em duas linhas celulares de melanoma: MNT-1 e A375. Nesta avaliação foram usados quatro tipos diferentes de nanopartículas: $NaYF_4$:Lu,Yb,Er(47%,18%,2%)@SiO_2 (UCNPs@SiO_2), $NaYF_4$:Lu,Yb,Er(47%,18%,2%)@SiO_2-Au (UCNPs@SiO_2-Au), $NaYF_4$:Yb, Er(20%,2%)@mSiO_2-PO_4 (UCNPs@mSiO_2-PO_4) e $NaYF_4$:Yb,Er(20%,2%)@mSiO_2-COOH (UCNPs@mSiO_2-COOH).

A caracterização físico-química das nanopartículas (UCNPs@SiO_2 e UCNPs@SiO_2-Au) foi feita por Dispersão Dinâmica da Luz de maneira a avaliar o seu tamanho e o índice de polidispersão. O potencial zeta também foi avaliado. Para avaliar a biocompatibilidade, foi realizado o ensaio colorimétrico de MTT (brometo de 3-(4,5-dimetil-tiazol-2-il)-2,5-difenil tetrazólio) mostrando que as nanopartículas são biocompatíveis em quase todas as concentrações e tempos de exposição testados para a linha celular MNT-1, facto que já não se verifica nas concentrações de exposição mais elevadas para a linha celular A375. Como confirmação do ensaio de MTT, foi realizado o ensaio Neutral Red Uptake mas apenas para a linha celular MNT-1 e para as UCNPs@SiO_2.

No que diz respeito à otimização das condições de irradiação para aplicação da terapia fototérmica, foi usado um laser de 980nm e testadas as nanopartículas UCNPs@SiO_2 e UCNPs@SiO_2-Au. Testou-se o aquecimento obtido em meio de cultura com e sem vermelho de fenol bem como o aquecimento obtido em água. Várias densidade de potência foram testadas abrangendo um intervalo de 0,3W/cm^2 a 4W/cm^2 durante 15min em placas de 96 poços e em cuvete.

Através destes estudos conclui-se que a linha celular A375 é mais sensível às altas concentrações de nanopartículas, enquanto que a linha celular MNT-1 é mais tolerante. Conclui-se, também, que a funcionalização das UCNPs com nanopartículas de ouro parece ter impacto negativo na biocompatibilidade. No que diz respeito às condições de irradiação do laser, mais investigação é necessária de maneira a que, após se determinar o tempo e a densidade de potência ideais, a terapia fototérmica possa ser testada utilizando cultura de células *in vitro*. Nos testes efetuados com as nanopartículas UCNPs@mSiO_2-PO_4 e UCNPs@mSiO_2-COOH, cujo objetivo foi avaliar o carregamento e libertação da doxorrubicina, constatou-se que as nanopartículas fosfonadas

carregam mais eficientemente a doxorrubicina em relação às nanopartículas carboxiladas e que a libertação deste fármaco ocorre mais rapidamente em meios mais ácidos.

keywords Melanoma, Upconversion Nanoparticles, Photothermal Therapy, Drug Delivery

abstract

Melanoma is the most aggressive type of skin cancer with high mortality rates. It must be detected at an early stage as it can be surgically removed with a high survival rate. Although existing therapies and surgery have made great progress in recent years, melanoma continues to have a high resistance to therapies and, if discovered at an advanced stage, treatment options are scarce and of low efficacy.

Upconversion nanoparticles (UCNPs) have attracted attention in this field due to their excellent properties, as for instance their ability to convert photons in the low-energy near-infrared region into high-energy radiation ranging from the ultraviolet to the visible region. These nanoparticles usually present low cytotoxicity and high luminescent stability, deep penetration into tissues and do not exhibit photobleaching.

Photothermal therapy, which uses radiation to create a localized heating effect only in target areas, is a promising solution for the treatment of melanoma. Upconversion nanoparticles could be used as photothermal agents, as they absorb in the near-infrared region and do not cause damage to biological tissues (in this region, the absorption of biological tissues is minimal). Intense laser radiation can damage tissue and the nanoparticles themselves. Therefore, it is essential to determine the ideal irradiation conditions (time and power density) to generate localized heating in tumour tissues, keeping normal tissues and nanoparticles intact, to achieve optimal phototherapeutic results. Another strategy to treat only the areas affected by the disease, avoiding the appearance of side effects in other parts of the body, is the targeted delivery of drugs. In drug delivery using nanoparticles, the drug is loaded onto the nanoparticle and transported to the destination where it will be released. Upconversion nanoparticles are ideal candidates for this delivery as they can be activated by light or pH.

This work aimed to evaluate the potential of different types of UCNPs for the treatment of human melanoma. It was also focused on optimizing the irradiation conditions for the application of photothermal therapy and in the study of pH-mediated loading and release of the drug doxorubicin. For that, the biocompatibility of UCNPs with different compositions was evaluated in two melanoma cell lines: MNT-1 and A375. In this evaluation, four different types of nanoparticles were used, namely, NaYF4:Lu,Yb,Er(47%,18% ,2%)@SiO_2 (UCNPs@SiO_2), NaYF4:Lu,Yb,Er(47%,18%,2%)@SiO_2-Au (UCNPs@SiO_2-Au), NaYF4:Yb,Er(20%.2%)@mSiO_2-PO_4 (UCNPs@mSiO_2-PO_4) and NaYF4:Yb,Er(20%.2%)@mSiO_2-COOH (UCNPs@mSiO_2-COOH).

The physicochemical characterization of nanoparticles (UCNPs@SiO_2 and UCNPs@SiO_2-Au) was performed by Dynamic Light Scattering to evaluate their size and polydispersity index. The zeta potential was also evaluated.

To assess biocompatibility, the colorimetric MTT assay (3-(4,5-dimethyl-thiazol-2-yl)-2,5-diphenyl tetrazolium bromide) was performed, showing that the nanoparticles are biocompatible at almost all concentrations and exposure times tested for the MNT- 1 cell line, which is no longer seen at the highest exposure concentrations for the A375 cell line. As confirmation of the MTT assay, the Neutral Red Uptake assay was performed but only for the MNT-1 cell line and for UCNPs@SiO_2.

Regarding the optimization of irradiation conditions for the application of photothermal therapy, a 980nm laser was used, and the UCNPs@SiO_2 and UCNPs@SiO_2-Au nanoparticles were tested. The heating obtained in culture medium with and without phenol red was tested, as well as the heating obtained in water. Various power densities were tested covering a range from 0.3W/cm^2 to 4W/cm^2 during 15min in 96-well plates and in a cuvette.

Through this study, it was concluded that the A375 cell line is more sensitive to high concentrations of nanoparticles while the MNT-1 cell line is more tolerant. It was also concluded that the functionalization of UCNPs with gold nanoparticles seems to have a negative impact on biocompatibility. About the conditions of laser irradiation, further investigation is needed so that, after determining the ideal time and power density, a photothermal therapy can be tested using *in vitro* cell culture. In our assays carried out with the UCNPs@mSiO_2-PO_4 and UCNPs@mSiO_2-COOH nanoparticles, whose objective was to evaluate the loading and release of doxorubicin, it was found that the phosphonate nanoparticles load more efficiently doxorubicin in relation to the carboxylated nanoparticles and that the release of this drug occurs more quickly in more acidic environments.

TABLE OF CONTENTS

I – INTRODUCTION 1
1. CANCER 1
2. SKIN CANCER 11
2.1 MALIGNANT MELANOMA 11
2.1.1- Stages 12
2.1.2- Causative factors 14
2.1.3- Ultraviolet radiation 15
2.1.4- Types of melanoma 17
2.1.5- Genes and signalization pathways 19
2.1.6- Existent therapies 21
3. NANOTECHNOLOGY 24
3.1 NANOTECHNOLOGY IN CANCER 26
4. UPCONVERSION NANOPARTICLES (UCNPs) 28
4.1 DEFINITION, STRUCTURE AND PROPERTIES 28
4.2 ENERGY TRANSFER AND UC MECHANISMS 33
4.2.1- Energy Transfer 33
4.2.2- UC Mechanisms 34
4.3 UCNPS FUNCTIONALIZED WITH GOLD (AU) 41
5. BIOMEDICINE APPLICATIONS OF UCNPs 43
5.1 PHOTOTHERMAL THERAPY 43
5.2 PHOTODYNAMIC THERAPY 45
5.3 ANTIBACTERIAL PHOTODYNAMIC THERAPY (APDT) 46
5.4 DRUG DELIVERY 46
5.5 BIOIMAGING 47
II - OBJECTIVES 50
III – MATERIALS AND METHODS 51
1. Upconversion nanoparticles and chemicals 51
2. Cell lines and reagents 51
3. Physicochemical characterization of nanoparticles 51
4. Cell culture 52
5. Cell Viability 53
6. Laser Optimization Tests for hyperthermia 56
7. Doxorubicin Loading and Release Studies 58

8. Statistical analysis 59
IV – RESULTS 60
1. Physicochemical characterization of Nanoparticles 60
2. Cell Viability 62
2.1 Viability of melanoma cells after incubation with UCNPs@SiO_2 -MTT assay 62
2.2 Viability of MNT-1 cells after incubation with UCNPs@SiO_2 – Neutral Red Uptake Assay 64
2.3 Viability of melanoma cells after incubation with UCNPs@SiO_2-Au 65
2.4 Comparison of exposure to UCNPs@SiO_2 and UCNPs@SiO_2-Au in the two cell lines 67
2.5 Viability of MNT-1 cells after incubation with UCNPs@mSiO_2-PO_4 and UCNPs@mSiO_2-COOH 68
2.6 Comparison of exposure to UCNPs@mSiO_2-PO_4 and UCNPs@mSiO_2-COOH 70
3. Laser Optimization Tests for hyperthermia 71
4. Doxorubicin Loading and pH Mediated Release Studies 76
V – DISCUSSION 78
VI – CONCLUSIONS 85
REFERENCES: 87

LIST OF FIGURES

Figure 1: The hallmarks of cancer suggested by Douglas Hanahan and Robert Weinber 2
Figure 2: Stages of Melanoma) 13
Figure 3: Diverse applications of Nanotechnology 24
Figure 4: Nanotechnology applications in cancer diagnosis 26
Figure 5: Penetration depths for UV and NIR light 29
Figure 6: Basic compositions of UCNPs 29
Figure 7: TEM image of $NaYF_4$:Yb (20%), Er (2%) nanoparticles with 34.1 ± 1.9nm. 31
Figure 8: Schematic energy level diagrams of the sensitizer ion Yb^{3+} and activator Er^{3+} and Tm^{3+} 32
Figure 9: Scheme of energy transfer process during ESA upconversion. 35
Figure 10: Scheme of energy transfer process during ETU upconversion. 36
Figure 11: Scheme of energy transfer process during CSU upconversion. 37
Figure 12: Scheme of energy transfer process during CU upconversion. 38
Figure 13: Scheme of energy transfer process during CR upconversion. 38
Figure 14: Scheme of energy transfer process during PA upconversion. 39
Figure 15: Scheme of energy transfer process during EMU upconversion. 40
Figure 16: Scheme of energy transfer process during ECU upconversion. 41
Figure 17: Photothermal Therapy 45
Figure 18: Light microscopy images of A375 cells with different confluence 53
Figure 19: Light microscopy images of MNT-1 cells with different confluence 53
Figure 20: MTT assay protocol 55
Figure 21: Neutral Red Uptake assay protocol 56
Figure 22: Irradiation scheme using irradiation in 96-well plates 57
Figure 23: Irradiation scheme using a cuvette containing the samples 58
Figure 24: STEM images of a) UCNPs@SiO_2 and b) UCNPs@SiO_2-Au 60
Figure 25: Hydrodynamic diameter of UCNPs@SiO_2 and UCNPs@SiO_2-Au in DMEM 61
Figure 26: Polidispersity Index of UCNPs@SiO_2 and UCNPs@SiO_2-Au in DMEM 61
Figure 27: Zeta potential of UCNPs@SiO_2 and UCNPs@SiO_2-Au in DMEM 62
Figure 28: Effect of UCNPs@SiO_2 on the viability of MNT-1 cells at 24h and 48h of exposure – MTT assay. 63
Figure 29: Effect of UCNPs@SiO_2 on the viability of A375 cells at 24h and 48h of exposure – MTT assay 64

Figure 30: Effect of UCNPs@SiO_2 on the viability of MNT-1 cells at 24h and 48h of exposure – Neutral Red Uptake assay.....65
Figure 31: Effect of UCNPs@SiO_2-Au on the viability of MNT-1 cells at 24h and 48h of exposure – MTT assay 66
Figure 32: Effect of UCNPs@SiO_2-Au on the viability of A375 cells at 24h and 48h of exposure – MTT assay 67
Figure 33: Effect of UCNPs@SiO_2 on the viability of MNT-1 cells and A375 cells at a) 24h and b) 48h of exposure and effect of UCNPs@SiO_2-Au on the viability of MNT-1 cells and A375 cells at c) 24h and d) 48h of exposure – MTT assay.....68
Figure 34: Effect of UCNPs@mSiO_2-PO_4 on the viability of MNT-1 cells at 24h and 48h of exposure – MTT assay 69
Figure 35: Effect of UCNPs@mSiO_2-COOH on the viability of MNT-1 cells at 24h and 48h of exposure – MTT assay 70
Figure 36: Effect of UCNPs@mSiO_2-PO_4 and UCNPs@mSiO_2-COOH on the viability of MNT-1 cells at a) 24h and b) 48h of exposure – MTT assay.....71
Figure 37: Differences between temperature increase in DMEM and distilled water 74
Figure 38: Influence of phenol red on the temperature increase in the absence of nanoparticles 75
Figure 39: Comparison between the two irradiation schemes: irradiation in 96-well plates and irradiation using a cuvette containing the samples to be irradiated.....76
Figure 40: Doxorubicin release over time from loaded UCNPs@mSiO_2-PO_4 and UCNPs@mSiO_2-COOH nanoparticles at 37 °C and pH 7.4 and 5.2. Full profile for 48h (left) and first 6h (right).....77

LIST OF TABLES

Table 1: Breslow's tumour thickness 13

Table 2: Hydrodynamic diameter Dh (with respective polydispersity index PdI) and zeta potential of UCNPs@SiO_2 and UCNPs@SiO_2-Au dispersed in DMEM culture medium (25µg/ml and 100µg/ml) 60

Table 3: Temperature variation as a function of irradiation power density at 980nm. Results for distilled water and DMEM culture medium with phenol red 72

Table 4: Temperature variation as a function of irradiation power density at 980nm. Results for DMEM culture medium without phenol red.....73

Table 5: Doxorubicin loading efficiency and nanoparticle capacity of UCNPs@mSiO_2-PO_4 and UCNPs@mSiO_2-COOH nanoparticles. 76

LIST OF ABBREVIATIONS

$^1O_2$ - Singlet oxygen

Abs- Absorbance

Ag - Silver

AJCC - American Joint Committee on Cancer

ALM - Acral lentiginous melanoma

aPDT - Antibacterial photodynamic therapy

ATP - Adenosine triphosphate

Au - Gold

AuNPs - Gold nanoparticles

BCC - Basal cell carcinoma

CDKN2A - Cyclin-dependent kinase inhibitor 2A

Ce6 - Chlorine6

c-KIT - Kit receptor tyrosine kinase

CNTs - Carbon nanotubes

CO_2 – Carbon dioxide

COVID-19 - Coronavirus disease 2019

CR - Cross-relaxation

CSU - Cooperative sensitization upconversion

CT - Computed tomography

CU - Cooperative upconversion

CuZnSOD - Copper-zinc superoxide dismutase

CW - Continuous-wavelength

DAPI - 4',6-diamidino-2-phenylindole

D_h - Hydrodynamic diameter

DLS - Dynamic light scattering

DMEM - Dulbecco's Modified Eagle's Medium

DMSO - Dimethyl sulfoxide

DNA - Deoxyribonucleic acid

DOX - Doxorubicin

E1 - First excited state

E2 - Second excited state

ECACC - European Collection of Authenticated Cell Cultures

ECU - Energy cascaded upconversion

EGF - epidermal growth factor

EGFR - EGF receptor

EMT - Epithelial–mesenchymal transition

EMU - Energy migration upconversion

Er^{3+} - Erbium

ESA - Excited-state absorption

ETU - Energy transfer upconversion

FBS - Fetal Bovine Serum

FRET - Förster resonant energy transfer

G - Ground state

GLUT1 - Glucose transporter 1

GPCR - G-protein-coupled receptor

GSA - Ground state absorption

HIF - Hypoxia-inducible transcription factors

Ho^{3+} - Holmium

IFN-α - Interferon alpha

LM - Lentigo maligna

Ln^{3+} - Lanthanide ions

LPO - Lipid peroxidation

LRET - Luminescence resonance energy transfer

LSPR - Localized surface plasmon resonance

MAPK - Mitogen-activated protein kinase

MB - Methylene blue

MC1R - Melanocortin-1-receptor

MDA - Malondialdehyde

miSiO_2 - Mesoporous silica

MnSOD - Manganese SOD

MRI - Magnetic resonance imaging

MTT - 3-(4,5 dimethyl-2-thiazolyl)-2,5-diphenyl tetrazolium bromide

$NaYF_4$ - Sodium yttrium fluoride

Nd^{3+} - Neodymium

Neutral red - 3-amino-7-dimethylamino-2-methyl-phenazine hydrochloride

NIR - Near-infrared

NM - Nodular melanoma

NMSC - Non-melanoma skin cancer

PA - Photon avalanche

PBS - Phosphate buffered saline

PdI - Polydispersity index

PDT - Photodynamic therapy

PET - Positron emission tomography

PI3K - Phosphatidylinositol-3-kinase

PS - Photosensitizer

PTEN - Phosphatase and tensin homolog protein

PTT - Photothermal therapy

QDs - Quantum dots

Rb - Retinoblastoma

RET - Resonance energy transfer

RNA - Ribonucleic acid

ROS - Reactive oxygen species

RTKs - Receptors tyrosine kinase

SCC - Squamous cell carcinoma

SOD - Superoxide dismutase

SPECT - Single-photon emission computed tomography

SSM - Superficial spreading melanoma

STEM - scanning transmission electron microscopy

TEM - transmission electron microscopy

TGF - Tumour growth factor

Tm^{3+} - Thulium

UC - Upconversion

UCL - Upconversion luminescence

UCNPs – Upconversion nanoparticles

UV - Ultraviolet

UVA - Ultraviolet A

UVB - Ultraviolet B

UVC - Ultraviolet C

VEGF - Vascular endothelial growth factor

VEGF-A - Vascular endothelial growth factor A

WHO - World Health Organization

Yb^{3+} - Ytterbium

ZnPc - Zinc(II) phthalocyanine

α-MSH - Alpha-melanocyte–stimulating hormone

I – INTRODUCTION

1. CANCER

Globally, cancer is one of the leading causes of death and compromised the increasing life expectancy. According to estimates, in 2020 occurred 19.3 million new cancer cases and almost 10.0 million cancer deaths worldwide. These values are estimative only because, due to SARS-CoV-2, the virus responsible for coronavirus disease 2019 (COVID-19), many people weren't diagnosed with cancer (Sung et al., 2021). According to World Health Organization (WHO) in 2019, cancer is the first or second leading cause of death before the age of 70 years in 112 of 183 countries and ranks third or fourth in a further 23 countries (Sung et al., 2021).

Overall, cancer incidence and mortality are rapidly growing worldwide. The high morbidity and mortality of cancer are related to the increasing prevalence of risk factors such as overweight, smoking, the increased aging and growth of the population as well as changes in the distribution of the main risk factors for cancer (several of which are associated with socioeconomic development) (Gainkam et al., 2008; Sung et al., 2021).

Cancer is a severe problem affecting the health of all human societies. It is a variable disease at the tissue level becoming a big challenge for its specific diagnosis, followed by the efficacy of treatment (Fisher et al., 2013; Meacham & Morrison, 2013).

It was observed that in developed countries cancer incidence is higher but mortality is higher in developing countries (Ghoncheh & Salehiniya, 2016).

Cancer can be caused by environmentally induced gene mutations, which in turn trigger cells to proliferate at an abnormally rapid pace, originating either benign or malignant tumours (Honors et al., 2018). The diagnosis of a tumour and its management is based on the confirmation of its malignancy, and on its site of origin, histotype, grade, and spread throughout the body (Carbone, 2020).

The cytoplasm and nucleus of cells can be directly or indirectly influenced by environmental chemical substances with carcinogenic properties that lead to genetic disorders and gene mutations (Hassanpour & Dehghani, 2017). Viruses, bacteria, and radiation are other carcinogenesis factors, comprising about 7% of all cancers (Parkin, 2006). In general, cancer disrupts cellular relations and results in the dysfunction of vital genes. This disturbance is effective in the cell cycle and leads to abnormal proliferation (Hassanpour & Dehghani, 2017; Seto et al., 2010)

Proto-oncogenes are responsible for cell division and growth under normal conditions but become oncogenes during genetic mutation, which are most dangerous for cell existence (Shtivelman et al., 1985). In addition, the absence of tumour suppressor genes triggers uncontrolled cells division. Usually, repair genes translate to proteins and enzymes that have repairing properties (Hassanpour & Dehghani, 2017).

Cancer cells have significantly different structural and functional characteristics due to genomic changes that stimulate tumorigenesis, making them different from other normal cells. The hallmarks of cancer (Figure 1), first introduced by Douglas Hanahan and Robert A. Weinberg in 2000 and later updated in 2011 (Hanahan & Weinberg, 2011), have proved essential to understanding cancer's common traits, aiding in rational drug development and combinations to treat cancer. These authors have proposed 10 organizing principles that enable the growth and metastatic dissemination of cancer cells. These distinctive and complementary capabilities include the ability of tumour cells and their microenvironment to sustain proliferative signalling, evade growth suppressors, resist cell death, promote replicative immortality, induce angiogenesis, support invasion and metastasis, reprogram energy metabolism, induce genomic instability and inflammation, and trigger evasion of immune responses (Girotti et al., 2020; Hanahan & Weinberg, 2011).

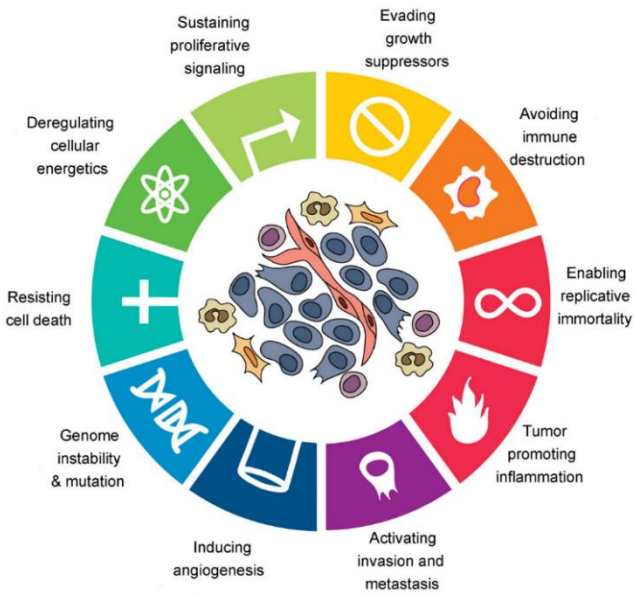

Figure 1: The hallmarks of cancer suggested by Douglas Hanahan and Robert Weinberg (adapted from Girotti et al., (2020))

Each hallmark constitutes a well-established process that a normal cell should undergo to enable tumour growth, survival, invasion and metastasis. They represent a broad range of features regulated by genetic, epigenetic, and posttranslational modifications, including phosphorylation, SUMOylation, and glycosylation, which together contribute to tumorigenesis and tumour progression (Hanahan & Weinberg, 2011).

- Hallmark 1: sustaining proliferative signalling

Cancer cells have a distinctive feature, which is the ability to maintain uncontrolled cell proliferation (Hanahan & Weinberg, 2011). Tumour cells show a reduced dependence on external stimulating signals from their microenvironment. Such stimulatory signals are activated and, in contrast to normal situations in which proliferative signalling is transitory, the signals are sustained chronically in different ways like elevation the number of surface receptors; induce structural alterations in the receptor molecules that facilitate ligand-independent firing; generate growth factor themselves or send signals to activate normal cells in the tumour microenvironment; and induce a constitutive stimulation of the cytoplasmic circuitry involved in different signalling pathways, among others. The most well-established and widespread mechanism of sustaining proliferative signalling involves mutational alteration of genes within cancer cells that convert such genes into active drivers of cell proliferation. These activated genes—defined as oncogenes—render otherwise transitory proliferation-promoting signals chronic (Hanahan & Weinberg, 2017; Hynes & MacDonald, 2009; Witsch et al., 2010). Mutations of the RAS gene are one of the most common traits in human cancer. The HRAS, KRAS, and NRAS proteins are constitutively active in cancer cells, promoting continuous proliferation in a variety of tumours (Sanchez-Vega et al., 2018).

- Hallmark 2: evading growth suppressors

Signals arising from the tumour microenvironment may also favour tumour growth by promoting the inactivation of tumour suppressors, thus limiting their capacity to halt cell cycle progression (Hanahan & Weinberg, 2011). Antiproliferative factors are produced to maintain cellular quiescence and tissue homeostasis. The signals block proliferation by inducing cells to enter in a reversible quiescent (G0) state. Tumour suppressor genes act avoiding cell proliferation, but sometimes their inactivation leads to unregulated cell growth. There are many tumour suppressors identified so far, with TP53 and retinoblastoma (Rb)

being the prototype molecules of this group. They play key roles in the mechanisms that help cells to decide between their proliferation and their senescence and apoptotic way. The Rb protein senses the complexity of extracellular factors and conveys this information to the nucleus, where the cell cycle proceeds or is halted until the conditions are optimal. TP53, on the contrary, senses the stress and other nutritional parameters from inside the cell. If those conditions are suboptimal or excessive genome damage is detected, the cell cycle is halted to preserve cell homeostasis or integrity (Burkhart & Sage, 2008; Deshpande et al., 2005; Girotti et al., 2020; Sherr & McCormick, 2002). Genetic profiling of genomes and transcriptomes indicates that a majority of human tumours contain defects—genetic or epigenetic—in the functions of the Rb and p53 tumour-suppressor pathways (Hanahan & Weinberg, 2017).

- Hallmark 3: avoiding immune destruction

Cancer cells can avoid immune destruction creating immunosuppressive microenvironments (Rabinovich et al., 2007). Cancer is characterized by the accumulation of a variable number of genetic alterations and the loss of normal cellular regulatory processes (Tian et al., 2011). The immune system plays a crucial role in resisting or eradicating the formation and progression of neoplasias, late-stage tumours, and micrometastases. Cells and tissues are continuously monitored by an ever-alert immune system, and such immune vigilance is responsible for recognizing and eliminating the vast majority of cancer cells and thus emerging tumours (Chen & Mellman, 2013). Solid tumours appear because they avoid their detection by the immune system, or they can limit the extent of immunological killing, thus evading eradication. The role of defective immunological monitoring of tumours would seem to be validated by the increases of certain cancers in immunocompromised individuals (Vajdic & Van Leeuwen, 2009).

- Hallmark 4: enabling replicative immortality

Cancer cells can overcome normal senescence resulting from telomeres shortening. Telomerase activation is an important step in carcinogenesis occurring in >90% of cancers (Harley et al., 1994).

Normal cells have a limited number of cell division cycles. That limitation is related to two processes that block cell proliferation: senescence (an irreversible, viable but quiescent, unproliferative state) and apoptosis (a state that induces cell death). When cells

escape from apoptosis and start to proliferate unlimitedly they are denominated as immortalized cells. This property is acquired by cancer cells. Telomeres are regions of repetitive nucleotide sequences located at the end of each chromatid. They protect the chromosomal DNA from deterioration or fusion with neighbouring chromosomes and be related to the replicative potential. Telomeres are shortened during each cell generation, and this progressive reduction provokes the loss of their ability to protect the ends of chromosomes, and consequently, the DNA instability and the entrance into apoptosis (Blasco, 2005; García-Caballero et al., 2015).

Telomerase is a specialized DNA polymerase that adds telomere repeat segments to the ends of telomeric DNA. It is almost absent in non-immortalized or somatic cells but expressed at significant levels in germ cells and in most spontaneously immortalized cells, including human cancer cells. This fact allows them to maintain their telomere length and proliferative potential, avoiding the events that trigger senescence and apoptosis (Heaphy & Meeker, 2011; Kawai et al., 2007).

- Hallmark 5: tumour-promoting inflammation

Tumour-associated inflammatory responses involve the secretion of multiple pro-inflammatory cytokines, chemokines, and growth factors that promote epithelial cell proliferation, fibroblast recruitment, and neovascularization (Arnold et al., 2015).

Solid tumours consist of neoplastic cells, non-malignant stromal cells, and migratory hematopoietic cells, including cells from the innate and adaptive immune system. Complex interactions between these cell types in this microenvironment regulate tumour growth, progression, angiogenesis, and metastasis (Candido & Hagemann, 2013; Zhang, Liu et al., 2012).

Initially was accepted the fact that the immune response was carried out to eradicate tumours, now the paradigm has changed, and it is accepted that immune cells can enhance tumorigenesis and progression, helping incipient neoplasias to acquire hallmark capabilities (Grivennikov et al., 2010; Qian & Pollard, 2010).

In some cancers, inflammatory conditions precede the development of malignancy; in others, oncogenic change drives a tumour-promoting inflammatory milieu. Most tumours are infiltrated by a variety of cell types of the immune system (the so-called infiltrating immune cells, or IIC), including macrophage subtypes, mast cells, and neutrophils, as well as T and B lymphocytes (Egeblad et al., 2010; García-Caballero et al., 2015; Hanahan & Coussens, 2012; Murdoch et al., 2008; Zhang, Liu et al., 2012). Besides differentiated

immune cells, partially differentiated myeloid progenitors can also be found in cancer, representing the link between circulating cells from bone marrow origin and the differentiated immune cells typically found in normal and inflamed tissues (García-Caballero et al., 2015; Murdoch et al., 2008).

The epidemiologic association between chronic inflammation and carcinogenesis supports the proposition that pre-existing inflammatory conditions can lead to the inception and progression of certain forms of cancer (Hanahan & Weinberg, 2017).

- Hallmark 6: activating invasion and metastasis

Metastasis is the result of a multistage sequence of limiting events called the metastatic cascade, meaning that if one step is blocked, the whole process is compromised. This process involves invasion of tumour cells to the surrounding tissue, intravasation, survival in the circulation, extravasation, and colonization of targeted organs. The success of each step, during early or late dissemination, relies on a multiplicity of factors hierarchically regulated at the transcriptional and posttranscriptional levels (Hanahan & Weinberg, 2011).

Alterations in molecules involved in the cell-to-cell and cell-to-extracellular matrix adhesion promote the invasion. Metastasis involves interactions between cancer cells and the local microenvironment. Metastatic cells rely on extrinsic signals from a supportive microenvironment to establish themselves as new colonies at a distant site (Egeblad et al., 2010; Qian & Pollard, 2010).

Transcription factors like Snail, Slug, Twist, and Zeb1/2, can induce the developmental regulatory program “epithelial–mesenchymal transition” (EMT), and therefore the acquisition of migratory, invasion, and apoptosis resistance abilities by epithelial cells. Cancer cell invasion can be carried out by different strategies and depends on the type of cancer. The EMT program regulates a particular type of invasiveness that has been termed “mesenchymal.” Other two mechanisms are the “collective invasion” and the “amoeboid invasion”. The first one involves nodules of cancer cells advancing massively into adjacent tissues and is characteristic of, for example, squamous cell carcinomas. In the second one, cancer cells show morphological plasticity, finding their way through the interstices in the extracellular matrix (Madsen & Sahai, 2010).

- Hallmark 7: inducing angiogenesis

Angiogenesis, the growth of new blood vessels out of pre-existing ones, is an essential requirement in the development and progression of cancer. Genetic and pharmacological inhibition of vascular signalling pathways has provided critical evidence that abnormal angiogenesis is a hallmark of cancer (Ferrara & Kerbel, 2005; Potente et al., 2011).

During embryogenesis, the development of the vasculature involves the creation of new blood vessels from endothelial precursors by a process termed vasculogenesis (Heinke et al., 2012). Once the primary vascular network is formed, the appearance of new blood vessels from pre-existing ones occurs by angiogenesis. Angiogenesis is a highly regulated process, very active in embryos but largely inactive in adults, limited to some processes related to reproductive cycles, wound healing, and bone repair. A deregulated and persistent activation of the "angiogenic switch" is essential for tumour growth and metastasis (Carmeliet, 2005a).

Like normal tissues, tumours require nutrients and oxygen, as well as an ability to remove metabolic wastes and carbon dioxide. The tumour-associated neovasculature, generated by angiogenesis, permits tumours to grow. Moreover, the new blood vessels present in the tumour microenvironment help in neoplastic growth (Hanahan & Folkman, 1996).

There are many pro-angiogenic factors. Vascular endothelial growth factor A (VEGF-A) is the prototypic pro-angiogenic factor and the major regulator of physiological and pathological angiogenesis (Ferrara et al., 2003). VEGF gene expression can be upregulated both by hypoxia and by oncogene signalling (Carmeliet, 2005b).

Angiogenesis is stimulated in an early stage of cancer development, but tumour vasculature differs from the normal vasculature showing abnormal characteristics, including fragility, chaotic arrangements, and imperfect vessel walls due to discontinuous endothelial cell lining and weak investiture with vascular smooth muscle cells (García-Caballero et al., 2015).

On the other hand, endothelial cells in tumour vasculature are usually irregularly shaped, forming an uneven luminal layer with loose interconnections and focal intercellular openings (Prokopiou et al., 2013). These characteristics allow macromolecule diffusion and aid the metastatic process by facilitating the entrance of tumour cells into the bloodstream (Pasqualini et al., 2002).

Cells at the diffusion limit from the nearest capillary activate various stress-response systems. The most important involves the hypoxia-inducible transcription factors (HIF), which regulate hundreds of genes, including ones that directly or indirectly induce angiogenesis and other stress-adaptive capabilities (Hanahan & Weinberg, 2017).

- Hallmark 8: genome instability & mutation

Cells may acquire random mutations and chromosomal rearrangements that contribute to tumour development and progression (Hanahan & Weinberg, 2011). The role of genome maintenance machinery is to detect and resolve DNA defects, ensuring low rates of spontaneous mutations during each cell generation (Lane, 1992). The cell genome is subject to routine DNA damage, from a variety of chemically reactive products of normal metabolism, from environmental insults, and from its replication during every cell division (Hanahan & Weinberg, 2017).

There are various forms of genomic instability. Most cancers have chromosomal instability, which refers to the high rate by which chromosome structure and number changes over time in cancer cells compared with normal cells. May also occur microsatellite instability which is a form of genomic instability characterized by the expansion or contraction of the number of oligonucleotide repeats present in microsatellite sequences (Negrini et al., 2010). In addition, the accumulation of mutations can be accelerated by compromising the surveillance systems that normally monitor genomic integrity and force genetically damaged cells into either senescence or apoptosis (Jackson & Bartek, 2009).

Genomic instability in tumour lesions has been attributed to the mutations in caretaker genes. These are genes that primarily function to maintain genomic stability. The classical caretaker genes are DNA repair genes and mitotic checkpoint genes. The tumour suppressor gene TP53 could also be considered as a caretaker gene because of its function in the DNA damage response (Lane, 1992). Thus, these caretaker genes can lose their properties as tumour suppressor genes in the course of tumour progression, either through inactivating mutations or via epigenetic repression (Barnes & Lindahl, 2004). Telomerase also is added to the list of critical caretakers responsible for maintaining genome stability and integrity (García-Caballero et al., 2015).

- Hallmark 9: resisting cell death

Cancer cells acquire the ability to escape death triggered by cell surface receptors, soluble factors, immune effector cells, and anticancer therapies, thus facilitating tumour progression (Hanahan & Weinberg, 2011).

Tumour cells increase in number not only due to their high proliferation rate but also to their capability to resist cell death (apoptosis) (Adams & Cory, 2007). There are factors involved in the reception and processing of extracellular death-inducing signals (the extrinsic apoptotic pathway) like Fas ligand/Fas receptor or TNF ligands/TNF receptor, and others involved in the monitoring and integration of intracellular signals (the intrinsic apoptotic pathway) in which the mitochondria is involved. The most important apoptosis effectors are the caspases (Pop & Salvesen, 2009). In this phase, the cell suffers morphological and biochemistry changes such as chromatin condensation, DNA damage, externalization of phosphatidylserine residues in membrane bilayers, cell cycle alterations, mitochondrial transmembrane potential reduction, intracellular acidification, reactive oxygen species production, and cellular proteins proteolysis, among others (Cryns & Yuan, 1998).

Apoptosis is controlled by a dialogue between the pro and the anti-apoptotic members of the Bcl-2 family of regulatory proteins, which include Bcl-xL, Bcl-w, Mcl-1, A1, and cytochrome c as inhibitors; and Bax, Bim, Puma, and Bak as activators (Adams & Cory, 2007; Willis & Adams, 2005). Several abnormality sensors that play key roles in tumour development have been identified: the loss of TP53 tumour suppressor function, the upregulated expression of Bcl-2, Bcl-xL, the downregulated expression of Bax, Bim, and Puma, and a significant loss or inactivation of lead members in the caspase family (Adams & Cory, 2007; Fiandalo & Kyprianou, 2012; Lowe et al., 2004).

Other two cell death phenomena should be mentioned, autophagy and necrosis. Autophagy plays a central role in regulating important cellular functions such as cell survival during starvation and cellular stress deficiency (Boya et al., 2013; Levine & Kroemer, 2008). Necrosis is the cell death that leads to cell destruction and release of its intracellular content into the surrounding tissue microenvironment. This process appears under genetic control and it probably helps tumour progression and invasion (Ouyang et al., 2012).

- Hallmark 10: deregulating cellular energetics

Acquisition of tumorigenic and metastatic capabilities requires a well-adjusted energy metabolism that fuels tumour growth (Girotti et al., 2020).

Under aerobic conditions, normal cells consume glucose which is transformed into pyruvate via glycolysis in the cytosol and thereafter to carbon dioxide in the mitochondria. Under anaerobic conditions, glycolysis is favoured, and relatively little pyruvate is dispatched to the oxygen-consuming mitochondria (García-Caballero et al., 2015).

Otto Warburg (O. Warburg, 1956) observed that certain cultured cancer cells have enhanced uptake of glucose, which is metabolized via glycolysis, even in the presence of oxygen levels that normally should favour oxidative phosphorylation. This phenomenon is known as the “Warburg Effect” or the “aerobic glycolysis” which produces, in addition to ATP, many of the building blocks for the cellular macromolecules that are required for cell growth and division (Hanahan & Weinberg, 2017).

Some tumours have been found to contain two subpopulations of cancer cells working symbiotically that differ in their energy-generating pathways. One of them consists of glucose-dependent cells that live under hypoxic conditions and secrete lactate, whereas the other cell subpopulation, better-oxygenated, preferentially import and utilize the lactate produced by their neighbours as their main energy source (Feron, 2009).

To compensate for the less efficient production of ATP, tumour cells increase the glucose import into the cytoplasm especially by upregulating GLUT1. The activity of GLUT1 is linked with activated oncogenes (e.g. RAS, MYC, Akt) (García-Caballero et al., 2015).

Malignant tumours often spread to surrounding tissues and move throughout the body using circulatory or lymphatic systems, causing metastasis. Due to the ability of cancer to metastasize, this makes localized treatment redundant and therefore problematic in the annihilation of the cancer cells (Honors et al., 2018; Swavey & Tr, 2013). It is necessary the develop of new strategies to fight this disease that kills more and more.

2. SKIN CANCER

According to the World Health Organization (WHO), skin cancer is the most common malignant disease amongst the Caucasian (D'Orazio et al., 2013) population with over a million new cases per year (Naves et al., 2017). According to its clinical behaviour and with the cells that originate it, it is classified into two categories: melanoma and non-melanoma skin cancer (NMSC) (D'Orazio et al., 2013). Basal cell carcinoma (BCC) and squamous cell carcinoma (SCC) are included in this last category. Both derivate from epidermal keratinocytes. Even though they have a bigger incidence, non-melanoma skin cancer is also less deadly and more easily treatable than malignant melanoma once that they stay at their original location with no tendency to spread (Simões et al., 2015).

2.1 MALIGNANT MELANOMA

Malignant melanoma is the most aggressive type of skin cancer showing high mortality rates (Naves et al., 2017). Worldwide, the incidence of melanoma has risen more than any other type of cancer (Monge-Fuentes et al., 2014). Melanoma is responsible for less than 10% of all types of skin cancer. However, it is linked with 80% of all deaths by skin cancer (Haridas et al., 2017). Nowadays melanoma is considered a multi-factorial disease with influences covering increased UV exposure, environment, hereditary risk factor, and improved surveillance and earlier recognition (Simões et al., 2015). The most important and potentially modifiable environmental risk factor for developing malignant melanoma is exposure to UV rays, because of their genotoxic effect (Rastrelli et al., 2016). Malignant melanoma is considered metastatically invasive once it tends to spread to surrounding tissues (Honors et al., 2018). Since melanoma presents both historical and clinical characteristics quite heterogenous and a significant number of mutations, it presents a low tumour regression rate, high rate of drug resistance and targeted therapies, low rate of patient survival, and a tendency for recurrences to occur (Bourneuf, 2017; George et al., 2016; Naves et al., 2017).

It has its origins in melanocytes (skin cells responsible for the production of melanin (Orthaber et al., 2017)) that, by suffering aberrant changes to their molecular and biochemical level, they end up becoming carcinogenic cells (Walker & Hayward, 2002). Melanocytes originate in the developing neural crest and migrate to the skin, to the hair follicles, to the eyes, and the ears (Gray-Schopfer et al., 2007). Although it is common to appear in pre-existing skin spots, it can occur in any part of the surface of the skin (Swavey & Tr, 2013).

The vascularization of the tumour happens naturally, by passive diffusion, where tumour cells obtain all the required nutrients to grow till it reaches the size range $2mm^3$. When the tumour cells are bigger than $2mm^3$, occurs angiogenesis to supply enough nutrients to the cancer cells, increasing the mass of the tumour once these areas become richly vascularized (Maeda et al., 2000).

It is thought that the development of the melanoma is accompanied by epithelial-to-mesenchymal (EMT) switch characterized by the melanocytes loss of E-cadherin expression and acquisition of some mesenchymal markers as SNAIL (transcription factor of zinc-finger family), SLUG (transcriptional repressor of E-cadherin), TWIST (Twist-related protein 1), and ZEB1 (Zinc finger E-box binding homeobox 1 transcription factor) (Caramel et al., 2013; Faião-Flores & Smalley, 2018).

2.1.1- Stages:

There are five stages of melanoma as shown in figure 2:

- Stage 0- melanoma is localized only on the superficial surface of the skin making the basal layer clear of any anomaly – melanoma *in situ*.
- Stage I – melanoma's thickness is smaller than 1mm. It is localized in the epidermis and penetrates the basal lamina spreading to the papillary dermis.
- Stage II- melanoma's thickness is between 1 and 2mm and it extends into the papillary-reticular dermis interface.
- Stage III – melanoma reaches the reticular dermis and its cells spread to at least one lymphatic node or the surrounding tissues.
- Stage IV – cell metastasis occurs to several organs, to other places of the skin, or lymphatic nodes far from the tumour's original place (Swavey & Tr, 2013).

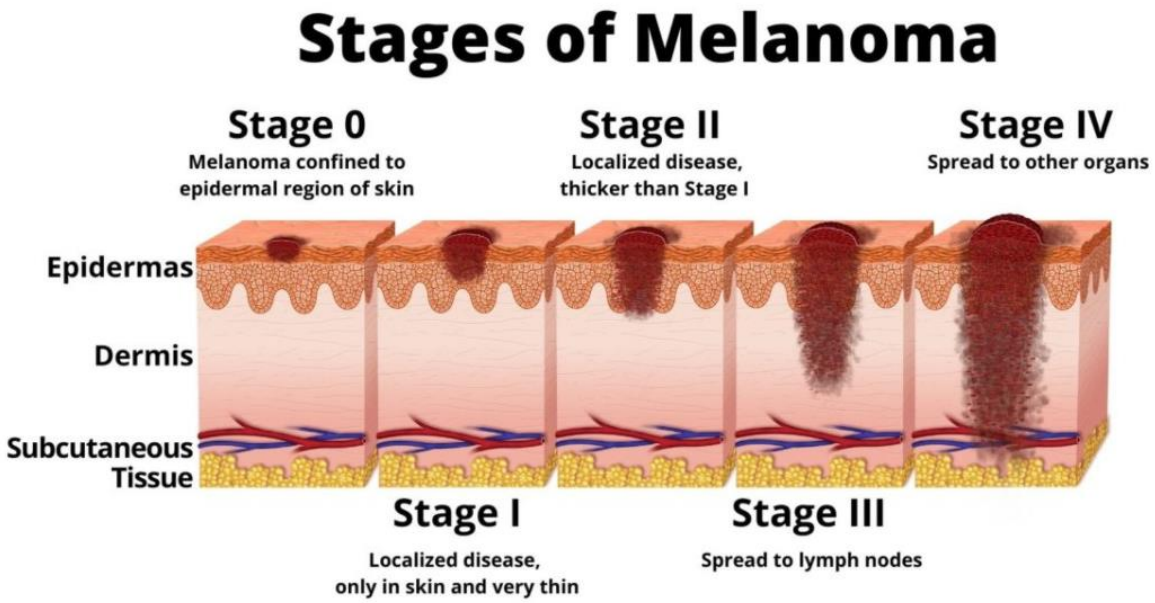

Figure 2: Stages of Melanoma (from ©https://www.aimatmelanoma.org/stages-of-melanoma/ accessed 8th October, 2021)

It is essential to diagnose the melanoma in its initial state before metastasis occurs because once it spreads, it is hard to find its origin making it harder to treat and it lowers the chances of survival (Honors et al., 2018). Once located in the dermis, melanoma has the potential to spread through the other body sites by entering the lymphatic system and bloodstream (Garbe et al., 2010). For this reason, it is important to be careful with the Breslow's tumour thickness which can be classified according to table 1. Using Breslow's tumour thickness, it is possible to make a prognosis of the patients, if there is a possibility of metastasis by knowing the survival rate for patients diagnosed with melanoma skin cancer (Naves et al., 2017).

Table 1: Breslow's tumour thickness (adapted from Naves et al., (2017))

STAGE	DEPTH
I	Tumour with ≤1.0 mm
IIA	1.01–2.0 mm
IIB	2.01–4.0 mm
III	Tumour depth ≥ 4.0 mm

The evaluation of primary tumours is done by applying the 2009 American Joint Committee on Cancer (AJCC) Melanoma Staging and Classification System that evaluates: tumour thickness, mitotic figures, ulceration, and microscopic satellites (Balch et al., 2009). The number of mitoses (achieved by histopathological measures) is a very important factor for the diagnosis of melanoma of reduced thickness (Breslow's thickness of less than 0.75mm). Characteristics like a dark colour and peripheral stretch marks are related to thin melanomas with mitosis, while brown colour and a net of atypical pigmentation are linked with a softer form of the sickness (Ribero et al., 2017).

2.1.2- Causative factors

There are several risk factors that contribute to the appearance of melanoma, such as:

- Skin type – people with lighter skin have a big risk of developing melanomas (Orthaber et al., 2017), once their risk of developing a sunburn due to UV rays is higher (Honors et al., 2018).
- Solar radiation – even though UVA and UVB rays induce the production of vitamin D, they are both carcinogenic because they are mutagenic and compromise the immune system (Simões et al., 2015). Sun exposure in childhood and adolescence as well as intermittent sun exposure are the biggest risk factors; factors like sunburns or the number of newly formed nevi are also considered to be high risk elements for the appearance of melanomas (Orthaber et al., 2017). Genomic and sequencing studies indicate UV radiation as the principal melanoma's mutagenic agent (Colebatch & Scolyer, 2018).
- Nevi – the number of dysplastic nevi (atypical) is also a risk factor. Those that have more than 6mm of diameter and an irregular shape and colour are considered to be atypical (Simões et al., 2015).
- Age – with the rise of age, there is a rise in the incidence of melanoma. Despite that, this is one of the most common types of cancer among young adults (Orthaber et al., 2017).
- Gender – generally speaking, the male population is more susceptible to melanomas than the female population (Orthaber et al., 2017). Men have a more tendency to the appearance of melanoma in the skin of their heads, neck, between their shoulders and hips while females usually develop melanoma in the lower part of their legs, between their shoulders or hips (Swavey & Tr, 2013). Physiological differences in the skin structure, differences in the immune system, the influence of

sex hormone levels, and the expression of estrogen receptors are the origin of this event (Liu-Smith et al., 2017; Roh et al., 2017).

- Immunosuppression – this can be considered a risk factor once it can lower the patient survival rate (Orthaber et al., 2017).
- Family history – if the patient has two or more close relatives with melanoma history, one's chances of developing melanoma get higher (Orthaber et al., 2017).
- Previously removed melanomas (Orthaber et al., 2017).

2.1.3- Ultraviolet radiation

Sunlight is a continuous spectrum of electromagnetic radiation that can be divided into three major spectrums of wavelength: ultraviolet, visible, and infrared (Soehnge et al., 1997). Ultraviolet radiation subdivides itself into ultraviolet A (UVA (315–400nm)), ultraviolet B (UVB (280– 315nm)) and ultraviolet C (UVC (100–280nm)) (Narayanan et al., 2010). Approximately 90–99% of the solar UV energy that reaches the earth's surface is UVA, where only 1–10% is UVB (Pastila & Leszczynski, 2007). UVC is absorbed by the ozone layer in the atmosphere, thus the effects of UVC are considered negligible to human health (Narayanan et al., 2010).

UV radiation is considered the major aetiological factor in skin cancer, but the relationship between dose, timing, and nature of exposure to tumour development remains unclear (Black et al., 1997). Ultraviolet radiation's role in the appearance of melanoma seems to be quite complex once that only a small amount of mutations caused by this type of radiation were detected in patients with melanoma comparing with those that were identified in patients diagnosed with non-melanoma skin cancer. Besides, it is known that intermittent exposure to ultraviolet rays is linked with the presence of melanoma. Melanoma occurs most frequently after intermittent exposure to the sun and in people with frequent sunburns. Epidemiologic observations suggest that chronic or low-grade exposures to ultraviolet light induce protection against DNA damage, whereas intense, intermittent exposures cause genetic damage (Gilchrest et al., 1999; Liu-Smith et al., 2017).

Recent studies suggested that DNA impairment requires the presence of other dysregulated genes (through epigenetic events) to initiate UV-induced melanomagenesis (Zaidi et al., 2008).

Whereas non-melanoma skin cancer represents a severe, but usually non-lethal, response to solar radiation (Black et al., 1997), malignant melanoma is one of the most

frequent malignant tumours in younger people and is characterized by its high capacity for invasion and metastasis (Hofmann et al., 2000).

On a molecular level, exposure to ultraviolet light increases skin pigmentation, partly due to the action of alpha-melanocyte–stimulating hormone (α-MSH) on its receptor, the melanocortin-1-receptor (MC1R). The binding of the hormone to the receptor stimulates intracellular signalling in melanocytes, and this signalling increases the expression of enzymes involved in the production of melanin. Light skin people show polymorphisms in gene MC1R lowering the activity of the receptor (Frändberg et al., 1998; Naysmith et al., 2004; Valverde et al., 1995) increasing the risk of melanoma (Kennedy et al., 2001).

In addition, ultraviolet radiation causes genetic changes in the skin, impairs cutaneous immune function, increases the local production of growth factors, and induces the formation of DNA-damaging reactive oxygen species that affect keratinocytes and melanocytes (Gilchrest et al., 1999; Thompson et al., 2005).

Exposure to UVA and UVB causes wavelength-dependent damage in human skin: UVB directly damages DNA (Sander et al., 2003; De Gruijl, 2000), inducing the formation of cyclobutane pyrimidine dimers (Meeran et al., 2008), while the deleterious effects of UVA on cellular targets involve photosensitizers and the generation of reactive oxygen species (ROS) (Sander et al., 2003; De Gruijl, 2000) which create breaks in DNA (Soehnge et al., 1997). ROS are involved in all stages of multistep cancer development (Marnett, 2000). Because of the potentially deleterious effects of ROS, cells use various mechanisms to modulate their intracellular and extracellular levels. The skin's enzymatic antioxidant defence includes copper-zinc superoxide dismutase (CuZnSOD), manganese SOD (MnSOD), and catalase. SOD converts superoxide anions into hydrogen peroxide, while catalase degrades hydrogen peroxide into water. These enzymes, which maintain a redox balance within cells, are modulated by UVB and UVA irradiation in skin cells *in vitro* and *in vivo* in murine skin (Sander et al., 2002; Sander et al., 2003; Okada et al., 1994; Sasaki et al., 1997).

When the formation of ROS exceeds the ability of the tissue's antioxidant defence system to quench them, damage to cell membranes by lipid peroxidation (LPO), damage to DNA, sulphur-containing enzymes and proteins, and carbohydrates are among the major effects (Sander et al., 2002; Sander et al., 2003). LPO leads to the formation of a, b-unsaturated aldehydes including malondialdehyde (MDA) which was shown to be mutagenic and carcinogenic (Sander et al., 2003).

UV radiation creates mutations to p53 tumour suppressor genes. These are genes that are involved in DNA repair or the apoptosis of cells that have lots of DNA damage.

Therefore, if p53 genes are mutated, they will no longer be able to aid in the DNA repair process; as a result, there is dysregulation of apoptosis, expansion of mutated keratinocytes, and initiation of skin cancer (Benjamin & Ananthaswamy, 2007), mostly in NMSC. Melanoma exhibits a very low frequency of p53 mutations (Simões et al., 2015).

2.1.4- Types of melanoma

Melanoma can be classified into three categories: cutaneous melanoma (91.2%), ocular melanoma (5.3%), and mucosal melanoma (1.3%) (Kawczyk-Krupka et al., 2013). Ocular melanoma, also known as uveal melanoma or choroidal melanoma, is the most common primary intraocular malignant tumour (Monge-Fuentes et al., 2014). Mucosal melanoma can occur in any mucous membrane of the body, including the nasal cavity and accessory sinuses, oral cavity, anorectum, and others (Mihajlovic et al., 2012).

2.1.4.1- Subtypes of cutaneous melanoma

Several histological subtypes of cutaneous melanoma are described, such as superficial spreading melanoma, nodular melanoma, polypoid melanoma, acral lentiginous melanoma, lentigo maligna melanoma, and some uncommon forms: desmoplastic melanoma, nevoid melanoma, amelanotic melanoma, and verrucous melanoma (Bourneuf, 2017; Tsao et al., 2012). The main categories are superficial spreading melanoma (SSM)- 70-75%, nodular melanoma (NM)- 20-25%, lentigo maligna (LM)- 5-10%, and acral lentiginous melanoma (ALM)- 5%. These data refer to White Caucasian populations (Saldanha et al., 2006).

Besides the histopathological differences between the different subtypes of cutaneous melanoma, other factors distinguish them.

- superficial spreading melanoma (SSM) is the most frequent form of melanoma (Carr et al., 2020). SSM has no preference for sun-damaged skin, being associated with intermittent and sporadic sun exposure. The upper back in both sexes and the legs in women are the most common sites. There is a tendency to multicoloration, not just with different shades of tan, but variations of black, red, brown, blue, and white (Forman et al., 2008; Monge-Fuentes et al., 2014). The lesion outline is usually sharply marginated with one or more irregular peninsula-like protrusions. The surface may have a palpable papule or a nodule that extends several millimetres

above the skin surface. SSM may emerge in an existing mole, or as a new lesion (Rastrelli et al., 2016). It undergoes lateral (radial) growth before vertical (invasive) growth occurs (Carr et al., 2020).

- nodular melanoma (NM) presents lesions that arise without a clinically apparent radial growth phase, but usually large atypical melanocytes can be found in the epidermis beyond the region of vertical growth (Forman et al., 2008; Monge-Fuentes et al., 2014). NM has a rapid growth and higher rate of metastasis (Rastrelli et al., 2016). Tumours appear primarily on sun-exposed areas of the head, neck, and trunk, and can be smooth and dome-shaped, fungating, friable, or ulcerated. Bleeding is usually a late sign (Forman et al., 2008; Monge-Fuentes et al., 2014). NM has a relatively uniform brown, black, or blue-black colour; also can be amelanotic (Rastrelli et al., 2016).

- the lentigo maligna (LM) begins as a tan macule that extends peripherally, with gradual uneven darkening over years, and tends to be more common in older patients with heavily sun-damaged skin (Forman et al., 2008; Monge-Fuentes et al., 2014). This cancer may evolve for decades before invading the papillary dermis. It has irregular outlines, and although the tumour is often relatively large and flat, a focus of invasion may be detected as a papule (Rastrelli et al., 2016).

- acral lentiginous melanoma (ALM) appears more commonly in palms, soles of feet, subungual, and occasionally, mucosal surfaces (Carr et al., 2020). Demonstrates a junctional growth pattern, indistinct margins, and over time, a vertical growth phase develops and shows little association with sun exposure (Forman et al., 2008; Monge-Fuentes et al., 2014). Represents the most prevalent histologic subtype in African, African American, Chinese, Taiwanese, and mixed racial heritage populations (Forman et al., 2008).

Melanomas are also classified in relation to melanin content. Most types of melanomas are melanotic, containing various degrees and types of pigmentation (melanin); however, any clinical subtype of primary cutaneous melanoma or metastatic melanoma may be amelanotic, presenting the absence of pigmentation in the tumour. Amelanotic melanoma represents 1.8-8.1% of all such tumours (Koch & Lange, 2000).

2.1.5- Genes and signalization pathways

Melanoma intratumoral and intertumoral heterogeneity places it among the most aggressive types of cancer. Intratumoral heterogeneity is characterized by genomic instability (occurring mutations as a result), genomic and epigenomic alterations (resulting in the expression of heterogeneous genes), and epigenetic dysregulation (Grzywa et al., 2017). The aggressiveness of melanoma can be explained by the ability of melanoma cells to escape the apoptosis process by overexpressing the apoptosis-inhibitory genes (as survivin and other inhibitory apoptosis proteins—IAPs) or through the reduction of the expression of the apoptosis stimulating genes that leads to failure of apoptosis and consequently to an increased risk of metastasis (Rigon et al., 2015).

Melanoma's complexity is also conferred by the different signalization pathways that are involved in its development, which coincide with the necessary ways to the development of melanocytes such as Notch, Wnt, endothelins, SOX (sex-determining region Y–like–SRY high-mobility group—HMG box) proteins, mitogen-activated protein kinase (MAPK) signalling pathway, phosphatidylinositol-3-kinase (PI3K) pathway, G-protein-coupled receptor (GPCR) family, and epithelial-to-mesenchymal transition (Liu et al., 2014; Paluncic et al., 2016).

There are two major groups of genes associated with skin cancer: high and low-risk genes. It was identified a region on the short arm of chromosome 9 associated with melanoma which was also absent in cancer cell lines. The deleted locus was later identified as harbouring the CDKN2A gene (cyclin-dependent kinase inhibitor 2A gene). Genetic CDKN2A mutations have been demonstrated in 25% to 50% of families with heritable melanoma (Nikolaou & Stratigos, 2014; Simões et al., 2015) causing a deficiency or loss of functions (mutations, homozygous deletions, or DNA methylation-induced epigenetic silencing) (Conde-Perez & Larue, 2014; Erlich & Fisher, 2018; Martín-Gorgojo & Nagore, 2018). Two other genes have been recognized within the same locus, one of which, P14ARF, overlaps CDKN2A and shares some coding regions, even though in a different reading frame. The other high-risk gene, CDKN2B, lies very close to CDKN2A and has a similar mechanism of action. The three proteins encoded by these genes (p16INK4a, p14ARF, and p15INK4b) are potential tumour suppressors and each plays a role in cell-cycle arrest (Peters, 2008).

CDK4, another very rare high penetrance familial melanoma gene, encodes the primary target of p16INK4a (Zuo et al., 1996). Currently, it is considered that these genes

may play a role in melanoma growth, although the evidence favours mutations in CDKN2A as the most predominant event (Simões et al., 2015).

Low-risk genes were associated with pigmentation. One of the most important alleles that influence skin cancer risk is the melanocortin-1-receptor (Simões et al., 2015), previously mentioned. Other low-risk candidate genes that have been explored for possible associations with skin malignancies include polymorphisms in various DNA repair genes and apoptosis (from the XP gene family (XPC, XPD)) BrCa2, TERT/CLPTM1L, TIPARP (formerly PARP-1), ATM, CASP8), but also in pigmentation (ASIP, TYR) and naevi proliferation (PLA2G6, MTAP, IRF4) (Debniak et al., 2008; Millikan et al., 2006; Nikolaou & Stratigos, 2014; Simões et al., 2015; Zhang et al., 2008).

Receptors tyrosine kinase (RTKs) are widely dysregulated in cancers. In cutaneous melanoma, alterations in the EGF receptor (EGFR), Met RTK (c-MET), and Kit receptor tyrosine kinase (c-KIT) result in changes to the associated signalling cascades (Simões et al., 2015). Activating mutations and/or gene amplification of KIT have been found in 28% of melanomas that arise in chronically sun-damaged skin (Eggermont, 2010). The EGFR can be activated by EGF, TGF (tumour growth factor), amphiregulin, and heparin-binding EGF. Following ligand binding, tyrosine-phosphorylated EGFR initiates the activation of downstream pathways, which results in cell proliferation, migration, adhesion, anti-apoptosis, angiogenesis, and metastasis (Khan et al., 2011; Wu et al., 2013). Downstream pathways include MAPK (also known as RAS/RAF/MEK/ERK signal transduction cascade) and Phosphatidylinositol-3-kinases (PI3K) signalling cascades (two major pathways that originate from the RTKs) and then dysregulation in these signalling pathways may result in aberrant cell proliferation and/or apoptosis, and eventual tumour development (Khan et al., 2011; Nikolaou et al., 2013). Dysregulation of this pathway may also involve membrane receptors, RAF and RAS proteins, and genes involved in other pathways such as PI3K, PTEN, Akt, which are also involved in regulating RAF activity. Furthermore, many studies have revealed that RAF/MEK/ERK pathway also influences chemotherapeutic drug resistance. Many human cancers show abnormal activation of this pathway, and BRAF and NRAS represent the most important identified mutations (Simões et al., 2015).

BRAF is a serine-threonine kinase that's is involved in cellular proliferation and it triggers the signalization pathway MAPK after its activation by the protein family RAS. This way of signalization is responsible for the control of important cellular processes, such as the progression of the cell cycle and differentiation and positive regulation (upregulation) of transcription. BRAF mutations lead to compromising of these processes being oncogenesis its final result (Leonardi et al., 2018; Liu et al., 2018; Roh et al., 2015). BRAF mutations are

very common in cutaneous melanoma while its presence in the non-cutaneous melanomas is low (Erlich & Fisher, 2018; Liu et al., 2018). Melanoma cancers exhibit BRAF mutations in up to 70% of cases that are responsible, in large part, for the constitutive hyperactivation of survival/antiapoptotic pathways such as the MAPK, NF-κB, and PI3K/AKT (Simões et al., 2015). The most prevalent mutation, which is detected in approximately 50% of melanomas, it's the replacement of valine with the glutamic acid in codon 600 (BRAF (V600E)). This mutation may be the result of a secondary effect of damage caused by UV radiation, like, for example, a non-classic DNA mutation induced by this type of radiation or the synthesis of reactive oxygen species (Erlich & Fisher, 2018; Tsao et al., 2012). This mutation was related in melanomas and melanocytic nevi, leading to the activation of the way RAS/RAF/MEK/ERK, performing a crucial part in the initiation of melanoma (Roh et al., 2015; Tsao et al., 2012). It was discovered a new BRAF mutation (an aminoacidic insertion in codon 599) in a patient with melanoma which reinforces the heterogeneity seen in this tumour (Trubini et al., 2018).

NRAS mutations represent the second most frequent cause that originates changes in the signalization pathway MAPK. This sort of mutation was indicated in 33% of primary and 26% of metastatic melanoma tumours and is correlated with sun exposure and nodular lesions, resulting in its constitutive activation even in the absence of activation (Simões et al., 2015). It was found in codons 12, 13, or 61. It is important to state that BRAF and NRAS mutations are both exclusive, meaning that it is rarely seen the presence of these two mutations simultaneously. Besides, it is important to mention that for these mutations to trigger a malignant transformation, additional mutations, such as the loss of tumour suppressants as p16INK4A or PTEN (phosphatase and tensin homolog protein), need to happen (Leonardi et al., 2018; Martín-Gorgojo & Nagore, 2018). By itself, BRAF or NRAS mutations can only cause an aberrant growth of the cells followed by a premature growth stop, leading to benign injuries that only acquire malignancy in the presence of other mutations (Conde-Perez & Larue, 2014).

2.1.6- Existent therapies

Prognoses of metastatic melanoma are performed by analysing the location of the primary tumour, tumour size, number of tumours, lymph node involvement, and the absence or presence of metastasis. To determine the stage of cancer, assessments such as physical examinations, imaging tests, laboratory tests, and pathology reports are performed on patients (Amin et al., 2017; Honors et al., 2018).

2.1.6.1- Surgery

The local treatment of cutaneous melanoma consists of radical excision of the skin tumour or the biopsy site. The tumour is classified using the Breslow's classification, which depends on the tumour depth (Orthaber et al., 2017). The excision is made around the affected place catching some of the surrounding tissues to assure that every affected tissue is removed and none cancerogenic cell remains in that area (Swavey & Tr, 2013). This is the primary treatment that offers a better chance of recovery when the melanoma is detected in its initial stages and metastasis has not yet occurred (Honors et al., 2018).

2.1.6.2- Chemotherapy

Another treatment for cancer is chemotherapy which has the ability to alleviate, control, or completely cure skin cancer; its success is dependent on the patient's severity of cancer at the time of diagnosis (Gogas et al., 2007). Chemotherapy relies on effective drugs to stop cancer cells from proliferating abnormally or to slow down their overall growth rate (Kang et al., 2015). Metastatic melanoma chemotherapeutic drugs include dacarbazine, paclitaxel, platinum compounds, and temozolomide (Megahed & Koon, 2014). Cisplatin (or its analogues) combined with other cytostatic drugs (carboplatin, nitrourea, taxanes, vindesine, and vinblastine) may be an option when the other drugs don't work (Simões et al., 2015). The low response rate (<20%) is due to various resistance mechanisms (Tang et al., 2017).

2.1.6.3- Radiotherapy

Radiotherapy is another therapy that is used for the treatment of melanoma (Barker & Postow, 2014). It is similar to chemotherapy in the sense that it can alleviate, control, or cure cancer depending on the severity and type of cancer the patient has been diagnosed with (Liniker et al., 2016). Radiation is employed to annihilate cancer cells through external or internal administration. With internal administration, radiation is precisely administered only to the affected area of a patient's body, whereas with external radiation the beam is applied to a much wider area and so is considered less precise (Honors et al., 2018).

2.1.6.4- Biological therapy

Biological therapies differ from chemotherapy since the drugs that are administered to patients aid the immune system in combating cancer rather than just directly killing rapidly proliferating cells (Honors et al., 2018). This type of therapy is often used in combination with other therapies (DeSantis et al., 2014). IFN-α treatment may be employed in patients with stage II and III melanoma as adjuvant therapy, in spite of being associated with substantial toxicity. In the absence of surgical options, systemic treatment is indicated. BRAF inhibitors like vemurafenib for BRAF mutated patients, as well as the CTLA-4 antibody ipilimumab (recombinant, fully human IgG1 monoclonal antibody against cytotoxic T lymphocyte-associated antigen 4) offer fresh therapeutic prospects apart from conventional chemotherapy. Nevertheless, therapeutic decisions in stage IV patients are controversial and should be primarily made by an interdisciplinary oncology team (Bhatia et al., 2009; Eggermont, 2010; Eigentler & Garbe, 2013).

The most conventional treatments used so far to fight cancer are often related to unwanted side effects. Although they continue to be the first line of treatment for cancer patients, new solutions need to be found. Since cancer cells and normal tissues are not fully differentiated, during surgery some cancer tissues may not be removed. Chemotherapy works throughout the body resulting in many side effects as well as resistance to certain drugs. Radiotherapy, despite acting in a specific region, also affects normal tissues leading to the appearance of skin damage, cell mutation, among other problems (Lee & Park, 2018).

Therefore, the development of more effective and safer methods for treating cancer is essential. New treatment systems that include nanomaterials have been developed. The next chapter will explore the applications of nanomaterials in the melanoma treatment.

3. NANOTECHNOLOGY

Nanotechnology could be described as any technology performed on a nanoscale with length scales in the 1 to 100 nanometres range and that has applications in the real world. Nanotechnology covers the production and application of physical, chemical, and biological systems at scales ranging from individual atoms or molecules to submicron dimensions, as well as the integration of the resulting nanostructures into larger systems. Nanotechnology has several applications, such as controlled drug delivery systems for diagnosis and therapy, it can provide targeted delivery of active biological substances, enhanced image contrast agents, chip-based nanolabs capable of monitoring and manipulating individual cells, nanoscale probes that can track the movements of cells and individual molecules, cancer treatment by detecting and destroying the tumour, restoration of human organs, and implants with higher biocompatibility (Figure 3). By providing constructs capable of combining multiple functionalities into a single nanoscale entity, nanotechnology also offers the opportunity to monitor and detect molecular and cellular changes associated with disease states. Once they penetrate the cell, nanostructures can detect a certain disease and cure it by delivering specific drugs to the zone of interest (Bhushan, 2010; McNeil, 2005; Stylios et al., 2005)

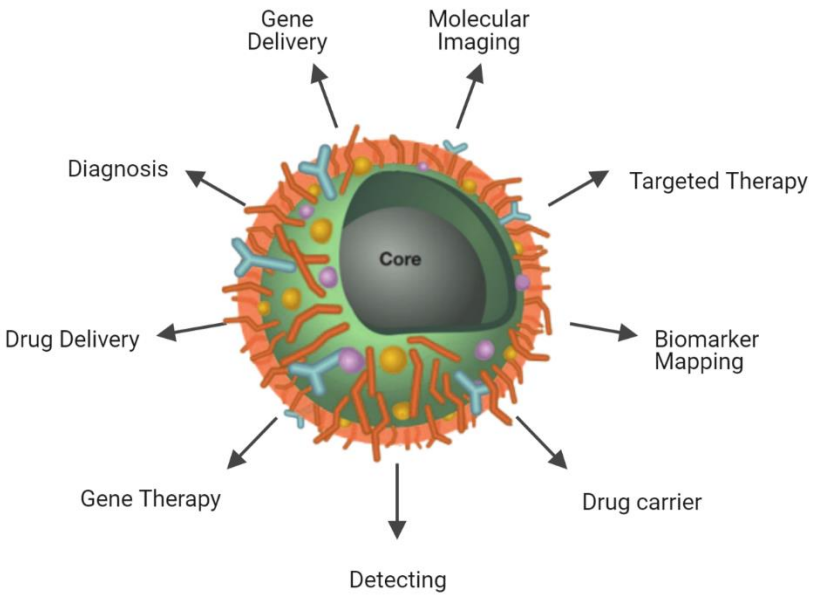

Figure 3: Diverse applications of Nanotechnology (adapted from Chaturvedi et al.,(2018); McNeil, (2005) and created in Biorender.com)

When nanotechnology is applied to biological systems, there are some important aspects to be considered like size, solubility, and targeting (active or passive) (McNeil, 2005; Wicki et al., 2015).

There are many different types of nanomaterials. Some examples are dendrimers, liposomes, carbon nanotubes, nanoshells, quantum dots, polymeric micelles, and nanoparticles. All these materials are designed with chemically modifiable surfaces to attach a variety of ligands that can turn these nanomaterials into biosensors, molecular-scale fluorescent tags, imaging agents, targeted molecular delivery vehicles, and other useful biological tools (Chaturvedi et al., 2018; McNeil, 2005).

Nanoparticles can be classified into different classes based on their properties, shapes, or sizes. They have unique chemical and physical properties due to their high surface area and nanoscale size. Their optical properties, reactivity, and other properties are dependent on the size, shape, and structure (Khan et al., 2019). Depending on the overall shape these materials can be 0D, 1D, 2D, or 3D (Tiwari et al., 2012).

Nanoparticles may be composed of three layers: (I) The surface layer, which may be functionalized with a variety of small molecules, metal ions, surfactants, and polymers; (II) The shell layer, which is chemically different material from the core and (III) The core, which is essentially the central portion of the nanoparticle and usually refers the nanoparticle itself (Shin et al., 2016).

Nanoparticles can be classified into various categories depending on their chemical and physical characteristics. There are carbon-based nanoparticles (e.g., fullerenes and carbon nanotubes (CNTs)), metal nanoparticles (e.g., gold and silver), ceramics nanoparticles (inorganic non-metallic solids), semiconductor nanoparticles (semiconductor materials possess properties between metals and nonmetals), polymeric nanoparticles, lipid-based nanoparticles, among others (Khan et al., 2019).

The multifunctionality of nanoparticles helps them incorporate biotargeting ligands such as antibodies, peptides, and small molecules or therapeutic drugs and transport them to the active site, as well as being useful in diagnosis and disease progress monitoring after chemotherapy. This technology facilitates early detection and a mixture of diagnostics with therapeutics. Personalized nanotechnology can also deliver cells or genes that are taken from the patient himself to improve the specific targeting of tumours and increasing the efficacy of treatment (Abadeer & Murphy, 2016; Liu, 2012).

3.1 NANOTECHNOLOGY IN CANCER

Nanotechnology-based diagnostic methods are being developed as promising tools for real-time, convenient, and cost-effective cancer diagnosis and detection. An essential advantage of applying nanoparticles for cancer detection lies in their large surface area to volume ratio relative to bulk materials. Due to this property, nanoparticle surfaces can be densely covered with antibodies, small molecules, peptides, aptamers, and others. These can bind and recognize specific cancer molecules. By presenting various binding ligands to cancer cells, multivalent effects can be achieved, which can improve the specificity and sensitivity of an assay. For cancer diagnosis, nanoparticles are being applied to the detection of extracellular cancer biomarkers (such as cancer-associated proteins, circulating tumour DNA, microRNA, DNA methylation, and extracellular vesicle), for detection of cancer cells (such as circulating tumour cells, detection through cell surface protein recognition and detection based on mRNA) and for *in vivo* imaging (passive targeting and active targeting) as represented in the figure 4 (Song et al., 2010; Zhang, Li et al., 2019).

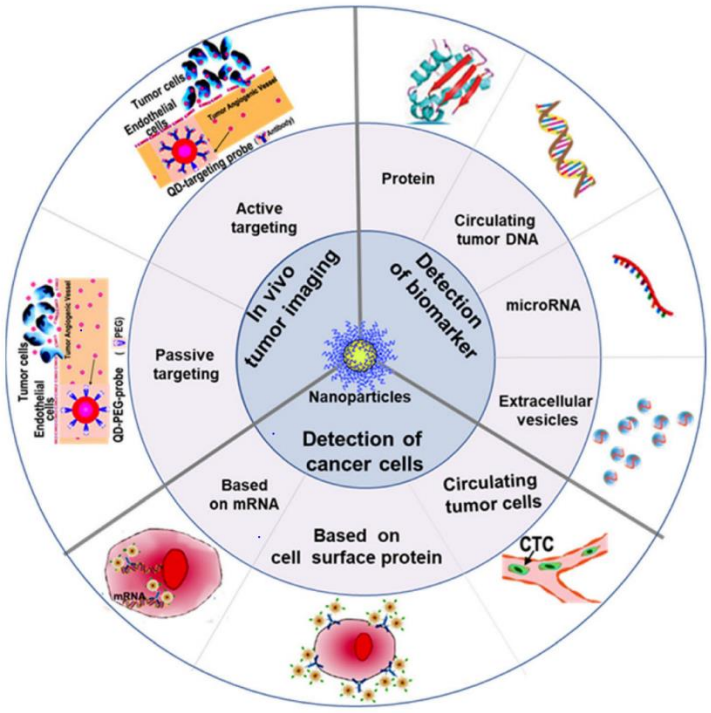

Figure 4: Nanotechnology applications in cancer diagnosis (from Zhang, Li et al., (2019))

Nanoparticles can be used to carry the chemotherapeutic drugs and release them in the tumour area, without disturbing healthy cells. They have the task to keep the

substances protected from degradation by the body before they arrive in the interest zone, to release them inside the tumour, and to keep control over them, in such a way that they can be discharged at the right time and in the most suitable concentration and distribution. The active targeting of the drug is the most suitable targeting approach for the successful delivery of nanoparticles in cancerous cells without causing any toxicity. It is a specific type of targeting that usually relies on ligand-receptor interaction, in which nanoparticles possess ligand that specifically binds to the receptor present on the tumour cell surface. Active targeting decreases nonspecific interaction by conferring the strong ligand-receptor binding to deliver the drug in peripheral tissues. Passive targeting is the diffusion-mediated transport of drugs which involves the preparation of a drug carrier complex that can escape to body defence machinery. The drug carrier complex circulates in the bloodstream and is to be taken to the target receptor. Various properties of drug carrier complex such as molecular weight, surface charge, hydrophobic or hydrophilic nature of the surface, and its size are key for efficient passive targeting of drugs (Albulet et al., 2017; Boisseau & Loubaton, 2011; Chaturvedi et al., 2018).

4. UPCONVERSION NANOPARTICLES (UCNPS)

4.1 DEFINITION, STRUCTURE AND PROPERTIES

Upconversion nanoparticles (UCNPs) are optical nanomaterials, commonly doped with trivalent lanthanide ions, that presenting a huge variety of electronic transitions within the 4f electron shells. The transition between f-f electrons on the 4f shell is protected, by electrons of higher 5s and 5p shells, from an influence of ligands and afterward, only a minimal perturbation of electronic configuration is experienced by the trivalent lanthanide ions, conferring unique luminescent properties. This shielding permit that these ions exhibit characteristic narrow-band emission and, since the f-f transitions are forbidden, the excited states have long lifetimes (Liu et al., 2017; Oliveira et al., 2019; Safdar et al., 2020; Wang, Han et al., 2010; Zhou et al., 2015).

These nanoparticles convert two or more near infrared (NIR) photons (lower energy photons) into one higher energy emission photon, in the ultraviolet, visible, and shorter wavelength NIR range, through a photon upconversion process (Chen et al., 2014; Wang & Liu, 2009). Because of this peculiarity, nanoparticles have a kind of nonlinear optical phenomenon, an anti-Stokes type of luminescence process. It is different from the Stokes type of luminescence process, which produces longer wavelength emissions after absorbing one photon with higher energy (Li et al., 2020).

Because these nanoparticles have several potential advantages in comparison to conventional fluorophores, like quantum dots, organic dyes, and fluorescent proteins, they have attracted a lot of attention (Gulzar et al., 2017). UCNPs exhibit low cytotoxicity, low photobleaching, high photostability, high quantum yield, long luminescence lifetime, non-blinking, large anti-Stokes shifts, among others (Chen, Li et al., 2016; Rafique et al., 2020; Wang et al., 2009; Wang et al., 2011; Wu et al., 2009).

The use of near-infrared (NIR) for excitation reduces phototoxicity compared with UV light. This fact permits a higher tissue penetration depth (Figure 5) and reduced the autofluorescence background showing an improved signal-to-noise ratio. In the near-infrared window (also known as an optical window or therapeutic window), the tissues have minimal light absorption avoiding the undesirable photodamage of cells (Chhetri et al., 2019; Wang et al., 2011).

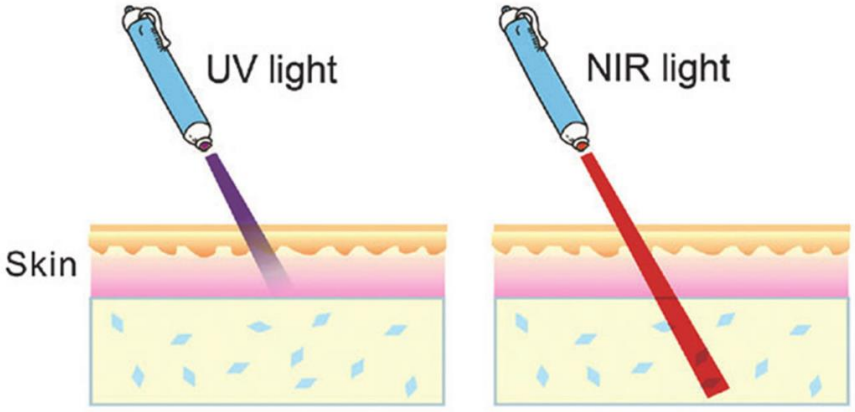

Figure 5: Penetration depths for UV and NIR light (adapted from Chen, Chen et al., (2015))

Usually, UCNPs are formed by three essential components: host matrix, sensitizer, and activator/emitter (Figure 6). Activators/emitters typically provide luminescent centres; sensitizers absorb NIR light, and transfer the absorbed light to activators to facilitate the emission of light; and host matrix provides a crystalline host lattice structure for activators and sensitizers to the correct place, giving it the suitable light conditions (Liang et al., 2020).

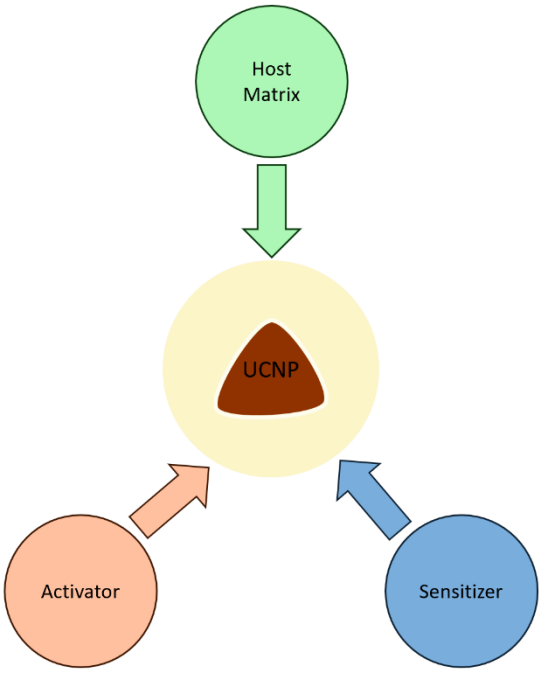

Figure 6: Basic compositions of UCNPs (adapted from Liang et al., (2020))

The optical properties of UCNPs are dependent on these components. They affect the spectral characteristics, conversion efficiency, and overall performance of UCNPs. To obtain high upconversion efficiency, it is crucial to co-dope sensitizer ions next to activator ions that have a closely matched intermediate-excited state, because the upconversion efficiency is highly dependent on the separating distance between the dopants (activators and sensitizers) (Chen, Peng et al., 2015; Chhetri et al., 2019; Tu et al., 2015).

Host matrix

The host matrix is an extremely important component in UCNPs and is related to upconversion luminescence (UCL) efficiency. Host matrix is essential for energy transfer during upconversion and determining the surrounding environments of dopant ions, such as spatial distance, and coordination numbers. Choose the appropriate host materials is very important because a few basic requirements are required, including optical stability and similar ionic size to that of the dopant ions. An ideal host matrix should have high chemical stability, low lattice phonon cut-off energies to minimize host absorption losses and maximize the luminescence output, and low local symmetry of the lattice for high upconversion emission (Chen, Li et al., 2016; Chhetri et al., 2019; Zhou et al., 2012).

The main materials used to synthesize UCNPs are fluorides, oxides, and chlorides. Metal-fluorides-based host materials have demonstrated chemical stability. Nowadays, the most widely investigated upconversion nanosystem is the $NaREF_4$, where RE means rare earth elements, including Y and all the lanthanides. $NaYF_4$ (sodium yttrium fluoride) looks to be the most suitable host material for UCNPs, as it fulfils the above-mentioned requirements for a great host matrix (Feng et al., 2013; Liang et al., 2020).

$NaYF_4$ has two different phases: cubic (α)-$NaYF_4$ and hexagonal (β)-$NaYF_4$ (Figure 7). In the hexagonal phase, the local crystal field is more asymmetric than in the cubic phase, making them better over the cubic $NaYF_4$ for UCL efficiency (Noculak & Podhorodecki, 2018). When the particle's physical size is reduced, high surface tension causes the phase transition from hexagonal to cubic, culminating in a significant decrease in luminescence for upconversion (Ayyub et al., 1995).

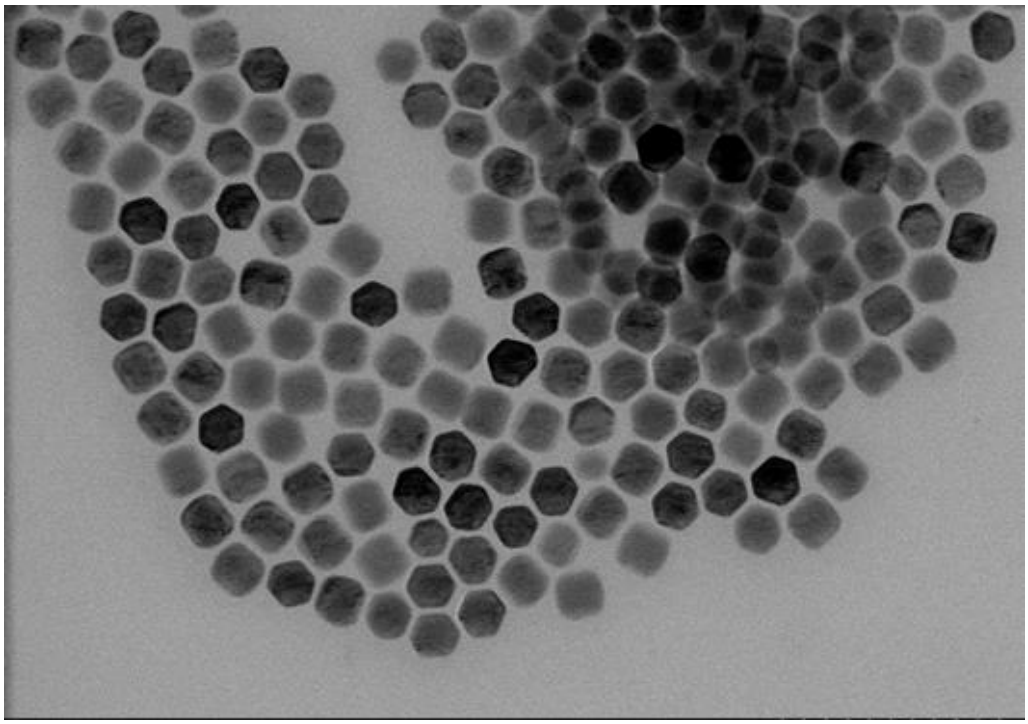

Figure 7: TEM image of $NaYF_4$:Yb (20%), Er (2%) nanoparticles with 34.1 ± 1.9nm.

Synthesis plays a crucial role in determining the composition, structure and properties of resulting materials. The resulting upconversion nanostructures may be either hydrophobic or hydrophilic, which have their merits and demerits. The upconversion nanostructures with controllable shape and size can be prepared by thermal decomposition, high temperature co-precipitation, and solvothermal method (Boyer et al., 2006; Li et al., 2008)

The low solubility of $NaREF_4$ in organic and aqueous solutions makes them easier synthesized using the co-precipitation method from corresponding precursors (Feng et al., 2013).

Dopants: Activators and Sensitizers

Dopant ions are divided into activators and sensitizers. Usually, UCNPs are composed of at least two different lanthanide ions. One plays the role of a sensitizer, while the other acts as an activator. Sensitizers absorb the energy of incident photons and non-radiatively transfer the energy to the close activators ions to emit upconverted luminescence (i.e., visible and UV) (Lee & Park, 2018; Safdar et al., 2020).

Typically, sensitizers are ions with a simple energy level structure, like ytterbium (Yb^{3+}) or neodymium (Nd^{3+}). The cross-section of the sensitizer ions used to absorb NIR it

is an important parameter for UCL efficiency. Usually, most lanthanide ions have a small absorption cross-section in NIR spectral region and do not produce sufficient UC efficiency. Nonetheless, Yb^{3+} or Nd^{3+} have larger absorption cross-sections and can transfer the absorbed energy to neighbouring excited ions (Chen, Li et al., 2016; Cheng et al., 2018; Xie et al., 2013). These ions are activators. The most common activators are erbium (Er^{3+}), thulium (Tm^{3+}), or holmium (Ho^{3+}) because of their long-lived intermediate energy states and due to their ladder-like arranged energy levels. They are essential for the entire UC emission process (Chhetri et al., 2019; Lu et al., 2014; Zhou et al., 2015). Their main upconversion emission bands are located in the green and red regions, the blue and NIR regions, and the green region, respectively (Lee & Park, 2018).

Yb^{3+} is one of the most ions used as a sensitizer because it only has one excited 4f level, $^2F_{5/2}$. The absorption band of Yb^{3+} has located around 980nm (corresponding to $^2F_{7/2} \rightarrow {}^2F_{5/2}$ transition). This transition matches quite well with several electronic transitions that are found in Er^{3+}, Tm^{3+}, and Ho^{3+}, facilitating the efficient energy transfer from Yb^{3+} to the emitting Ln^{3+} ions, as represented in the figure 8 (Chen, Li et al., 2016; Chhetri et al., 2019; Lingeshwar Reddy et al., 2018; Wang & Liu, 2009).

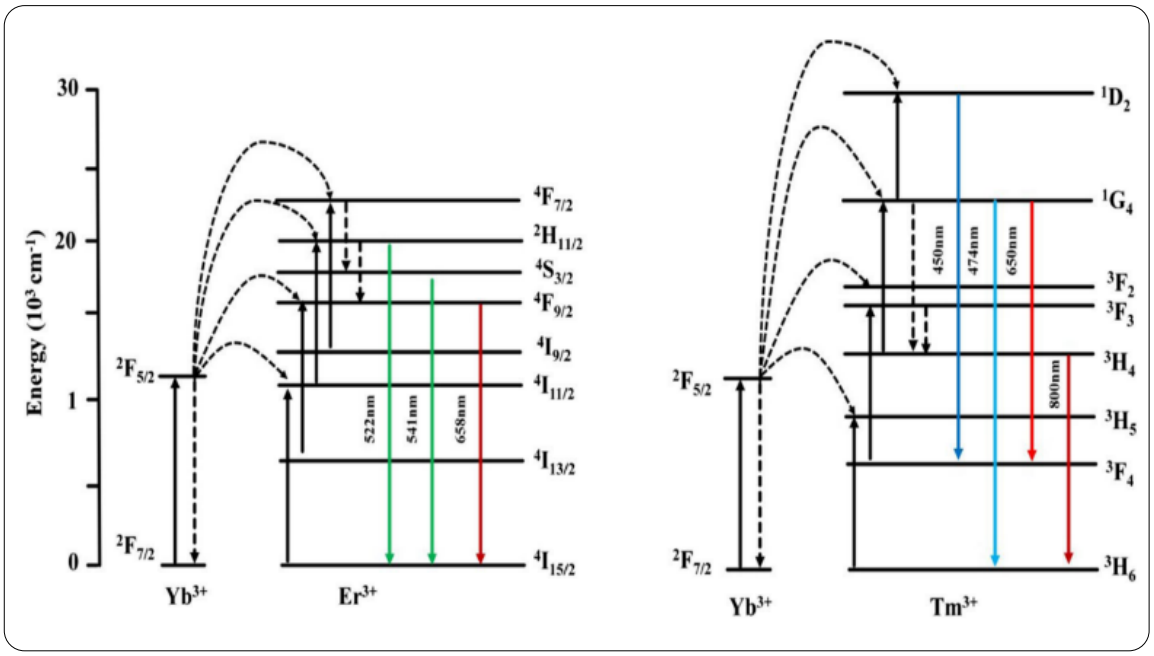

Figure 8: Schematic energy level diagrams of the sensitizer ion Yb^{3+} and activator Er^{3+} and Tm^{3+}. Full and dotted arrows indicate radiative and non-radiative energy transfer, respectively. Under excitation at 980nm, an electron of Yb^{3+} is excited from the $^2F7_{/2}$ to the $^2F_{5/2}$ level. The energy may be transferred to Er^{3+}/Tm^{3+} non-radiatively to excite it to the corresponding excited level. (from Liang et al., (2020))

To obtain the desired UC luminescence characteristics, it is essential the optimization of the material composition, since different Ln^{3+} dopant ions can exhibit different emission properties. Moreover, the relative concentration of the activator ions is extremely important because a too small concentration may not produce an efficient UC emission, and a too high concentration may result in concentration quenching. Yb^{3+} is usually codoped into the lattice at relatively high concentrations (around 20-30%), while the activator concentration is only <2%, reducing the energy loss from cross-relaxation (Safdar et al., 2020; Zhang, Yang et al., 2013).

Coating the shell on the surface of UCNPs (UCNPs@shell) gives them a hydrophilic surface for good dispersity in the physiological environment and also introduces the other functional units into theranostic platform. The coating of UCNPs with mesoporous silica ($mSiO_2$) has attracted great interest since silica shows good biocompatibility, and their surface is easily functionalized with various groups which allows combine UCNPs with different types of molecules to be used in different areas. Silica also confers good water solubility, specific cellular accumulation, and a large surface area (Kong et al., 2014; Rafique et al., 2020; Wang et al., 2019).

UCNPs are interesting materials due to their photophysical properties and their application potentials in various fields such as solid-state laser, solar cells, colour displays, or biomedicine (Klier & Kumke, 2015; Li et al., 2020; Ramasamy & Kim, 2014; Safdar et al., 2020). In the last years, applications in the biomedicine field have progressed significantly with the development of biocompatible, efficient, and accurate UCNPs to be applied in photodynamic therapy, *in vivo* and *in vitro* biological imaging, drug delivery, multimodal imaging, antibacterial activity, gene delivery and gene therapy, biodetection, clinical diagnosis, cancer therapy, intracellular temperature sensing, biolabels for cancer detection, fluorescence imaging, photothermal therapy, among others (Chávez-García et al., 2018; Chhetri et al., 2019; Debasu et al., 2020; Feng et al., 2013; Safdar et al., 2020; Wang, Thang et al., 2020; Zhang, Yang et al., 2013).

4.2 Energy transfer and UC Mechanisms

4.2.1- Energy Transfer

Energy transfer applies to all upconversion process. There are many types of energy transfer processes such as energy transfer in core@shell nanostructures, luminescence resonance energy transfer (LRET), and Förster resonant energy transfer (FRET) (Chen, Li et al., 2016).

In core@shell nanostructures, shell layers can be inactive or active in terms of UCL (Vetrone et al., 2009). Inactive shells usually reduce nonradiative decay losses of surface luminescence increasing UCL efficiency or introduce other functions to satisfy the requirements from specific applications. Active shells are very important in determining optical properties because they are responsible for the spatial separation of luminescent centres, and consequently, the energy transfer between core and shell can be reduced. Thus, core@shell nanostructures are beneficial to reduce the prejudicial energy transfer and increase UCL (Chen, Li et al., 2016).

Another energy transfer process is LRET. To occur resonance energy transfer (RET) is necessary a certain overlapping between the absorption band of acceptor and emission band of the donor. It is also essential that the distance between donor and acceptor be small to allow energy transfer. In UCNPs based LRET nanocomposites, UCNPs are usually used as an energy donor, while several metal nanoparticles, dyes, or quantum dots (QDs) act as acceptor (Chen, Li et al., 2016).

Förster resonant energy transfer (FRET) is an energy transfer process in which the energy of a chromophore in the excited state (donor) can be transferred to a neighbour molecule that is in the ground state (acceptor). This can occur at a distance greater than the collisional radii. When the donor and the acceptor are close, energy can be transferred without the generation of any photons, through long range dipole−dipole interactions. There are many parameters that depends on the rate of the energy transfer, such as the quantum yield of the donor, the distance between the donor and the acceptor, the extent of the overlap between the emission spectrum of the donor and the absorption spectrum of the acceptor, and the relative orientation of the donor regarding the acceptor transition dipoles (Melle et al., 2018).

4.2.2- UC Mechanisms

There are a lot of possible UC mechanisms. The photon upconversion process in lanthanide-doped nanoparticles can occur in eight different ways: excited-state absorption (ESA), energy transfer upconversion (ETU), cooperative sensitization upconversion (CSU), cooperative upconversion (CU), cross-relaxation (CR), photon avalanche (PA), energy migration upconversion (EMU), and energy cascaded upconversion (ECU) (Li et al., 2020; Safdar et al., 2020).

These upconversion mechanisms involve the sequential absorption of two or more near-infrared photons into multiple specific intermediate energy states, which is followed by

the emission of a high-energy photon (with a wavelength shorter than the absorbed light). This is a nonlinear optical mechanism (Chhetri et al., 2019).

4.2.2.1- Excited State Absorption (ESA)

ESA (Figure 9) is based on the principle that a ground state lanthanide ion sequentially absorbs two photons to emit a single higher energy photon. In this UC mechanism, an ion that is in a ground state (G) absorbs a photon and is promoted to the first excited state (E1) through the process known as ground state absorption (GSA). The E1 state has a long lifetime and, before decaying to the ground state, another pump photon is absorbed, promoting the ion from the E1 state to the second excited state (E2). Upconversion emission occurs when existing decay from the E2 state to the ground state. The emitted photon has higher energy (and shorter wavelength) than the absorbed photons. To get a highly efficient ESA is necessary a ladder-like arrangement of the energy states of ions. In reality, only just a few lanthanide ions show such energy level structures. Er^{3+}, Ho^{3+}, Tm^{3+}, and Nd^{3+} are some examples (Auzel, 2004; Chhetri et al., 2019; Li et al., 2020; Safdar et al., 2020; Wang & Liu, 2009).

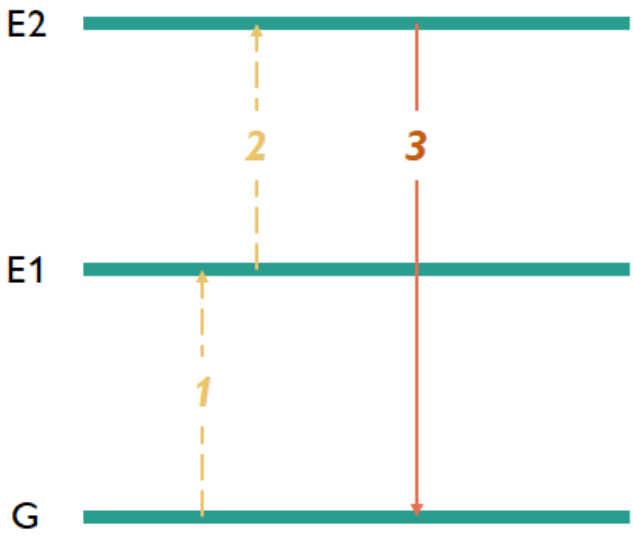

Figure 9: Scheme of energy transfer process during ESA upconversion. The yellow lines represent photon excitation, and the orange lines represent emission processes (adapted from Li et al., (2020))

4.2.2.2- Energy Transfer Upconversion (ETU)

The ETU process (Figure 10) is characterized by the use of two lanthanide ions instead of one, like what happens in ESA. For an ETU process occurs, an ion 1 (sensitizer) is excited, by absorbing a pump photon, and goes from the ground state for the excited E1 state. At the same time, an ion 2 (activator) also absorbs energy from the pump photon and transit, simultaneously, for the E1 state (like what happens with ion 1). Then, ion 1 transfers the stored energy (non-radiative energy transfer process) to ion 2. Thus, the activator goes to the excited E2 state by energy transfer, and the sensitizer relaxes back to the ground state. In this process, the energy transfer is highly sensitive to the distance between the sensitizer and activator that in turn is determined by the ions concentration. The ETU mechanism is extremely important for UCNPs because the most efficient UCNPs use it (Chhetri et al., 2019; Li et al., 2020; Wang & Liu, 2009).

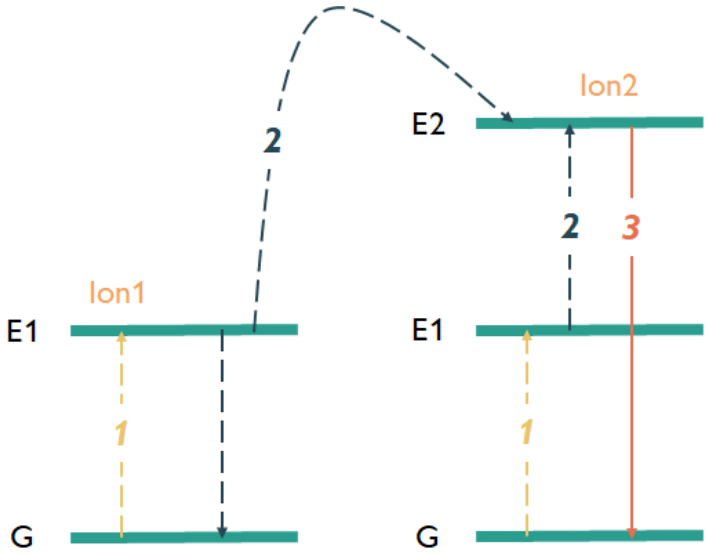

Figure 10: Scheme of energy transfer process during ETU upconversion. The yellow lines represent photon excitation, the blue lines represent energy transfer, and the orange lines represent emission processes (adapted from Li et al., (2020))

4.2.2.3- Cooperative Sensitization Upconversion (CSU)

The CSU (Figure 11) is a process that involves the interaction of three ion centres, where ion 1 and ion 3 are sensitizers (usually being the same chemical element), and ion 2 is an activator. When ions are excited, ion 1 and ion 3 are promoted to excited E1 state. Then, both ion 1 and ion 3 will interact with ion 2 and simultaneously transfer the

accumulated energy to ion 2, exciting to a higher excited state E2. The excited ion 2 deexcites to its ground state and emit an upconverted photon (Li et al., 2020; Safdar et al., 2020).

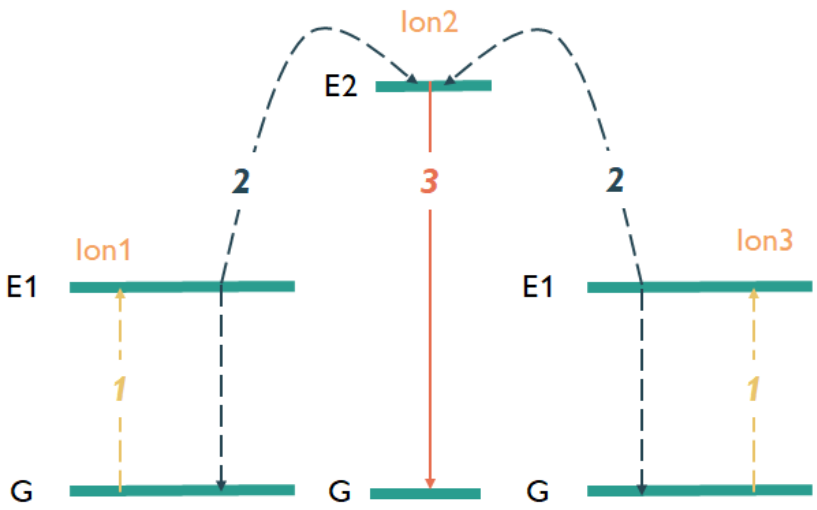

Figure 11: Scheme of energy transfer process during CSU upconversion. The yellow lines represent photon excitation, the blue lines represent energy transfer, and the orange lines represent emission processes (adapted from Li et al., (2020))

4.2.2.4- Cooperative Upconversion (CU)

CU (Figure 12) is a similar process to CSU, previously described. This process also involves three ions. Ion 1 and ion 3 is excited and then return to the ground state emitting simultaneously a photon whose energy is equal to the sum of the two excited ions. Nonetheless, there is no real emission level involved in this process, this being the main difference between the CU mechanism and CSU mechanism (Li et al., 2020; Safdar et al., 2020).

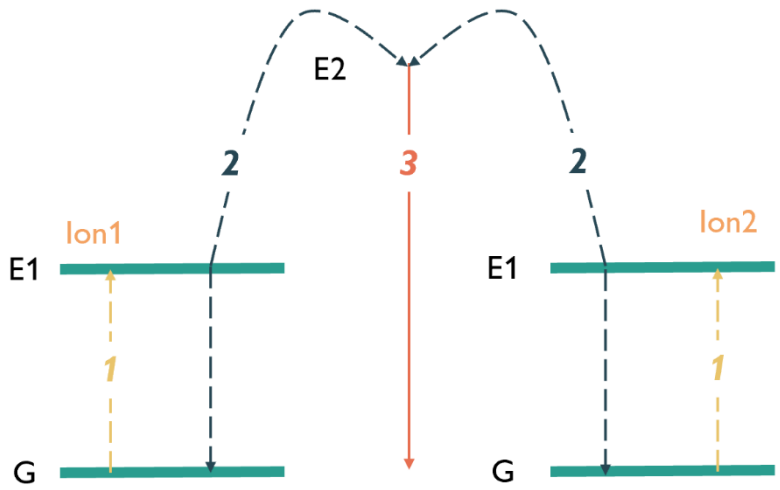

Figure 12: Scheme of energy transfer process during CU upconversion. The yellow lines represent photon excitation, the blue lines represent energy transfer, and the orange lines represent emission processes (adapted from Li et al., (2020))

4.2.2.5- Cross Relaxation (CR)

CR (Figure 13) is a process that results from an ion-ion interaction, being a non-radiative energy transfer process. In this mechanism, ion 1 transfers part of its excited energy to ion 2. Ion 1 and Ion 2 can be either the same or different chemical elements. The efficiency of this process is related to the dopant concentrations. When both ions are the same chemical element, CR will trigger a “concentration quenching mechanism" which significantly dampens the emission intensity (Li et al., 2020; Safdar et al., 2020).

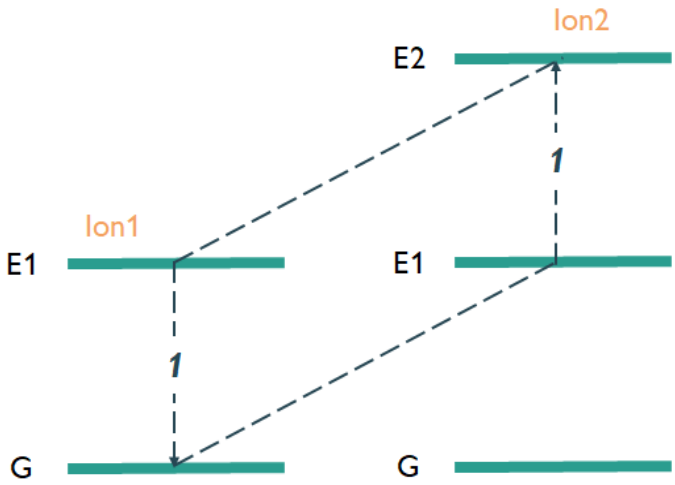

Figure 13: Scheme of energy transfer process during CR upconversion. The blue lines represent energy transfer (adapted from Li et al., (2020))

4.2.2.6- Photon avalanche (PA)

PA (Figure 14) is a process with high complexity and requires an excitation power of a certain threshold to occur. Above this threshold, there is a production of upconversion luminescence but below that threshold, an insignificant luminescence is observed. This process has a strong dependence on cross-relaxation between luminescent centres and the excitation power density. PA is a looping process that involves ESA for light excitation and an efficient CR that produces feedback. Is divided into three main steps. Initially, the level E1 of ion 2 is populated by non-resonant weak ground state absorption. In this repeatable process, an ESA process occurs to elevate ion 2 from the E1 level to the E2 level. After, an efficient CR process occurs between ion 1 and ion 2. In the last step, ion 1 transfers its energy to ion 2 to populate its level E1 and forms a full loop. This process generally requires a pump threshold and a long time to develop, making it easy to distinguish it from ESA and ETU. Since PA is a repeatable process, continuous avalanche transitions may occur, which result in a strong upconversion emission (Chen et al., 2014; Chien et al., 2018; Li et al., 2020; Safdar et al., 2020; Shanmugam et al., 2014; Wang & Liu, 2009).

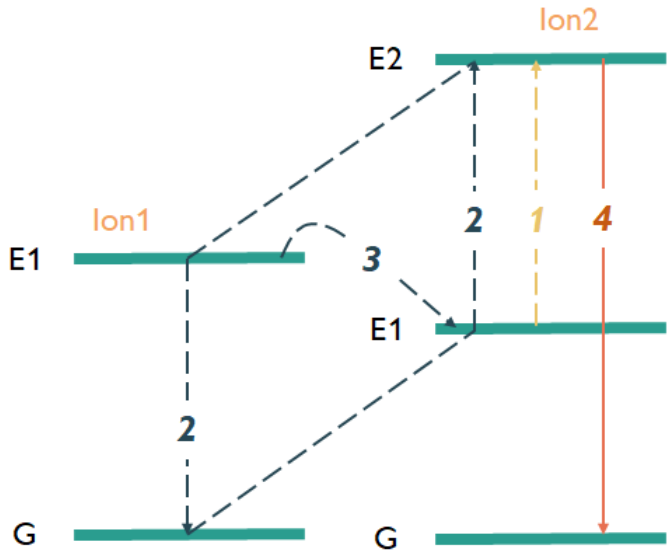

Figure 14: Scheme of energy transfer process during PA upconversion. The yellow lines represent photon excitation, the blue lines represent energy transfer, and the orange lines represent emission processes (adapted from Li et al., (2020))

4.2.2.7- Energy Migration Upconversion (EMU)

In core-shell nanoparticles, the EMU process (Figure 15) involves four types of lanthanide ions: sensitizer, accumulator, migrator, and activator. The sensitizer ion is used to harvest pump photons and then transfer its energy to an accumulator ion, which will pass to a higher state. This one will deliver the energy to a migrator ion. Through random energy hopping migrator ion release energy to the activator ion, which emits an upconverted ion. To avoid deleterious cross-relaxation and decrease of emission intensity the sensitizer/ accumulator and the activator are spatially restricted to different layers of the core-shell structure (Li et al., 2020; Safdar et al., 2020).

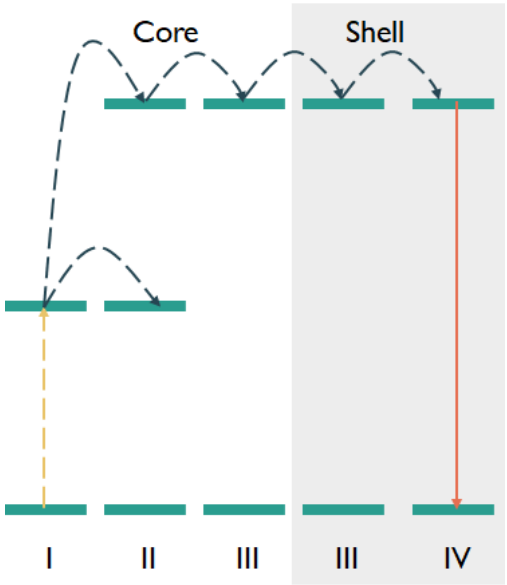

Figure 15: Scheme of energy transfer process during EMU upconversion. The yellow lines represent photon excitation, the blue lines represent energy transfer, and the orange lines represent emission processes (adapted from Li et al., (2020))

4.2.2.8- Energy Cascaded Upconversion (ECU)

The ECU process (Figure 16) is a hybrid inorganic-organic system that is constituted for an epitaxial core/shell upconverting nanocrystal and NIR dyes anchored on the core/shell nanocrystal surface. In this mechanism, NIR dye can harvest NIR light and initialize multistep directional non-radiative energy transfer. First, NIR dye transfers energy to type I lanthanide ions (intermediate sensitizers), incorporated at the shell layer. Then, type I lanthanide ions transfer energy to type II lanthanide ions (sensitizers) in the core domain. Finally, type II lanthanide ions transfer energy to type III lanthanide ions (activators) in the core to produce upconversion via the ETU mechanism. This multistep cascade energy

transfer strategy leads to high efficiency for the transfer of harvested light energy (Abdul Hakeem et al., 2021; Li et al., 2020).

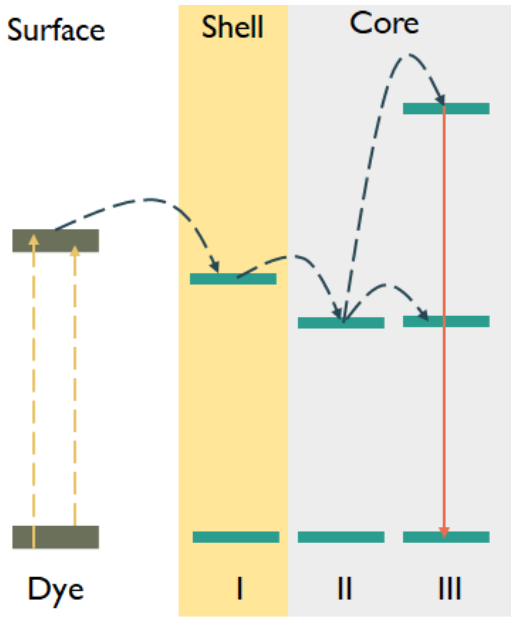

Figure 16: Scheme of energy transfer process during ECU upconversion. The yellow lines represent photon excitation, the blue lines represent energy transfer, and the orange lines represent emission processes (adapted from Li et al., (2020))

4.3 UCNPs FUNCTIONALIZED WITH GOLD (AU)

Despite the numerous advantages, UCNPs can show low brightness compromising their range during *in vivo* applications. The low brightness of UCNPs have two main causes. One is the extremely low quantum efficiency. The other reason is the low absorption cross-section of the lanthanide ions. Although Yb^{3+} ions, commonly used as sensitizers, has a larger absorption cross-section than the other lanthanide ions, it may not be sufficient. There are three ways to solve this problem. One way is through the development of an active shell for upconversion nanocomposites which objective is to increase the upconversion efficiency by doping the sensitizer Yb^{3+} ions in the shell layer. The other possibility is to use a NIR organic dye as an energy absorber to enhance the absorption abilities of UCNPs. The third option is to functionalize UCNPs with noble metals like gold (Au) or silver (Ag) (Feng et al., 2013; Wang, Wang, et al., 2010).

There are several Au-based nanomaterials, such as nanoshells, nanorods, nanostars, nanocages and nanoparticles (Wang et al., 2017).

Gold nanoparticles (AuNPs) have a large surface-to-volume ratio, excellent biocompatibility, and low toxicity. Spherical nanoparticles show a size relative absorption peak from 500 to 550nm (Yeh et al., 2012). Gold nanoparticles can interact with light through

surface plasma resonance. They have applications in a variety of fields such as chemistry, materials science, physics, medicine, and life sciences (Hammami et al., 2021).

Nowadays, noble metals have been quite studied due to their great optical properties, such as strong visible light absorbing and scattering. The energy transfer process most extensively exploited when it comes to metal nanoparticles is the localized surface plasmon resonance (LSPR). It can occur between noble metals, like Au, and phosphors when the free electrons of noble metals collectively oscillate when excited by the incident photons at the resonant frequency (Chen, Li et al., 2016; Sui et al., 2019).

5. BIOMEDICINE APPLICATIONS OF UCNPS

In recent years, the design of multifunctional UCNPs for diverse applications has attracted a lot of interest in various fields, especially in biomedicine (Duan et al., 2018).

Theranostics, the integration of diagnostic and therapy, has been proposed as a promising strategy to fight against various fatal diseases, such as cancer. UCNPs have been explored for potential applications in cancer diagnostics and treatment owing to their excellent properties. Acting as theranostic agents, UCNPs have attractive features like:

- the fact that their excitation wavelength (980nm or 808nm, generally) be located in the "optical transmission window" of biological tissues (700-1000nm), allowing for greater depth of penetration;
- their high photostability that permits UCNPs utilization in monitoring *in vivo* and *in vitro*;
- how they are excited by NIR light, there is no background autofluorescence when UCNPs served as UCL imaging probes because exogenous and endogenous fluorophores in the organisms can't be excited by this light;
- a large surface that can be modified to conjugate with biomolecules, hydrophilic ligands, and various therapeutic agents;
- non-toxic elements in composition conferring an excellent potential for biomedical applications (Cheng et al., 2013; . Wang et al., 2019; Xie et al., 2010).

The advances in some biomedicine applications of UCNPs are described below.

5.1 PHOTOTHERMAL THERAPY

UCNPs can be applied in photothermal therapy (PTT). Conventional cancer treatments, such as chemotherapy and radiotherapy, have a lot of disadvantages, including toxic side effects (like a decrease in immune function, physical weakness, digestive disturbance, inflammatory reaction, and renal toxicity, etc.), a lower specificity at the targeted location, and limited efficacy as a result of drug resistance, thus restricting their wide use in cancer therapy. With the rapid development of physics, electronics, and nanotechnology, near-infrared light (700–1400nm)-triggered photothermal therapy has attracted wide interest for fighting cancer because NIR light falls in the optically biological window of human tissues, i.e., in the spectral region where tissue scattering and absorption are minimized (Chen, Roy et al., 2016; Cheng et al., 2014; Lim et al., 2015).

Photothermal therapy is based on efficient heat generation under illumination with a laser radiation source to induce tissue hyperthermia (above 42ºC) through nanomaterials, resulting in tumour ablation and subsequently cell death with minimal side effects on non-cancer cells (Figure 17). This technique displays great advantages compared to traditional tumour ablation methods and has attracted much attention due to minimal injury, short treatment period, multiple selections of excitation sources, accurate location for tumour sites, deep tissue penetration capacity, reduced side effects, and favourable biosafety to normal tissues. NIR light possesses numerous advantages over ultraviolet or visible light, including the absence of photodamage to living organisms, a low scattering and autofluorescence background, and a high penetration depth and spatial resolution (Abadeer & Murphy, 2016; Wang et al., 2017; Wang, Yang et al., 2020; (Zhang, Xu et al., 2019).

The basic principle of PTT is that the tumour cells and normal cells have a different sensitivity to heat; namely, compared to tumour cells, normal cells are more resistant to high temperatures and typically recover faster than cancer cells when exposed to either heat or the combination of heat and radiation. In addition, normal tissues have more blood flow than cancerous tissue so that they dissipate heat better. Thus, at the same high temperature, tumour cells are more likely to be killed than normal cells (DeNardo & DeNardo, 2008; Wang et al., 2017).

The features of an excellent photothermal agent include (i) high optical absorption coefficients and thermal dissipation rates and strong NIR absorption for efficient photothermal conversion, (ii) right size and well-engineered surface chemistry to allow long blood circulation time and efficient tumour accumulation upon systemic administration, and (iii) good biocompatibility and ideal biodegradability to avoid toxicity related to the agent itself. Currently, numerous nanomaterials with strong NIR absorption and high photothermal conversion efficiency have been employed as photothermal agents for PTT, such as various gold nanostructures, metal chalcogenides nanoparticles, carbon nanomaterials, and organic polymers. For UCNPs based PTT studies, UCNPs are combined with these mentioned photothermal agents to offer imaging-guided PTT, which is regarded as an effective theranostic strategy (Wang et al., 2017; Wang et al., 2019).

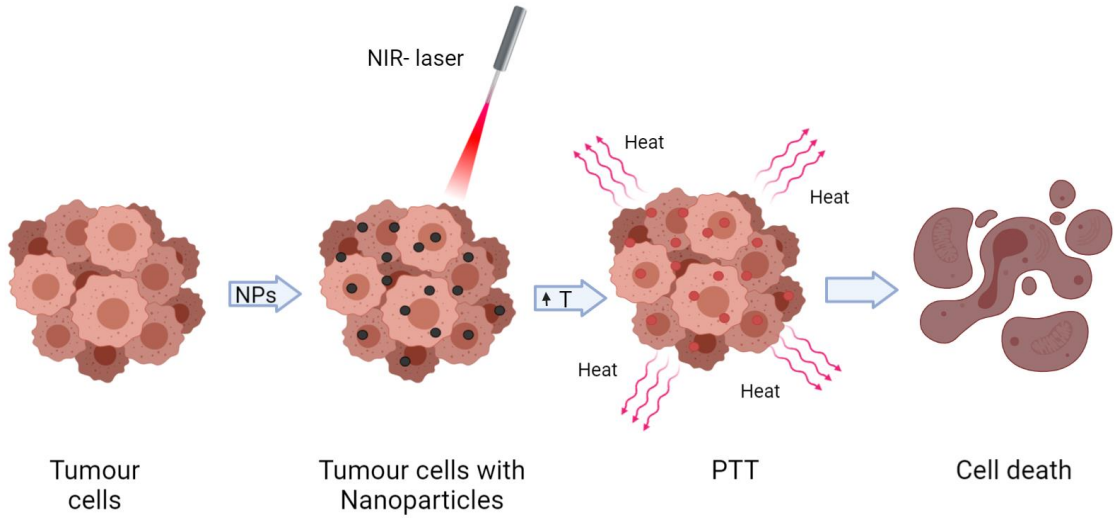

Figure 17: Photothermal Therapy (created on Biorender.com)

5.2 PHOTODYNAMIC THERAPY

Another potential biomedical application of UCNPs is photodynamic therapy (PDT). PDT is a therapy that uses photosensitizers (PS) to generate reactive oxygen species to kill target cells. This therapy is activated by the light. PDT is considered a good strategy in the treatment of certain diseases such as cancer or microbial infections due to its advantages of targeting restricted to the diseased tissues and reduced long-term side effects (Chen, Ågren et al., 2015; Ding et al., 2018; Li et al., 2020; Wang et al., 2011).

The most common photosensitizers are Chlorine6 (Ce6), zinc(II) phthalocyanine (ZnPc), methylene blue (MB), psoralen, or porphyrin derivatives, semiconductor nanomaterials, among others (Chen, Li et al., 2016; Chhetri et al., 2019).

PDT is a therapy minimally invasive, effective, and economic to treat cancer cells. This mechanism involves three steps. The first step consists of the delivery and uptake of photosensitizer by the target cells. The second is the irradiation with appropriate light. And the last step is the generation of reactive oxygen species such as singlet oxygen ($^1O_2$) that damage tumorous cells without a major commitment of the surrounding cells (Dolmans et al., 2003; Lim et al., 2012; Wang et al., 2016; Zhang et al., 2007).

However, this therapy only can be applied in surface diseases or on the lining of internal organs or cavities due to the limited penetration depth in tissues achieved by the light that is used (light in the blue-red region). Besides that, PDT is also limited in the

treatment of large tumours that have metastasized. To fight this problem and obtain deep tissue-penetration treatment, UCNPs serves as optical nanotransformer converting the deep-penetrating NIR light to visible wavelengths that can excite PS and bring on PDT (Chhetri et al., 2019; Li et al., 2020).

Various strategies such as mesoporous silica coatings or polymer coatings have been used to incorporate PS molecules onto the surface of coated UCNPs (Qian et al., 2009; Yang et al., 2014).

PDT can be combined with other therapies like PTT, chemotherapy, immunotherapy, radiotherapy, or gene therapy (Chhetri et al., 2019; Tian et al., 2015; Wang, Thang et al., 2020).

5.3 Antibacterial photodynamic therapy (aPDT)

Nowadays, there are many infectious diseases related to bacterial biofilms. These biofilms are responsible for protecting bacteria from the effect of antibiotics, helping them in resistance to antibiotics. To carry out biofilm removal and sterilization treatment at the same time were created antimicrobial PDT platforms by attaching appropriate photosensitizers on the surface of functionalized UCNPs. NIR-triggered UCNPs aPDT showed a good therapeutic effect against gram-positive and gram-negative bacteria related to a variety of infectious diseases and showed good promise for multidrug-resistant bacteria (Liang et al., 2020; Wang, Thang et al., 2020).

5.4 Drug Delivery

In the last years, there are emerged alternatives more safe and efficient for cancer treatments. Drug delivery systems, in particular nanoparticles used as drug carriers, appear such an alternative to conventional cancer treatments due to their advantages: high loading capacity, specific target drug delivery, and consequently, low side effects to healthy cells (Lee & Park, 2018).

For a drug delivery carrier to be considered effective it must have good biocompatibility, good stability of *in vivo* circulation, and the capacity to deliver the drug effectively. One of the different types of used nanoparticles in drug delivery is UCNPs. Their optical properties make them more efficient nanocarrier materials in drug delivery systems. Besides that, small size facilitates the endocytosis of cells, and these UCNP-based systems

used for drug delivery allow track and efficient evaluation of drug release in real-time. In fact, UCNPs can be used as luminescent indicators to help locate the position of the nanocomposites and thus to realize where is the drug. The simplest system is constituted by silica-coated UCNPs, in which drugs are load. This loading process can be done into the nanocavity by simple physical adsorption or by hydrophobic-hydrophobic interactions inside the porous silica layer. They can still be used as indicators to monitor the release of drugs in the delivery system based on the energy transfer process (Chen et al., 2018; Dukhno et al., 2018; Feng et al., 2013; Ge et al., 2018; Lee & Park, 2018; Liang et al., 2020).

UCNPs can be functionalized with targeting moieties, such as TAT peptide, folic acid, or RGD peptide which intends to direct UCNPs to the exact local of the drug release (Li et al., 2020).

There are several methods for drug release, namely light, pH, heat, diffusion, osmolarity, magnetic field, among others (Hossen et al., 2019; Zhang et al., 2016).

Photoinduced drug delivery systems use photoreactions such as photocleavage and photoisomerization to control drug release:

* Drug delivery using photocleavage

This is an appealing method to trigger drug release. It can occur through three methods: the direct cleavage of the bond between the molecule and the carrier, a change in the charge on the carrier surface used to induce electrostatic repulsion between the molecules and the carrier, and the destruction of the carrier itself (Lee & Park, 2018).

* Drug delivery using photoisomerization

Photoisomerization is a reaction that leads to a spatial conformation change of isomers under optical irradiation. This reaction can be used as a switch to control the drug release. One of the most used molecules in this process is azobenzene, which is used a lot with UCNPs (Lee & Park, 2018).

5.5 BIOIMAGING

Bioimaging is a technology that has attracted a lot of attention in the medical field. The most used bioimaging techniques are computed tomography (CT), magnetic resonance imaging (MRI), positron emission tomography (PET), fluorescence imaging, and single-photon emission computed tomography (SPECT) (Chen, Li et al., 2016; Feng et al., 2013).

Traditional bioimaging probes are usually composed of organic fluorophores or fluorescent proteins that have the disadvantage of having poor light stability and producing strong background fluorescence in the visible light region. A way to solve this problem is to

use lanthanide-based UCNPs due to all the advantages that they possess, like stable chemical properties, deep penetration, no background fluorescence, no auto-fluorescence, high signal-to-noise ratio, long luminescence lifetime, non-blinking, large anti-Stokes shifts low cytotoxicity, low photobleaching, among others (Liang et al., 2020; Wu & Butt, 2016).

Upconversion nanomaterials have been the subject of major developments to produce upconversion probes for functional bioimaging. Until now, these probes have been successfully designed for cell tracking and for *in vivo* monitoring of the lymph nodes, tumours, and specific analytes. Multimodality bioimaging probes have also been widely used (Feng et al., 2013).

Most commonly used UCNPs use Yb^{3+} as a sensitizer which requires a laser excitation of 980nm. At this wavelength, water molecules also tend to absorb radiation. As biological samples have water in their constitution, they tend to absorb the energy causing attenuation of the excitation signal and possible overheating of biological specimens that can cause tissue damage and cell death (Safdar et al., 2020; Wang, Liu et al., 2013).

A strategy used to overcome this limitation is to adjust the excitation wavelength to an interesting range of values in order of 800nm. A wavelength on this region not only improves the penetration depth but also reduces the tissue-overheating problem since this wavelength has a minimal absorbance for all biomolecules. The incorporation of Nd^{3+} as a sensitizer instead of Yb^{3+} is a good solution because Nd^{3+} has a shorter wavelength excitation band cantered 808nm rather than 980nm (Chen, Li et al., 2016; Safdar et al., 2020).

* UCNPs for lymph bioimaging

The lymphatic system is very important in the tumour metastasis process. However, is difficult to study because there are few imaging techniques with adequate sensitivity. UCNPs are ideal fluorescence probes used for *in vivo* lymph imaging because the probes injected can easily reach the sentinel lymph nodes through lymphatic vessels and exhibit intense UCL signals (Cao et al., 2011; Kobayashi et al., 2009).

* UCNPs for tumour-targeted imaging

Due to the optical properties of UCNPs, they are largely used in actively targeted imaging of tumours. Tumour targeting is one of the most attractive functional imaging applications because of the importance of tumour detection. To target UCNPs to the tumour, they are usually functionalized with folic acid, peptides, or antibodies. In this way, they

connect more easily to the desired location and emit light that will allow the tumour to be located (Feng et al., 2013; Liang et al., 2020).

* Multimodality imaging

Another type of upconversion nanomaterial attracting great attention for *in vivo* bioimaging is the multimodality probe. Single modal imaging techniques like MRI, CT, PET, and optical imaging are not sufficient in many cases for the conclusive diagnosis of metastatic or circulating cancer cells in biological tissues. Multimodal bioimaging based on UCNPs, which combines UCL imaging with other imaging technologies, like MRI or CT permits capture of complementary and high-throughput diagnostic information, thus facilitating the diagnostic process (Chen, Li et al., 2016; Chhetri et al., 2019; Feng et al., 2013; Li et al., 2020).

II - OBJECTIVES

For biological applications, the biocompatibility of materials is always of paramount concern. Thus, the first part of the practical work focused on determining the biocompatibility of various nanomaterials in melanoma cells, namely, MNT-1 pigmented human melanoma cells and A375 amelanotic human melanoma cells. The second part seeks to explore two of the existing bioapplications - photothermal therapy and drug delivery.

This work can be divided into specific aims:

- Analysis of the physicochemical properties of nanoparticles;
- Verify the biocompatibility of the nanoparticles in different melanoma cell lines;
- Optimization of laser irradiation conditions for photothermal therapy;
- Study of loading and pH mediated releasing of doxorubicin.

III – MATERIALS AND METHODS

1. Upconversion nanoparticles and chemicals

$NaYF_4$:Lu,Yb,Er(47%,18%,2%)@SiO_2 (UCNPs@SiO_2) coated with a silica shell were provided by Professor Xiaogang Liu group from Singapore (Liu Lab-National University of Singapore). Subsequently, these upconversion nanoparticles were loaded with spheric gold nanoparticles (14nm) by Dra. Ana Luísa Daniel group at the department of Chemistry of University of Aveiro - **$NaYF_4$:Lu,Yb,Er(47%,18%,2%)@SiO_2-Au** (UCNPs@SiO_2-Au).

$NaYF_4$:Yb,Er(20%,2%)@mSiO_2-PO_4 (UCNPs@mSiO_2-PO_4) and **$NaYF_4$:Yb,Er (20%,2%)@mSiO_2-COOH** (UCNPs@mSiO_2-COOH) which are respectively phosphonated and carboxylated functionalized UCNPs, were provided by Dr Ute Resch-Genger group from BAM, Berlin.

2. Cell lines and reagents

The MNT-1 cell line was provided by Doctor Manuela Gaspar (iMed.ULisboa, Portugal) and A375 cell line was purchased from the European Collection of Authenticated Cell Cultures (ECACC) and supplied by Sigma-Aldrich (Spain). Dulbecco's Modified Eagle's Medium (DMEM), Fetal Bovine Serum (FBS) and fungizone were purchased from Gibco, Life Technologies (Grand Island, NY, USA). L-glutamine, penicillin-streptomycin and phosphate buffered saline (PBS) were from Grisp (Porto, Portugal). Trypsin-EDTA (0.25% trypsin and 1 mM EDTA), dimethyl sulfoxide (DMSO; ≥99.7%), 3-(4,5 dimethyl-2-thiazolyl)-2,5-diphenyl tetrazolium bromide (MTT; 98%), neutral red (3-amino-7-dimethylamino-2-methyl-phenazine hydrochloride) and glacial acetic acid were purchased from Merck (St. Louis, MO, USA). Doxorubicin hydrochloride (≥98%; DOX HCl) was purchased from Cayman Chemical (USA).

3. Physicochemical characterization of nanoparticles

The morphology and size were assessed by scanning transmission electron microscopy (STEM) using a 200 kV Hitachi HD-2700 (Hitachi High-Technologies Europe GmbH, Germany) STEM microscope equipped with energy-dispersive X-ray spectroscopy and secondary electron detectors.

Hydrodynamic diameter (Dh) and polydispersity index (PdI) of the UCNPs were measured by dynamic light scattering (DLS), and zeta potential was evaluated by electrophoretic mobility. Both experiments were carried out on Malvern ZetaSizer Nano ZS (Malvern Instruments), which uses multi-scatter laser diffraction to determine the nanoparticle size and their agglomeration. Particle size, PdI and zeta potential were measured in DMEM medium at concentrations of 25µg/ml and 100µg/ml and three replicates for each concentration were done. For particle size and PdI determination, the samples were placed into standard cuvettes and illuminated by a He-Ne laser at λ=633nm. For zeta potential determination, the samples were placed in clear zeta cells, and their temperature was equilibrated at 25ºC before sample reading. UCNPs@SiO_2 were dispersed 5min in an ultrasonic bath and 5 seconds in the vortex while UCNPs@SiO_2-Au were disperse 10-15 seconds in an ultrasonic bath and 5 seconds in the vortex to avoid AuNPs release. The dispersion conditions were the same for the following assays with cell lines.

4. Cell culture

In this work, two cell lines were used for our experiments: A375 amelanotic human melanoma cells (Figure 18) and MNT-1 pigmented human melanoma cells (Figure 19). Cells were maintained in 25cm^2 cell culture flasks and cultured in Dulbecco's modified Eagle's medium supplemented with 10% (v/v) Fetal Bovine Serum (FBS), 2mM L-glutamine, 100U/ml penicillin, 100µg/ml streptomycin and 2.5µg/ml fungizone. Cells were incubated in a humidified atmosphere at 37ºC and 5% CO_2.

Cells were daily observed using an inverted phase-contrast Eclipse TS100 microscope (Nikon, Tokyo, Japan) to monitor the morphology and growth. The confluence and the presence of microbiological contamination were also checked. When cells were approximately at 80% confluence, they needed to be sub-cultivated. For that, the old medium was removed and then PBS was added to wash the cells. PBS also removes any residual FBS which is responsible for inactivating Trypsin. To dissociate cells, breaking cell-to-cell and cell-to-substrate attachment, Trypsin-EDTA was added and then the flask was incubated at 37ºC for about 4min. Subsequently, to inactivate Trypsin, a volume of culture medium of at least double the volume of trypsin was added.

The next step was to count the cells using a hemocytometer or Neubauer chamber. Knowing the density that we want to seed, through the formula $civi = cfvf$, we obtain the

initial volume that we must remove from the cell suspension and place it in the new flask or plate with the right proportion of medium.

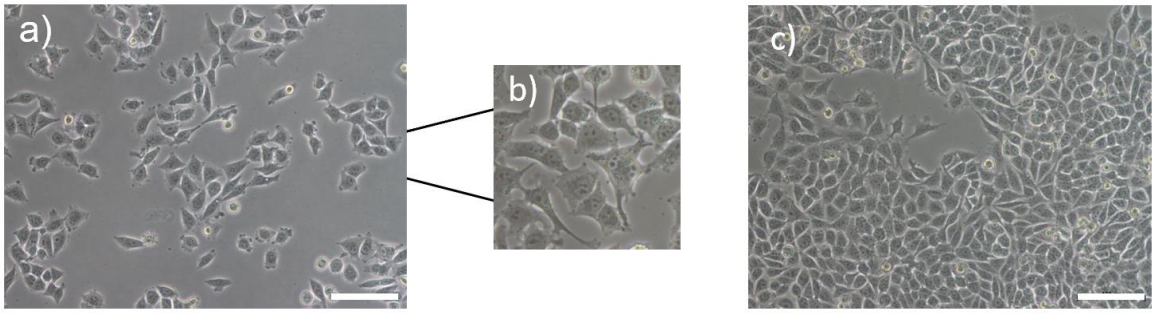

Figure 18: Light microscopy images of A375 cells with different confluence: a) 100x magnification at ~40% confluence; b) 200x magnification; c) 100x magnification at ~80% confluence. Bar corresponds to 100µm.

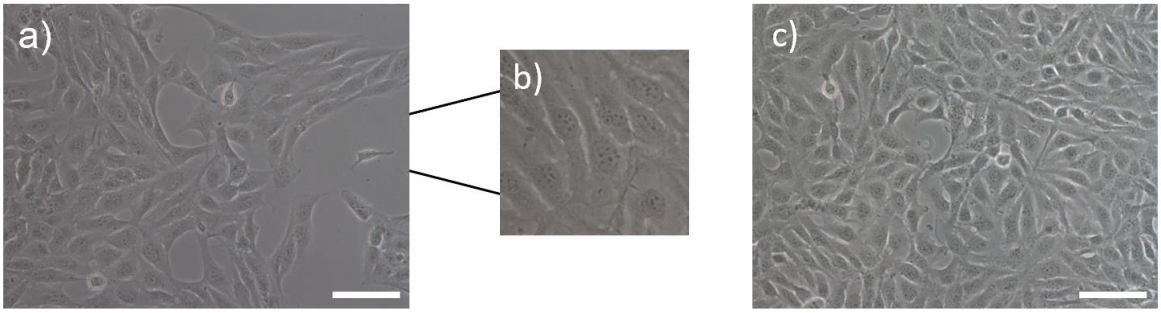

Figure 19: Light microscopy images of MNT-1 cells with different confluence: a) 100x magnification at ~60% confluence; b) 200x magnification; c) 100x magnification at ~95% confluence. Bar corresponds to 100µm.

5. Cell Viability

The viability of MNT-1 and A375 cell lines exposed to UCNPs was tested by MTT assay. In this colorimetric assay, viable cells can convert a soluble tetrazolium yellow salt (MTT) into an insoluble purple formazan precipitate, by the action of mitochondrial reductase (Kumar et al., 2018). MNT-1 cells were seeded in 96-well plates at a concentration of 35000 cells/ml and 25000 cells/ml for 24h and 48h of exposure, respectively, while A375 cells were seeded at a concentration of 35000 cells/ml and 20000 cells/ml for 24h and 48h, respectively. After seeding, the plates were incubated for 24h at 37ºC in a 5% CO_2 humidified atmosphere for cell adhesion to the plate. Then, culture medium was replaced with 100µl of fresh culture medium containing sequentially diluted UCNPs (UCNPs@SiO_2 or UCNPs@SiO_2-Au or UCNPs@mSiO_2-PO_4 or UCNPs@mSiO_2-COOH (these last two just for MNT-1 cells)) at the following concentrations: 12.5; 25; 50;

100 and 200µg/ml. Cells exposed to the medium were used as a negative control, and cell viability was measured after 24h and 48h.

After the incubation time, the medium was removed and 100µl of fresh medium was replaced in each well. Then, 50µl of MTT (previously dissolved in PBS at the concentration of 1mg/ml) was added to each well and incubated for 4h at the previously described conditions. After that time, the culture medium with MTT was removed and replaced by 150µl of DMSO for formazan crystal solubilization. The plates were left to shake for 2h. The next step was the measure of the absorbance of the samples with a microplate reader (Synergy HT Multi-Mode, BioTek, Winooski, VT) at 570nm (Figure 20).

Cell viability was also determined by Neutral Red Uptake Assay, but only for MNT-1 cell line and UCNPs@SiO_2 nanoparticles. In this assay, viable cells can incorporate and bind, in the lysosomes, the dye neutral red (Repetto et al., 2008). Different concentrations of Neutral Red Medium were tested, namely, 40µg/ml and 75µg/ml. Neutral Red Medium was prepared the day before the assay from the Neutral Red Stock Solution 4mg/ml. To prepare that Stock Solution 40mg of neutral red dye were dissolved in 10ml PBS. To prepare Neutral Red Medium, Neutral Red Stock was dissolved in culture medium at a proportion of 1:100 and incubated overnight at the same temperature as the cells.

MNT-1 cells were seeded in 96-well plates at a concentration of 35000 cells/ml and 25000 cells/ml for 24h and 48h of exposure, respectively. Then, the plates were incubated at the same conditions described above.

In the next step, culture medium was replaced with 100µl of fresh culture medium containing sequentially diluted UCNPs at different concentrations 12.5; 25; 50; 100 and 200µg/ml. Cells exposed to the medium were used as a negative control, and cell viability was measured after 24h and 48h.

After the incubation time, the medium was removed, and 100µl of Neutral Red Medium (previously centrifuged for ~10min at 600g to remove any precipitated dye crystals) was replaced in each well and incubated for 2h at 37ºC in a 5% CO_2 humidified atmosphere. After that time, the plates were inspected with an inverted microscope to check the possible precipitation of neutral red, and then the Neutral Red medium was removed. The next step was the wash the cells with 150µl of PBS. After removing PBS, 150µl of Neutral Red Destain Solution was added to extract the dye. Neutral Red Destain Solution was prepared with 50% ethanol 96%, 49% deionized water, 1% glacial acetic. The plates were left to shake for 10min. The absorbance of the samples were measured with a microplate reader (Synergy HT Multi-Mode, BioTek, Winooski, VT) at 540nm (Figure 21).

The ratio of cell metabolic activity (MA, a usual marker for cell viability) for both assays was calculated as: MA = [(Sample Abs –DMSO Abs) / (Control Abs – DMSO Abs)]*100.

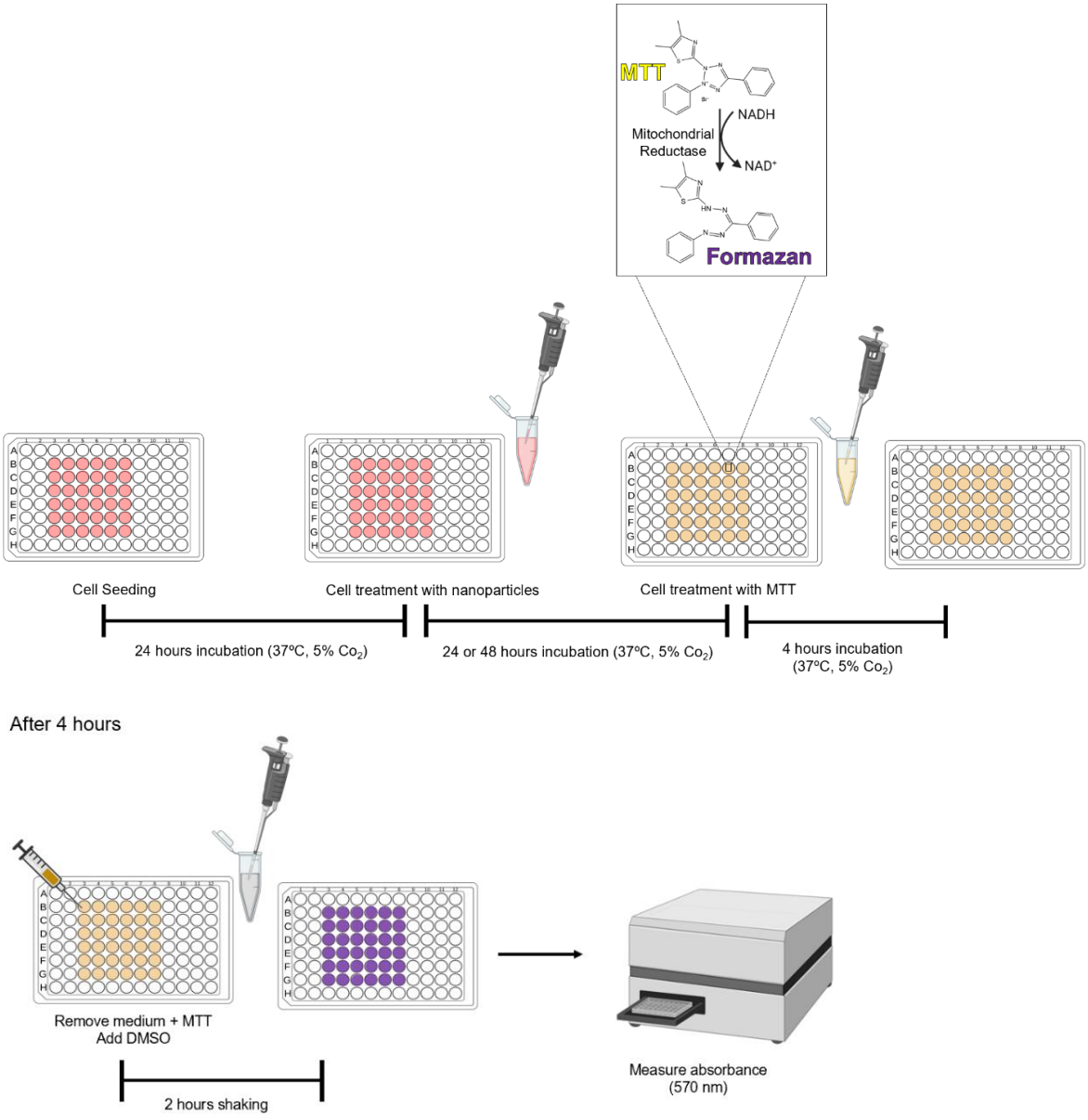

Figure 20: MTT assay protocol

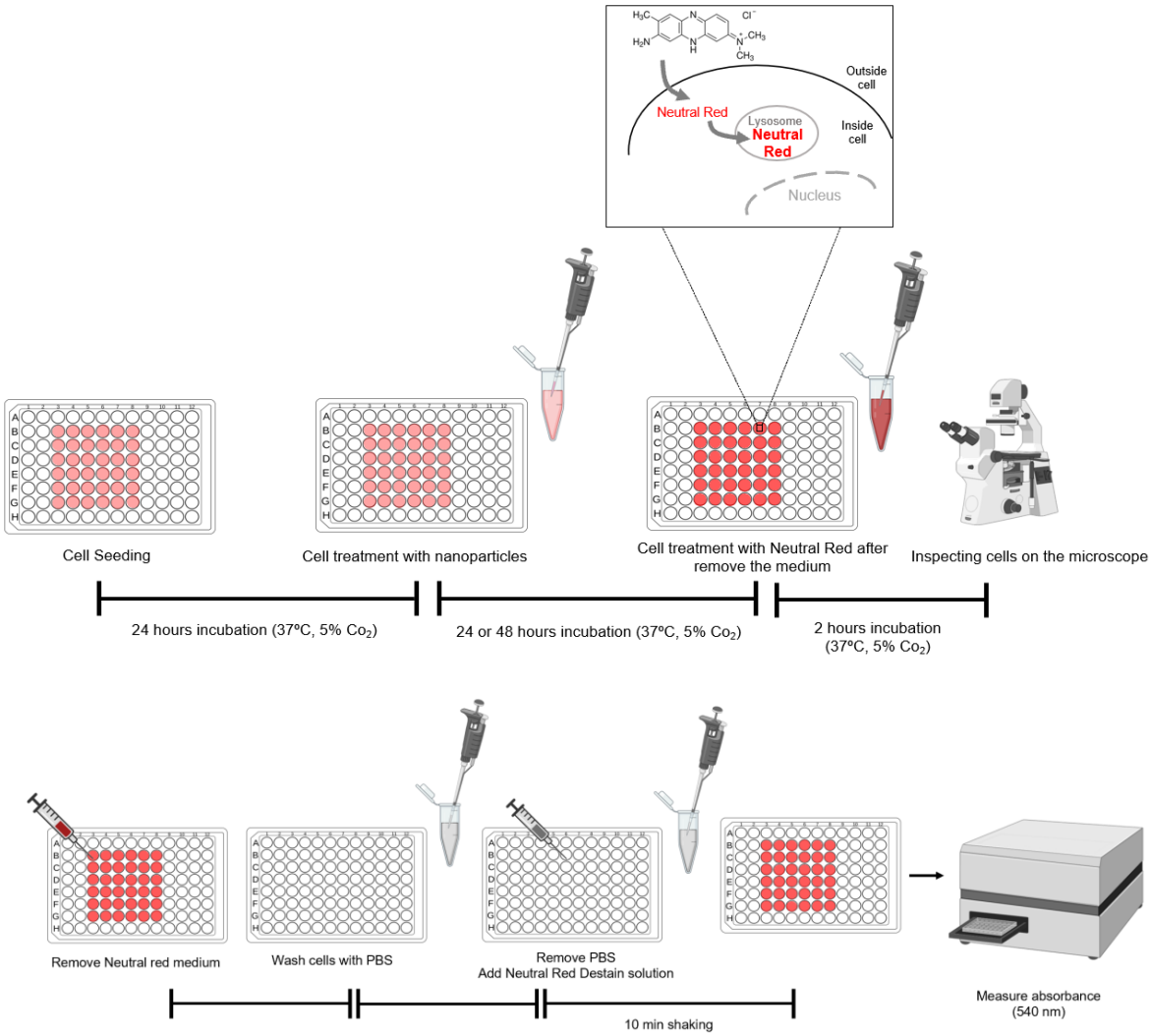

Figure 21: Neutral Red Uptake assay protocol

6. Laser Optimization Tests for hyperthermia

Tests were carried out to determine the optimal irradiation conditions of UCNPs@SiO_2 or UCNPs@SiO_2-Au for the application of photothermal therapy. A continuous-wavelength (CW) 980nm NIR laser wavelength was used. The samples were subjected to 15min of NIR irradiation and various power densities were tested, namely, 0.3W/cm^2; 0.7W/cm^2; 1W/cm^2; 1.5W/cm^2; 3W/cm^2; 3.5W/cm^2, and 4W/cm^2. Two irradiation schemes were used, one with irradiation in 96-well plates (Figure 22), and the other using a cuvette containing the samples to be irradiated (Figure 23). The samples were tested at concentrations of 25µg/ml and 100µg/ml diluted in DMEM with phenol red, in DMEM without

phenol red, or in distilled water. For control, the dilution medium without nanoparticles was used.

The temperature was measured using a thermocouple (Picolog). Initial and final temperatures were recorded to know the temperature difference reached after laser irradiation. In some tests, partial temperatures were also recorded.

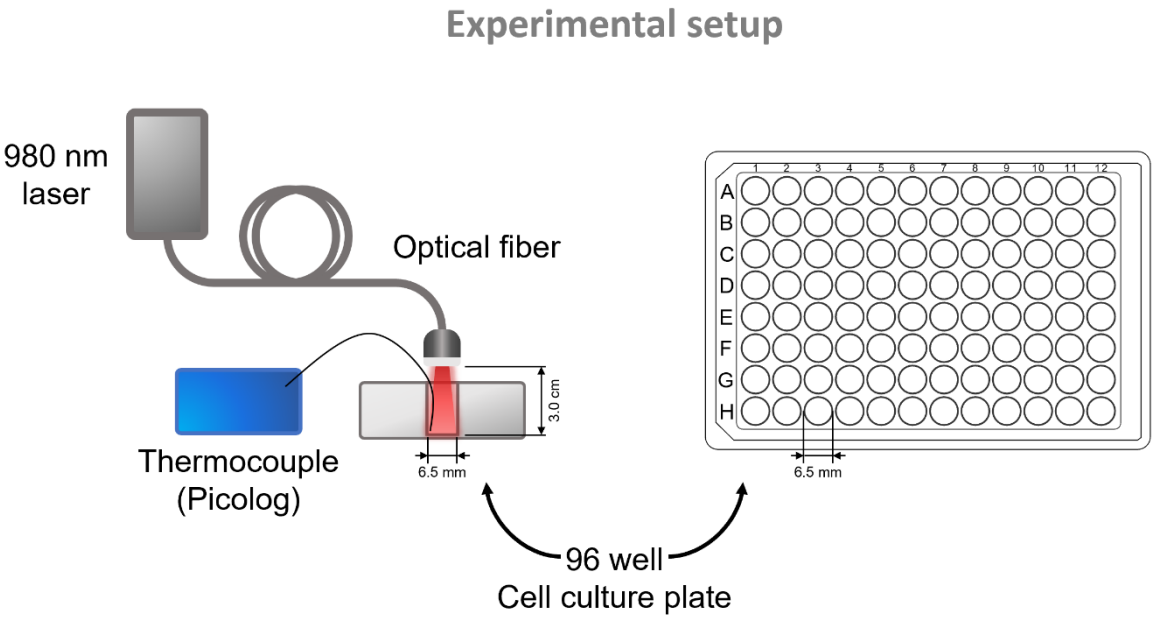

Figure 22: Irradiation scheme using irradiation in 96-well plates

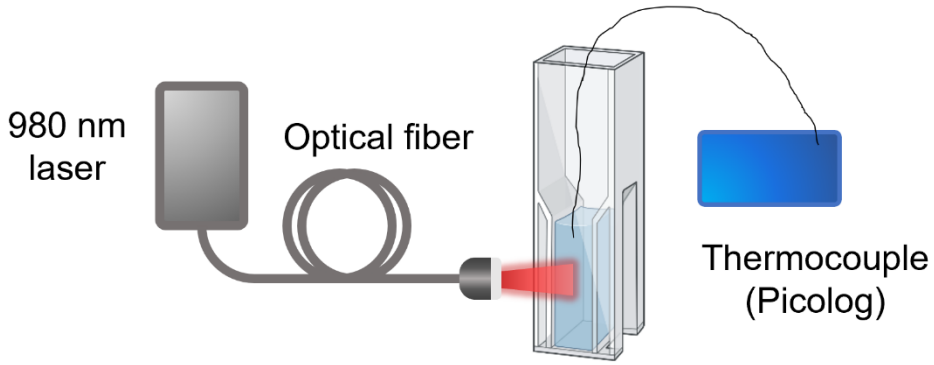

Figure 23: Irradiation scheme using a cuvette containing the samples

7. Doxorubicin Loading and Release Studies

The first step for loading doxorubicin into the UCNPs@mSiO$_2$-PO$_4$ and UCNPs@mSiO$_2$-COOH nanoparticles was to prepare a solution of doxorubicin hydrochloride in a concentration of 209.56µg DOX/ml (measured UV-Vis) in sodium phosphate buffer (pH 6). Then, nanoparticles were accurately weighed and incubated in 2ml of the solution (1.25mg NPs/ml). The mixtures were vertically stirred (Heidolph Reax 2, Heidolph Instruments, Schwabach, Germany30 rpm) for 24h at room temperature in the dark. To separate the nanoparticles, they were centrifuged at 7000 rpm for 5 minutes. The solution's remaining doxorubicin content ([DOX]final) was determined by UV-Vis spectrophotometry at 480nm. The loading efficiency and the nanoparticle capacity were calculated using equations 1 and 2, respectively (Unsoy et al., 2014).

$$Loading\ Efficiency\ (\%) = \frac{[DOX]_{initial} - [DOX]_{final}}{[DOX]_{initial}} \times 100 \qquad (1)$$

$$Nanoparticle\ Capacity\ (m_{DOX}/m_{NP}) = \frac{m_{loaded\ doxorubicin}}{m_{nanoparticles}} \qquad (2)$$

To obtain the doxorubicin release profiles, the loaded nanoparticles (2.5mg NP) were transferred to 10ml of sodium phosphate buffer with a pH value of 5.2 and 7.4. The solution was vertically stirred (Heidolph Reax 2, Heidolph Instruments, Schwabach, Germany30 rpm) at 37°C for 48h in the dark. At predetermined time intervals, an aliquot (1ml) of the solution was taken and replaced by an equal volume of fresh buffer. The

nanoparticles were centrifuged before taking the supernatant sample. The sample was then analysed using UV-Vis spectrophotometry (480nm) to assess DOX concentration.

8. Statistical analysis

For MTT and Neutral red uptake assays, at least 2 independent assays with three replicates each were performed. All data were expressed as mean ± standard deviation (SD). All statistical analyses were performed in SigmaPlot version 14.0 for software (Systat Software Inc.). Data were analysed by one-way ANOVA, followed by Dunnet's and Dunn's method (as a parametric and non-parametric test, respectively).

IV – RESULTS

1. Physicochemical characterization of Nanoparticles

Figure 24 shows transmission electron microscopy (TEM) images of the UCNPs@SiO_2 and UCNPs@SiO_2-Au nanoparticles. The TEM image showed the individualized $NaYF_4$ structure with spherical and cubic morphologies, being each core well encapsulated with a silica shell. The UCNPs@SiO_2 had a core size of 78nm and a shell size of 10nm (Figure 24a). Figure 24b shows the UCNPs@SiO_2 functionalized with spheric gold nanoparticles with a size of 14nm.

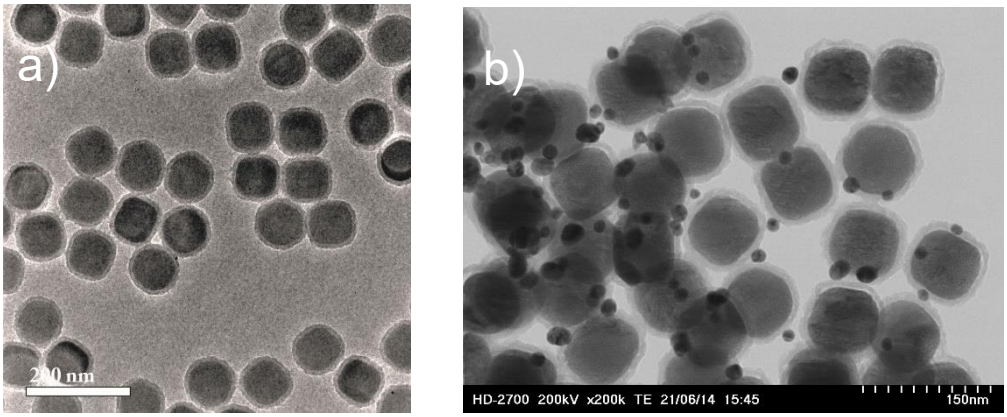

Figure 24: TEM images of a) UCNPs@SiO_2 and b) UCNPs@SiO_2-Au

Table 3 shows the results of hydrodynamic diameter (Dh), polydispersity index (PdI), and zeta potential (ζ). The UCNPs@SiO_2 were dispersed 5min in an ultrasonic bath and few seconds in the vortex, while UCNPs@SiO_2-Au were dispersed 10-15 seconds in an ultrasonic bath and few seconds in the vortex.

Table 2: Hydrodynamic diameter Dh (with respective polydispersity index PdI) and zeta potential of UCNPs@SiO_2 and UCNPs@SiO_2-Au dispersed in DMEM culture medium (25µg/ml and 100µg/ml). Data are presented as average ± standard deviations calculated from 3 replicate measurements.

Nanoparticles	Concentration	D_h (nm)	PdI	ζ (mV)
UCNPs@SiO_2	25µg/ml	72.27 ± 2.77	0.61 ± 0.04	-7.77 ± 0.59
	100µg/ml	113.77 ± 3.43	0.24 ± 0.01	-7.84 ± 0.68
UCNPs@SiO_2-Au	25µg/ml	168.83 ± 73.02	0.76 ± 0.22	-8.96 ± 1.13
	100µg/ml	345.10 ± 75.93	0.84 ± 0.17	-10.93 ± 0.76

The average hydrodynamic diameter for UCNPs@SiO_2 was 72.27 ± 2.77nm for 25µg/ml and 113.77 ± 3.43nm for 100µg/ml. For the UCNPs@SiO_2-Au, the average hydrodynamic diameter was much larger, being approximately 168.83 ± 73.02nm for 25µg/ml and 345.10 ± 75.93nm for 100µg/ml (Figure 25).

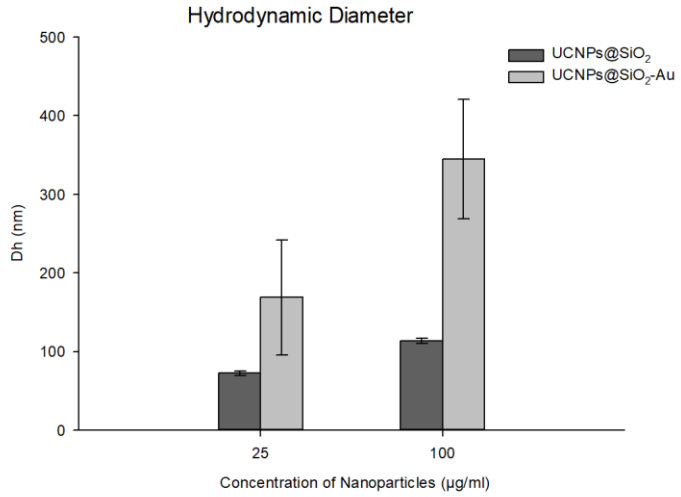

Figure 25: Hydrodynamic diameter of UCNPs@SiO_2 and UCNPs@SiO_2-Au in DMEM . Results are shown as average ± standard deviation (SD).

The PdI obtained for 25µg/ml was 0.61 ± 0.04 and in the highest concentration decreased to 0.24 ± 0.01, for UCNPs@SiO_2. For UCNPs@SiO_2-Au the PdI obtained for 25µg/ml was 0.76 ± 0.22 and for 100µg/ml was 0.84 ± 0.17 (Figure 26).

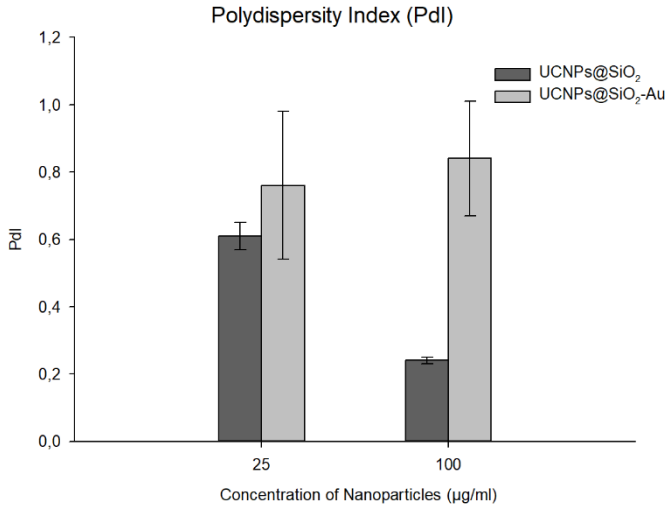

Figure 26: Polidispersity Index of UCNPs@SiO_2 and UCNPs@SiO_2-Au in DMEM. Results are shown as average ± standard deviation (SD).

Although there were differences between the two nanoparticles (especially for the highest concentration), all PdI values were below 1. However, suspensions of Au-functionalized nanoparticles tended to approximate a polydisperse distribution.

In relation to the zeta potential, the values were very close. For UCNPs@SiO_2, the difference in zeta potential for the two concentrations was minimal. For 25µg/ml suspension, the zeta potential value was -7.77 ± 0.59mV and for 100µg/ml it was -7.84 ± 0.68mV. For UCNPs@SiO_2-Au these values were slightly lower (-8.96 ± 1.13mV for 25µg/ml and -10.93 ± 0.76mV for 100µg/ml) but the difference was not very significant (Figure 27).

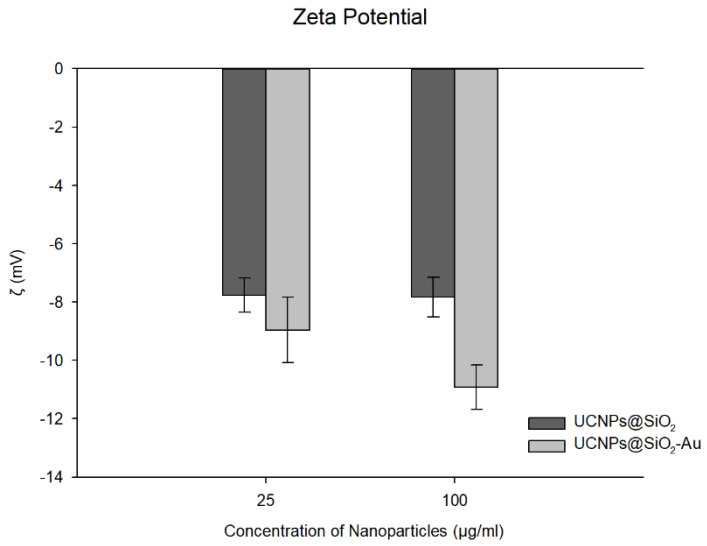

Figure 27: Zeta potential of UCNPs@SiO_2 and UCNPs@SiO_2-Au in DMEM. Results are shown as average ± standard deviation (SD).

2. Cell Viability

2.1 Viability of melanoma cells after incubation with UCNPs@SiO_2 -MTT assay

MTT assay was performed to measure cell viability on melanoma cells after 24h and 48h of exposure to nanoparticles. The results are expressed as the percentage of viable cells after treatment.

For 24h assay, the viability of MNT-1 did not decreased significantly. No statistical differences were observed, showing that these nanoparticles do not affect the MNT-1 cell viability when they were exposed for 24h. After 48h exposure, a significant decrease in cell viability was noted with the increase of the nanoparticles concentration. Relative to controls,

the viability of exposed cells was significantly reduced ($p<0.05$) upon exposure to UCNPs@SiO_2 at 100µg/ml and 200µg/ml (Figure 28).

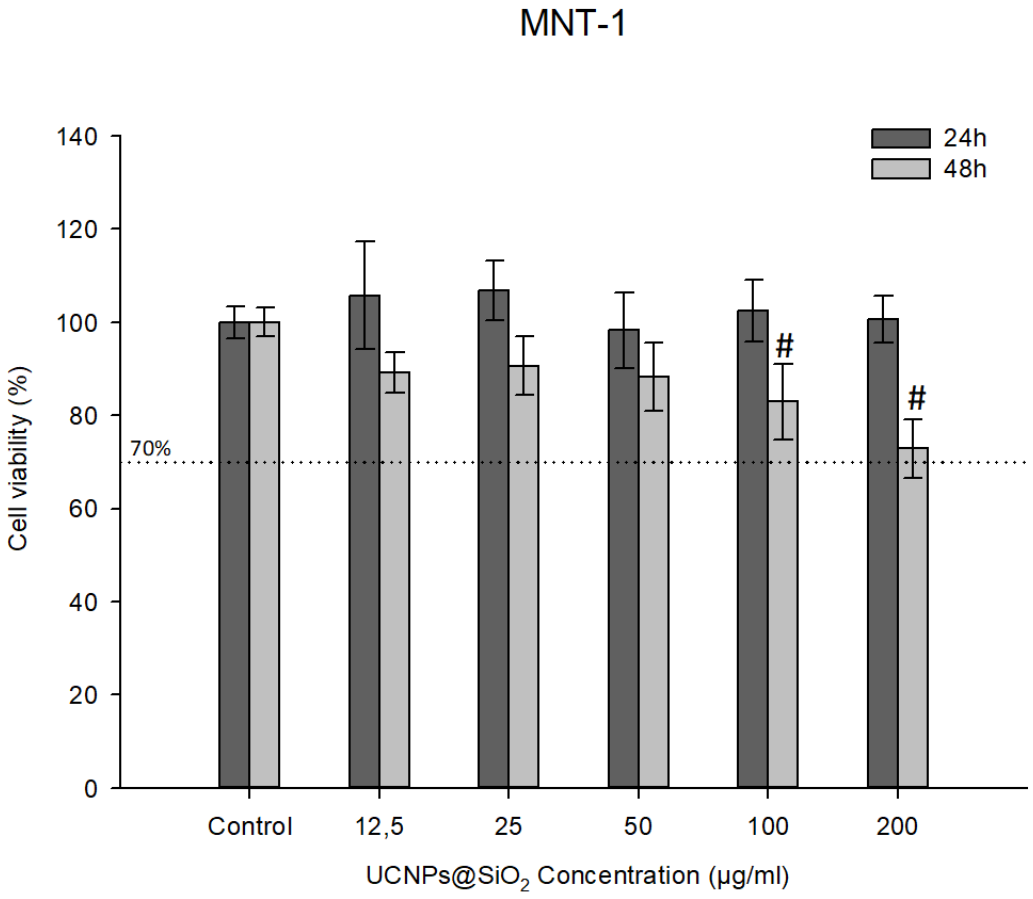

*Figure 28: Effect of UCNPs@SiO_2 on the viability of MNT-1 cells at 24h and 48h of exposure – MTT assay. Results are shown as average ± standard deviation (SD). * (24h) or # (48h) indicates a significant statistical difference in relation to control condition ($p<0.05$)*

The investigated concentrations led to A375 cell viability decrease in a dose-dependent manner being significant at contrations of 50µg/ml, 100µg/ml, and 200µg/ml. It was also verified a significant decrease in viability over time ($p<0.05$). After 24h exposure, an increase in the concentrations of nanoparticles from control to 50µg/ml, 100µg/ml, and 200µg/ml promoted a significant decrease in cell viability. For 48h exposure, a similar response was found (Figure 29).

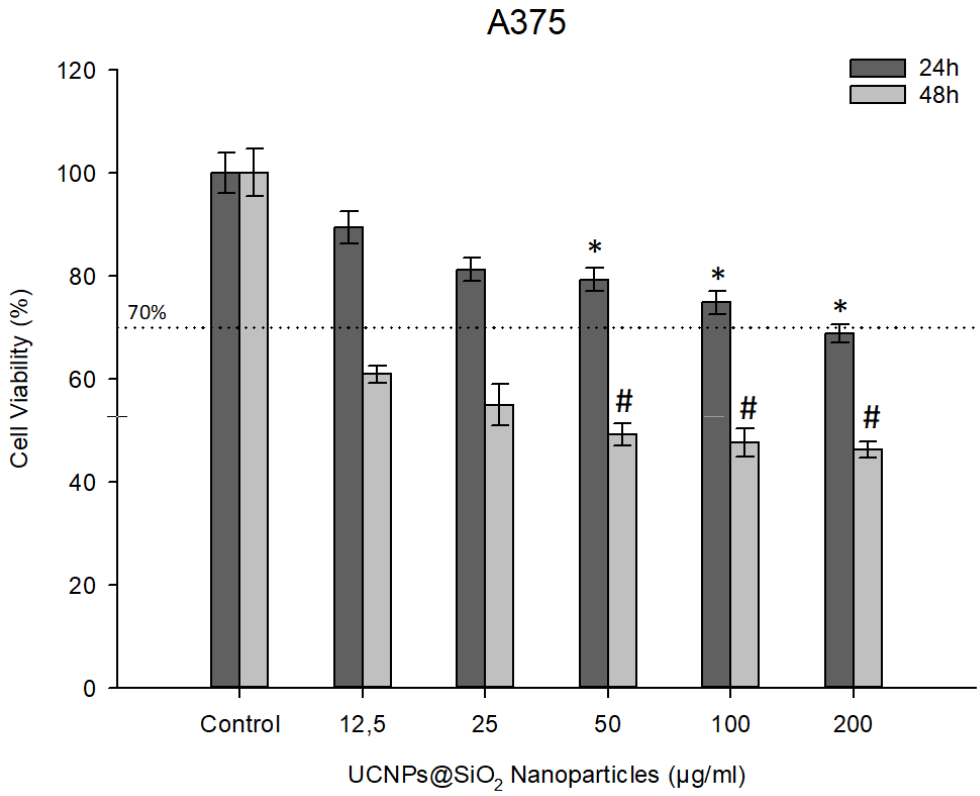

*Figure 29: Effect of UCNPs@SiO_2 on the viability of A375 cells at 24h and 48h of exposure – MTT assay. Results are shown as average ± standard deviation (SD). * (24h) or # (48h) indicates a significant statistical difference in relation to the control condition (p<0.05).*

2.2 Viability of MNT-1 cells after incubation with UCNPs@SiO_2 – Neutral Red Uptake Assay

Neutral Red Uptake assay was performed to measure cell viability on MNT-1 cells after 24h and 48h of exposure to nanoparticles. This assay was performed to verify the results obtained through the MTT assay and it was only performed for the MNT-1 cell line and UCNPs@SiO_2. The results are expressed by the percentage of viable cells after treatment.

As with the MTT assay, there was also no significant decrease in viability for the 24h exposure for almost all concentrations. However, at the highest concentration, the viability of MNT-1 decreased significantly ($p<0.05$). At 48h of exposure, the neutral red uptake assay is in agreement with the MTT assay for the two highest concentrations but, at the concentrations of 12.5µg/ml and 50µg/ml, the viability of exposed cells was also significantly reduced ($p<0.05$) in relation with controls (Figure 30).

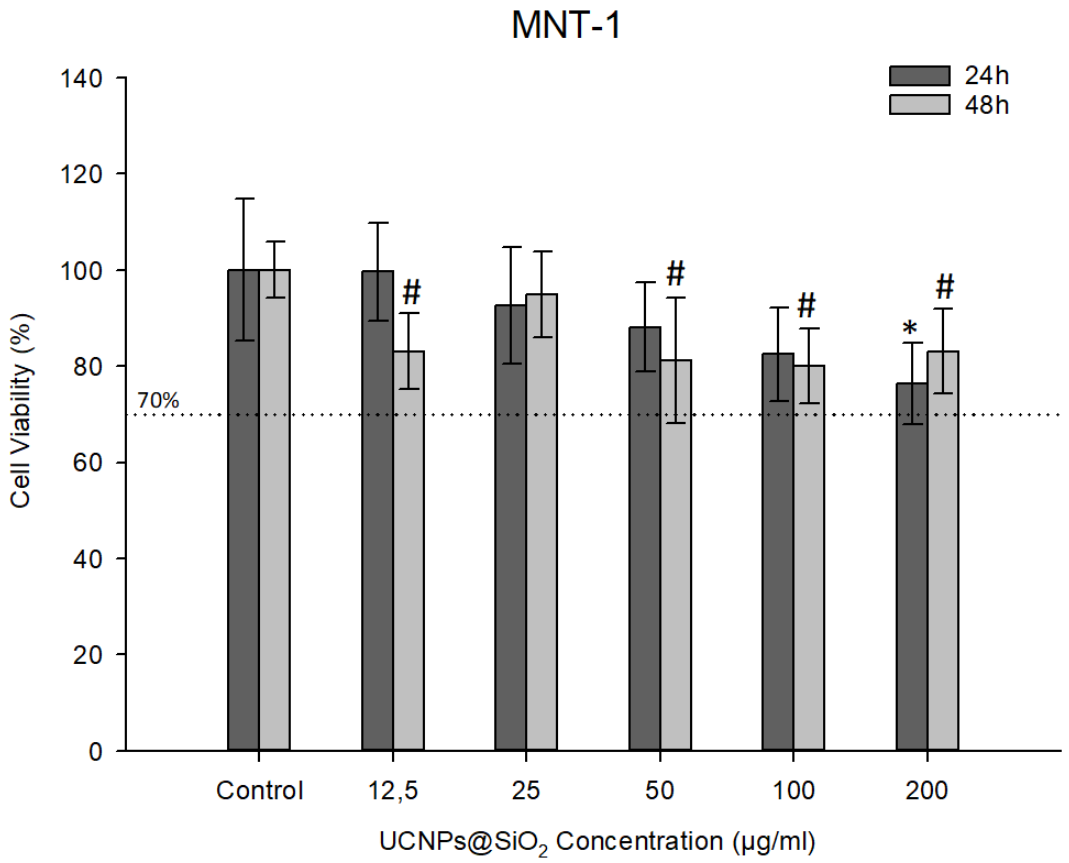

*Figure 30: Effect of UCNPs@SiO_2 on the viability of MNT-1 cells at 24h and 48h of exposure – Neutral Red Uptake assay. Results are shown as average ± standard deviation (SD). * (24h) or # (48h) indicates a significant statistical difference in relation to the control condition ($p<0.05$).*

2.3 Viability of melanoma cells after incubation with UCNPs@SiO_2-Au

MTT assay was performed to measure cell viability on melanoma cells after 24h and 48h of exposure to nanoparticles. The results are expressed as the percentage of viable cells after treatment.

For 24h assay, the viability of MNT-1 did not decreased significantly, except for the highest concentration, in spite of a viability decrease trend with UCNPs@SiO_2-Au concentration. At concentrations of 12.5µg/ml, 25µg/ml, 50µg/ml, and 100µg/ml, a decrease in cell viability was found, becoming significant compared to the control only with the concentration of 200µg/ml. After 48h exposure, a significant decrease in cell viability was noted with increasing nanoparticles concentration. Relative to controls, the viability of exposed cells was significantly reduced ($p<0.05$) upon exposure to UCNPs@SiO_2-Au at 50µg/ml, 100µg/ml, and 200µg/ml. A significant reduction in cell viability was also observed at a concentration of 12.5µg/ml (Figure 31).

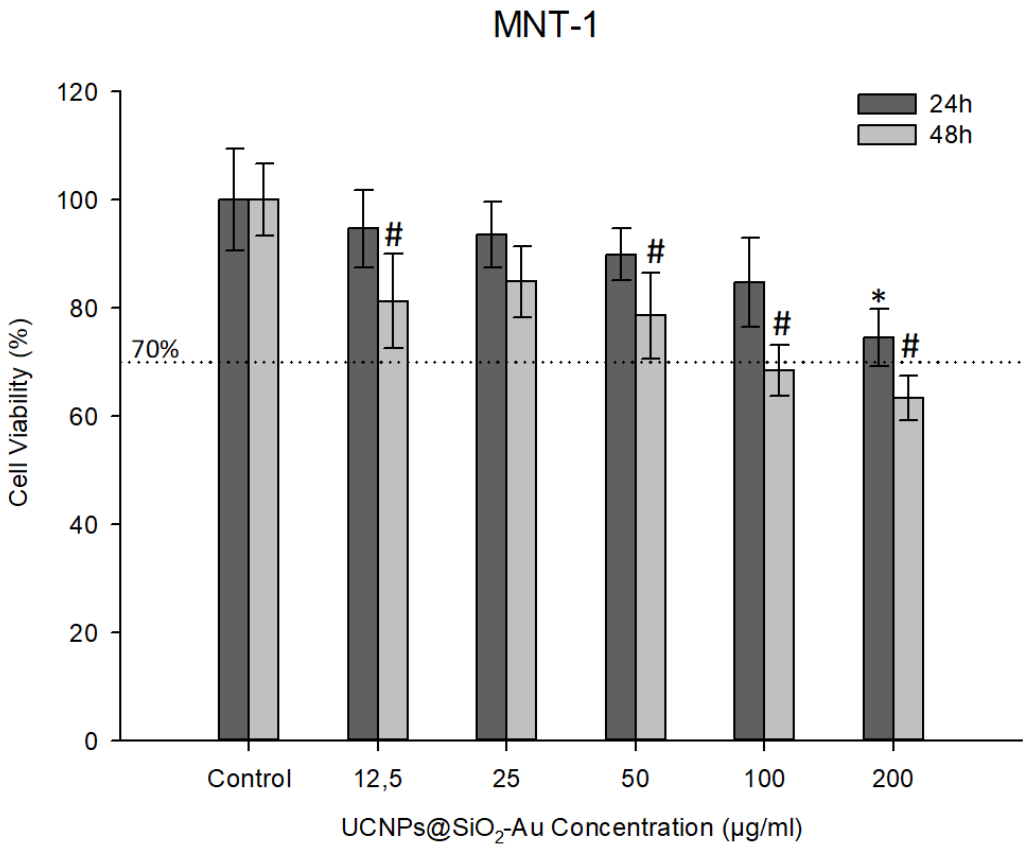

*Figure 31: Effect of UCNPs@SiO_2-Au on the viability of MNT-1 cells at 24h and 48h of exposure – MTT assay. Results are shown as average ± standard deviation (SD). * (24h) or # (48h) indicates a significant statistical difference in relation to the control condition ($p<0.05$).*

The viability of A375 cells was negatively affected by UCNPs@SiO_2-Au. Upon exposure to nanoparticles at concentrations higher than 25µg/ml (including this value), cell viability was significantly reduced after 24h and 48h. Cell viability is less than 70% at a concentration of 25µg/ml and above for both exposure times. For example, for 100µg/ml the viability was 45.80% and 26.95% for 24h and 48h, respectively (Figure 32).

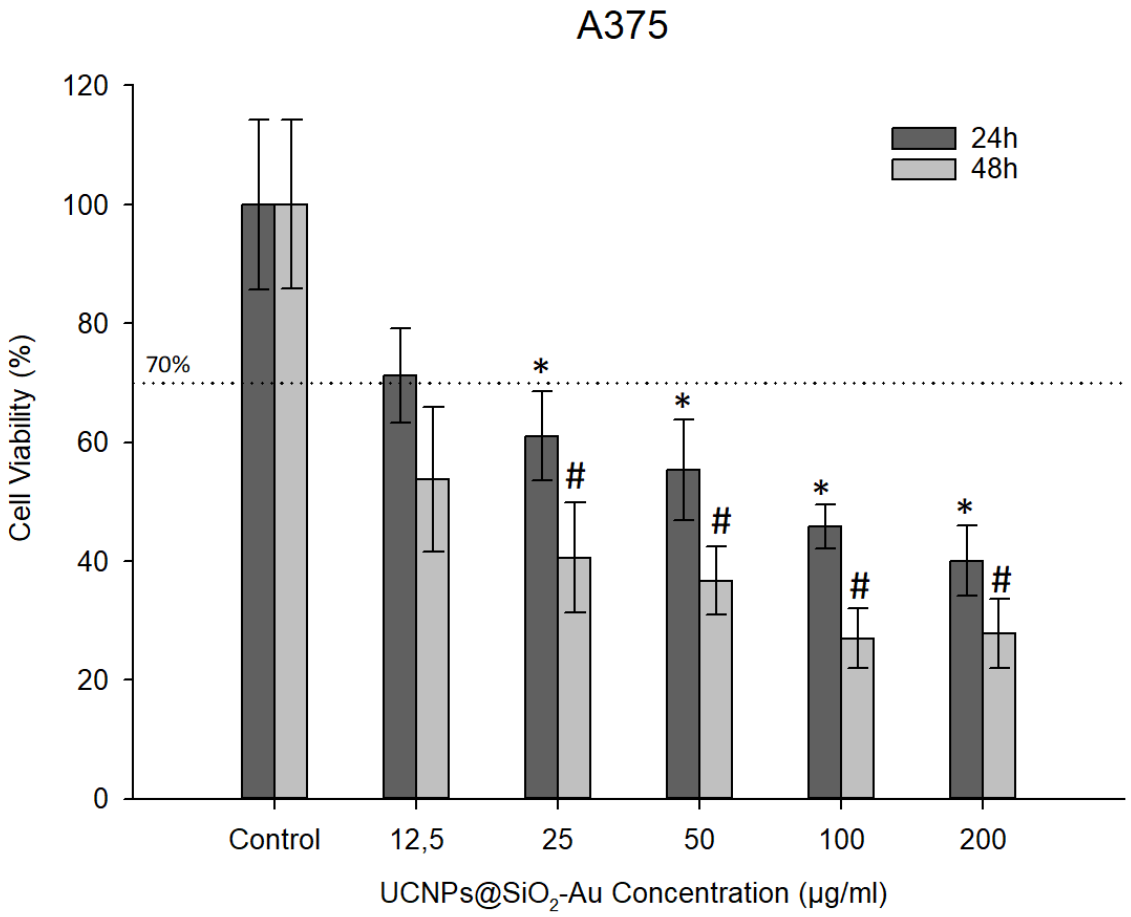

*Figure 32: Effect of UCNPs@SiO_2-Au on the viability of A375 cells at 24h and 48h of exposure – MTT assay. Results are shown as average ± standard deviation (SD). * (24h) or # (48h) indicates a significant statistical difference in relation to the control condition ($p<0.05$).*

2.4 Comparison of exposure to UCNPs@SiO_2 and UCNPs@SiO_2-Au in the two cell lines

A375 cells proved to be more sensitive to both nanoparticles than MNT-1 cells. Differences were observed between cell lines at all exposure concentrations ($p<0.05$). For 48h of exposure, the differences are quite significant, especially for the highest concentrations. (Figure 33).

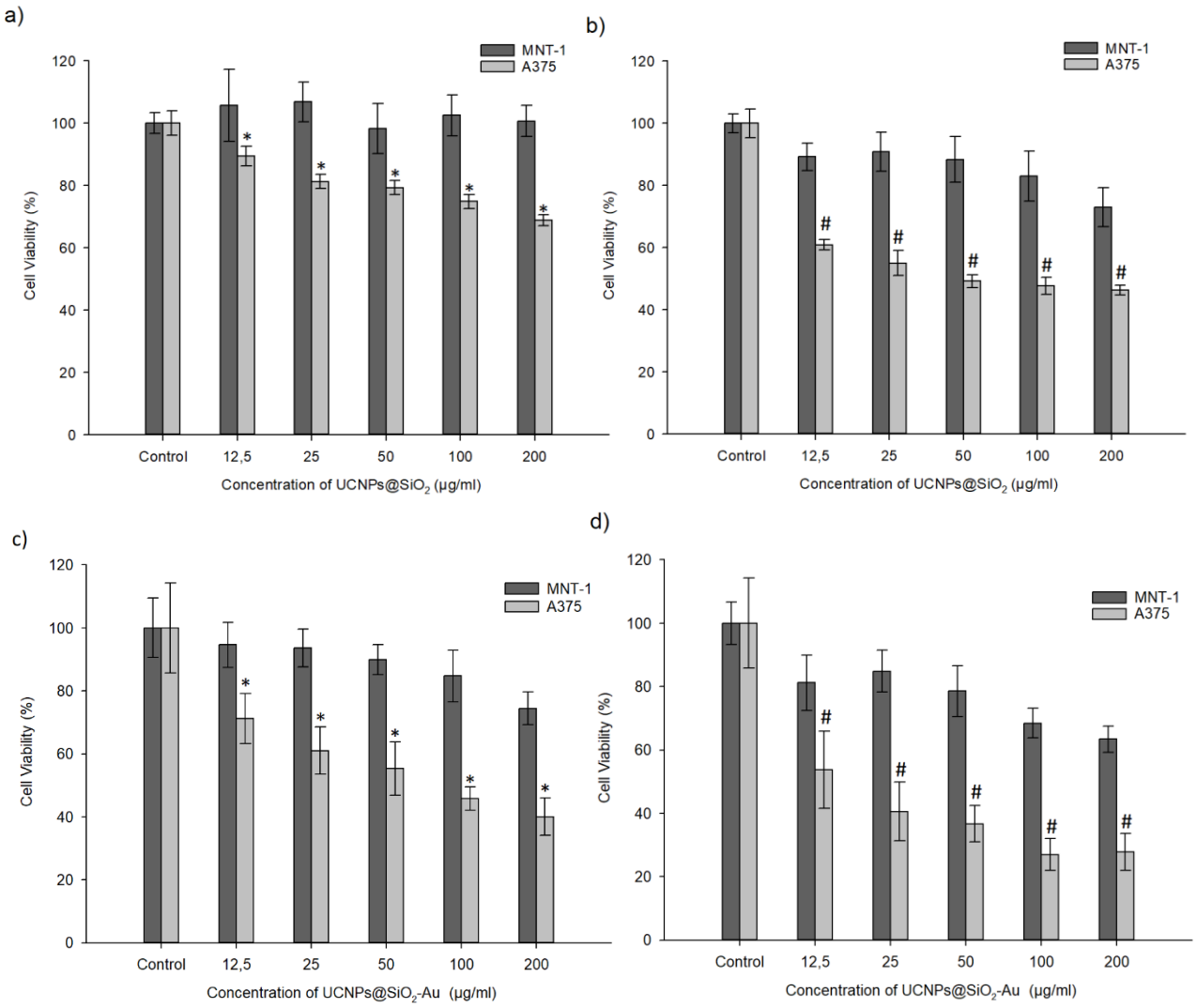

*Figure 33: Effect of UCNPs@SiO_2 on the viability of MNT-1 cells and A375 cells at a) 24h and b) 48h of exposure and effect of UCNPs@SiO_2-Au on the viability of MNT-1 cells and A375 cells at c) 24h and d) 48h of exposure – MTT assay. Results are shown as average ± standard deviation (SD). * (24h) or # (48h) indicates a significant statistical difference in relation to the control condition ($p<0.05$).*

2.5 Viability of MNT-1 cells after incubation with UCNPs@mSiO$_2$-PO$_4$ and UCNPs@mSiO$_2$-COOH

MTT assay was performed to measure cell viability on melanoma cells after 24h and 48h of exposure to nanoparticles. The results are expressed as the percentage of viable cells after treatment. After 24h exposure, an increase in the concentrations of UCNPs@mSiO$_2$-PO$_4$ caused a statistically significant decrease ($p<0.05$) in cell viability for all conditions. After 48h exposure, a significant decrease in cell viability was noted with

increasing nanoparticles concentration. Relative to controls, the viability of exposed cells was significantly reduced ($p<0.05$) upon exposure to UCNPs@mSiO$_2$-PO$_4$ at 25µg/ml, 50µg/ml, 100µg/ml, and 200µg/ml (Figure 34).

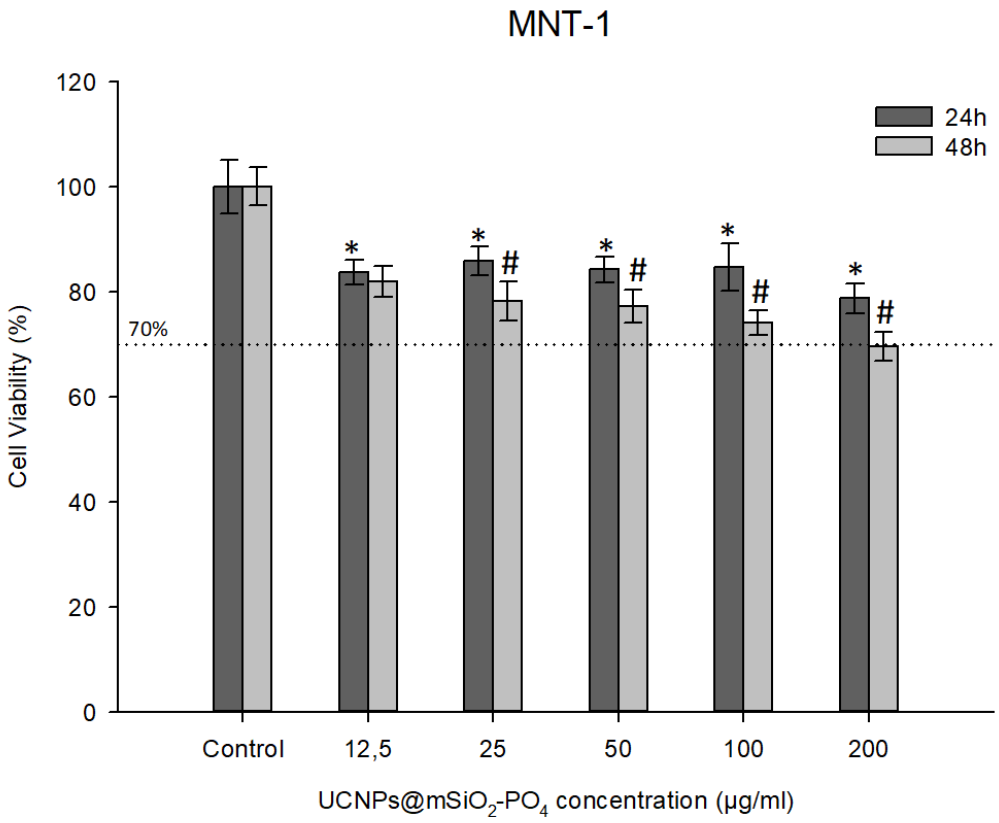

*Figure 34: Effect of UCNPs@mSiO$_2$-PO$_4$ on the viability of MNT-1 cells at 24h and 48h of exposure – MTT assay. Results are shown as average ± standard deviation (SD). * (24h) or # (48h) indicates a significant statistical difference in relation to the control condition ($p<0.05$).*

For 24h assay, the viability of MNT-1 did not decreased significantly. No statistical differences were observed, showing that these nanoparticles do not affect the MNT-1 cell's viability when they are exposed for 24h. After 48h exposure, a significant decrease in cell viability was noted with increasing nanoparticle's concentration. Relative to controls, the viability of exposed cells was significantly reduced ($p<0.05$) upon exposure to UCNPs@mSiO$_2$-COOH for all the concentrations (Figure 35).

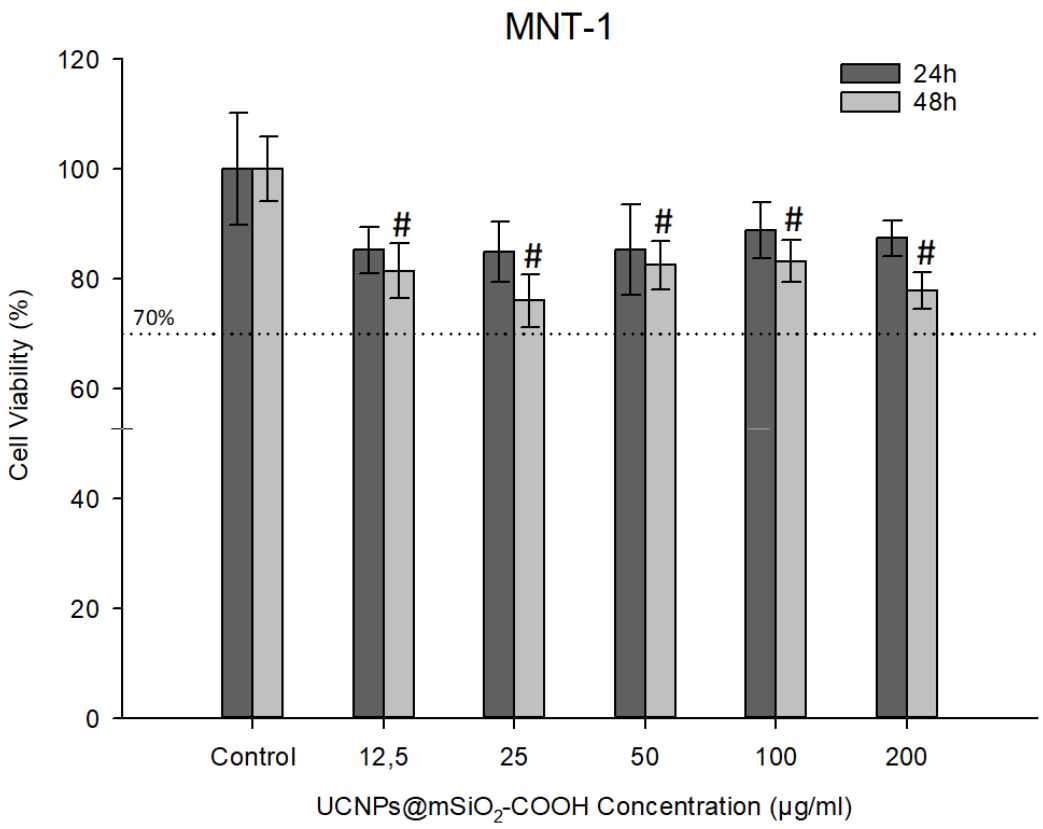

*Figure 35: Effect of UCNPs@mSiO$_2$-COOH on the viability of MNT-1 cells at 24h and 48h of exposure – MTT assay. Results are shown as average ± standard deviation (SD). * (24h) or # (48h) indicates a significant statistical difference in relation to the control condition (p<0.05).*

2.6 Comparison of exposure to UCNPs@mSiO$_2$-PO$_4$ and UCNPs@mSiO$_2$-COOH

Through the graphics, we are able to see that there were no statistically significant differences (p<0.05) for the 24h of exposure between both nanoparticles, showing that these nanoparticles did not affected the cell viability. For 48h, there was only one difference between them in the highest concentration tested (figure 36).

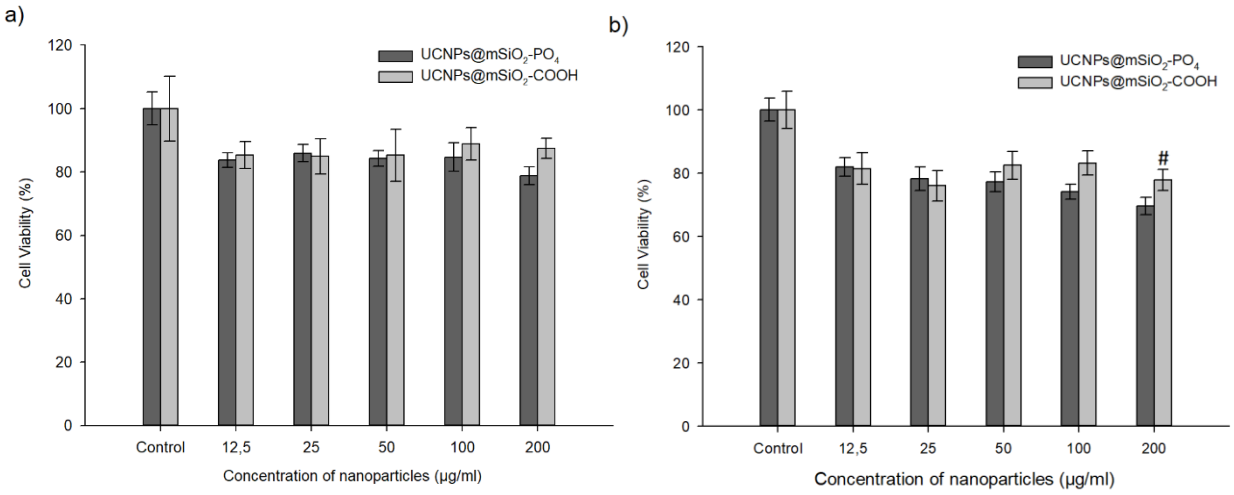

*Figure 36: Comparison of exposure to UCNPs@mSiO₂-PO₄ and UCNPs@mSiO₂-COOH on the viability of MNT-1 cells at a) 24h and b) 48h of exposure – MTT assay. Results are shown as average ± standard deviation (SD). * (24h) or # (48h) indicates a significant statistical difference in relation to the control condition (p<0.05).*

3. Laser Optimization Tests for hyperthermia

This assay was carried out to determine the ideal conditions of laser irradiation for photothermal therapy application. To investigate the photothermal properties of UCNPs@SiO_2 and UCNPs@SiO_2-Au, the temperature of the nanoparticle's colloidal solutions was measured as a function of the laser irradiation time when irradiated with a certain power density (which was variable between the various assays). During the measurement, a thermocouple connected to a TC-08 thermocouple data logger (Pico Technology) was immersed in the colloidal solution, recording the temperature throughout the entire irradiation time. All solutions were irradiated for 15min regardless of the type of nanoparticles, their concentration, or the medium used to dilute them. The results obtained are shown in the following tables.

Table 3: Temperature variation as a function of irradiation power density at 980nm. Results for distilled water and DMEM culture medium with phenol red. Results are shown as average ± standard deviation (SD), if applicable.

Conditions	Test type	Increase (ºC)
Power Density = 0.3W/cm^2 **Current** = 0.68A	Thermocouple without DMEM	0.40
	DMEM	1.59
	DMEM + 25µg/ml UCNPs@SiO_2	1.62
	DMEM + 100µg/ml UCNPs@SiO_2	1.67
	DMEM + 25µg/ml UCNPs@SiO_2-Au	2.15
	DMEM + 100µg/ml UCNPs@SiO_2-Au	1.66
Power Density = 0.7W/cm^2 **Current** = 0.89A	Thermocouple without DMEM	1.99
	DMEM	7.64 ± 0.12
	DMEM + 25µg/ml UCNPs@SiO_2	7.05 ± 0.14
	DMEM + 100µg/ml UCNPs@SiO_2	6.70
	DMEM + 25µg/ml UCNPs@SiO_2-Au	6.48
	DMEM + 100µg/ml UCNPs@SiO_2-Au	6.14
Power Density = 1W/cm^2 **Current** = 1.05A	Thermocouple without DMEM	2.54
	DMEM	6.33
	DMEM + 25µg/ml UCNPs@SiO_2	7.26
	DMEM + 100µg/ml UCNPs@SiO_2	6.95
	DMEM + 25µg/ml UCNPs@SiO_2-Au	9.89
	DMEM + 100µg/ml UCNPs@SiO_2-Au	7.89 ± 0.22
Power Density = 1.5W/cm^2 **Current** = 1.32A	DMEM	11.19
	DMEM + 100µg/ml UCNPs@SiO_2	8.47 ± 0.31
Power Density = 3W/cm^2 **Current** = 2.12A	DMEM	25.16 ± 7.25
	DMEM + 100µg/ml UCNPs@SiO_2	26.85 ± 9.88
	DMEM + 25µg/ml UCNPs@SiO_2-Au	27.77 ± 0.54
	DMEM + 100µg/ml UCNPs@SiO_2-Au	29.24 ± 2.21
Power Density = 3.5W/cm^2 **Current** = 2.39A	DMEM + 100µg/ml UCNPs@SiO_2	17.47
Power Density = 4W/cm^2 **Current** = 2.65A	DMEM	30.12 ± 2.74
	DMEM + 25µg/ml UCNPs@SiO_2	32.77
	DMEM + 100µg/ml UCNPs@SiO_2	20.73 ± 3.10
	dH_2O	31.36
	dH_2O + 25µg/ml UCNPs@SiO_2	24.86
	dH_2O + 100µg/ml UCNPs@SiO_2-Au	27.34

Table 4: Temperature variation as a function of irradiation power density at 980nm. Results for DMEM culture medium without phenol red. Results are shown as average ± standard deviation (SD), if applicable.

Conditions	Test type	Increase (ºC)
Power Density = 0.7W/cm^2 **Current** = 0.89A	DMEM	12.19 ± 1.95
Power Density = 1W/cm^2 **Current** = 1.05A	DMEM	14.86
Power Density = 1.5W/cm^2 **Current** = 1.32A	DMEM	16.52
	DMEM + 25µg/ml UCNPs@SiO_2	10.42
	DMEM + 100µg/ml UCNPs@SiO_2	24.01
	DMEM + 25µg/ml UCNPs@SiO_2-Au	19.24
Power Density = 1.5W/cm^2 **Current** = 1.32A **2º irradiation scheme**	DMEM	24.94
	DMEM + 25µg/ml UCNPs@SiO_2	26.30
	DMEM + 100µg/ml UCNPs@SiO_2	24.63
	DMEM + 25µg/ml UCNPs@SiO_2-Au	26.36
	DMEM + 100µg/ml UCNPs@SiO_2-Au	25.68

Table 3 refers to all measurements that used DMEM culture medium with phenol red and includes the results of the single measurement made with distilled water. Table 4 shows the results of all measurements made with DMEM culture medium without phenol red. The concentrations of nanoparticles tested were 25µg/ml and 100µg/ml.

To know if any component of the culture medium interfered with heating, the temperature variation was tested with distilled water.

As can be seen from Figure 37, the results show that heating in DMEM culture medium and distilled water was practically the same in the absence of nanoparticles. When nanoparticles were added to the solution prepared with DMEM, there was an opposite effect to the desired one occurring less heating. Furthermore, this power density (4W/cm^2) caused very large temperature increases, as can be seen in table 4, making it unfeasible for testing with cells.

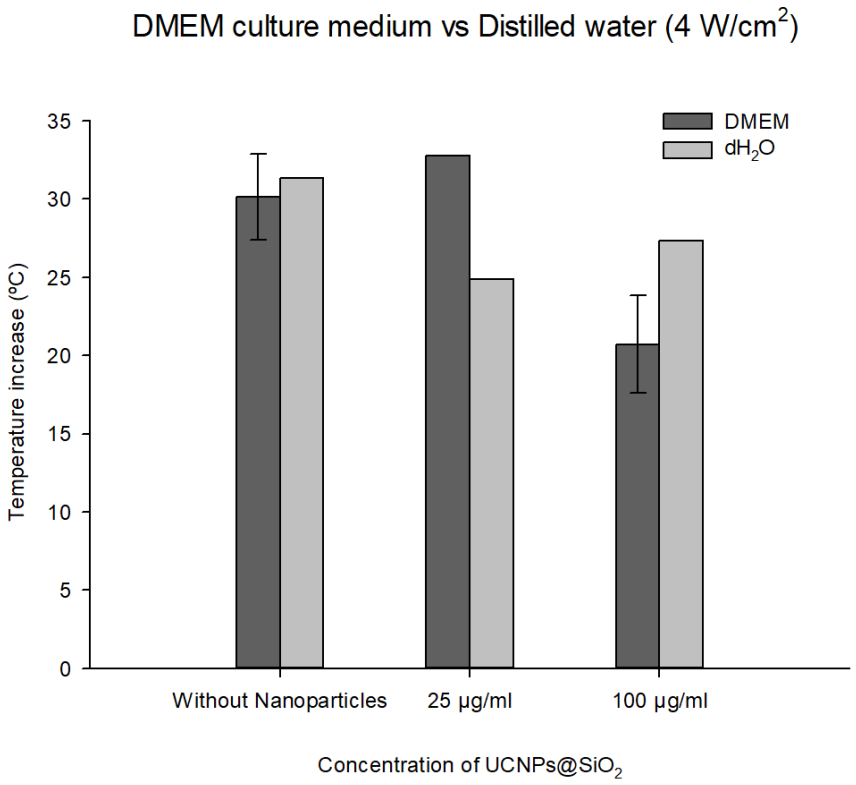

Figure 37: Differences between temperature increase in DMEM and distilled water

In this way, lower power densities (0.3W/cm^2, 0.7W/cm^2, 1W/cm^2, and 1.5W/cm^2) were tested. When colloidal solutions of nanoparticles were irradiated with these power densities, there were no large increases in temperature. Once again, the addition of nanoparticles seems to cause a smaller increase in temperature, especially in the concentration of 100µg/ml when compared to the concentration of 25µg/ml.

To investigate if the colour of the medium influences these measurements (Figure 38), a comparative test was carried out in which the temperature increase was evaluated in solutions without nanoparticles prepared with DMEM culture medium with and without phenol red.

The results show that there was a clear influence of phenol red in the temperature variation. When phenol red was absent, the temperature rise was greater. This condition is not the desired one since, in the absence of nanoparticles, it is not desirable for large temperature increases to occur, since this increase must be due to the action of the nanoparticles and not due to laser irradiation.

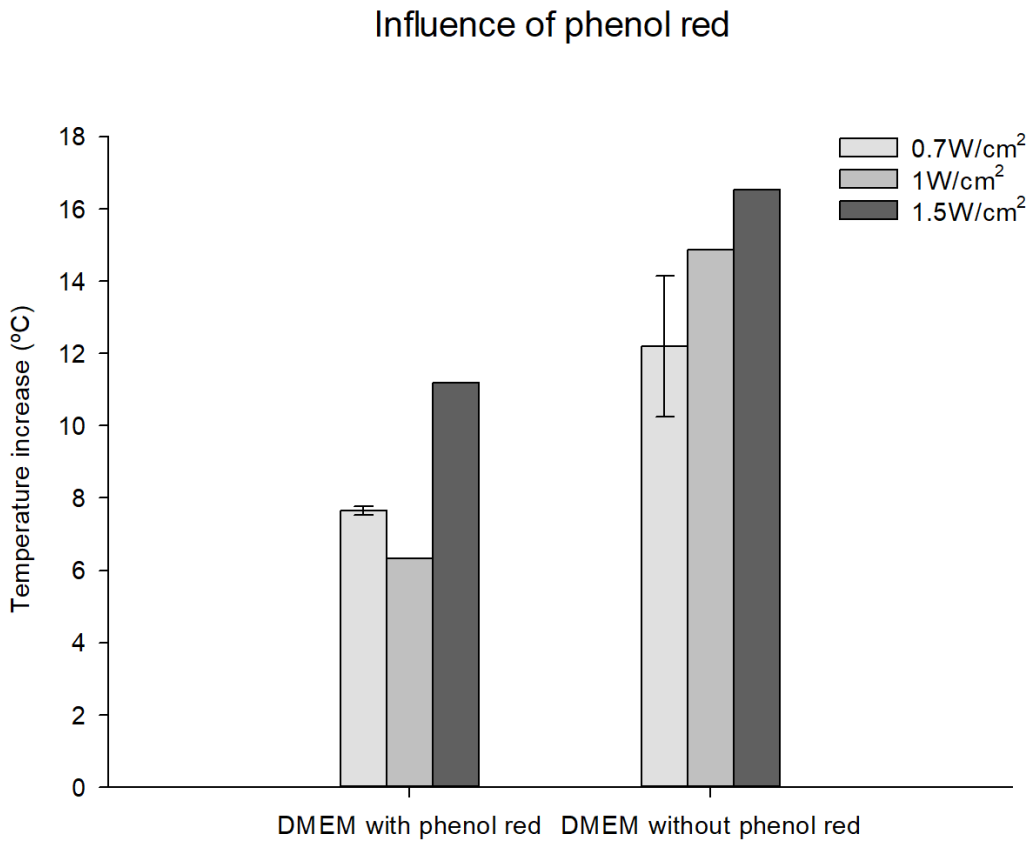

Figure 38: Influence of phenol red on the temperature increase in the absence of nanoparticles

In this study, two irradiation schemes were also tested, one using irradiation in 96-well plates and the other using a cuvette containing the samples to be irradiated. The fact that there are significant differences in temperature rise values showed that there was no agreement between these two methods. Thus, more studies would have to be done to be able to determine which method provides the most accurate and consistent measurements (Figure 39).

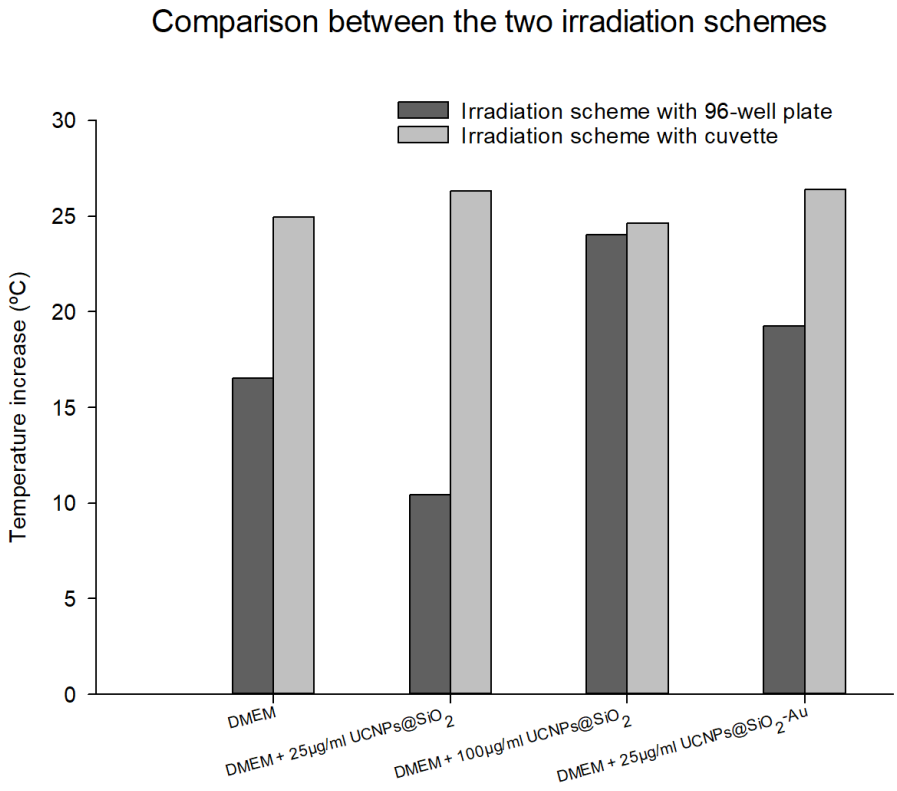

Figure 39: Comparison between the two irradiation schemes: irradiation in 96-well plates and irradiation using a cuvette containing the samples to be irradiated. Samples was prepared with DMEM.

4. Doxorubicin Loading and pH Mediated Release Studies

The UCNPs@mSiO$_2$-PO$_4$ and UCNPs@mSiO$_2$-COOH nanoparticles were loaded with DOX using a buffer solution at pH 6 and a DOX concentration of 209.56µg DOX/ml. The results of loading efficiency and nanoparticle capacity are shown in Table 5.

Table 5: Doxorubicin loading efficiency and nanoparticle capacity of UCNPs@mSiO$_2$-PO$_4$ and UCNPs@mSiO$_2$-COOH nanoparticles.

Initial [DOX] (µg/ml) (Measured UV-Vis)	Sample	Efficiency (%)	Average (%)	Loaded DOX (µg/mg)	Average (µg/mg)
209.56	Phosphonated	63.09	64.43 ± 1.33	105.77	105.89 ± 0.12
		65.76		106.01	
	Carboxylated	37.51	40.13 ± 2.61	68.36	73.12 ± 4.76
		42.74		77.88	

The UCNPs@mSiO$_2$-PO$_4$ nanoparticles exhibit drug loading of 105.89 ± 0.12µg of DOX per mg of NPs corresponding to a loading efficiency of 64.43 ± 1.33%. UCNPs@mSiO$_2$-COOH nanoparticles exhibit drug loading of 73.12 ± 4.76µg of DOX per mg of NPs corresponding to a loading efficiency of 40.13 ± 2.61%. The functionalization with the carboxyl group appears to decrease the loading efficiency. Therefore our results show that phosphonated UCNPs adsorb more DOX than carboxylated UCNPs.

The *in vitro* drug release studies were carried out using nanoparticles at physiological (pH 7.4) and tumour microenvironment (pH 5.2) pHs to find out the pharmacokinetics in normal plasma and tumour environment.

Figure 40 shows the cumulative release of DOX from the UCNPs@mSiO$_2$-PO$_4$ and UCNPs@mSiO$_2$-COOH nanoparticles at pH 5.2 and 7.4, in buffered solutions. After 1h, a burst release occurs in all formulations. After 6h, the cumulative DOX release at pH 7.4 in UCNPs@mSiO$_2$-PO$_4$ was 68.53% while at pH 5.2 was 93.93% and, in UCNPs@mSiO$_2$-COOH, the cumulative DOX release at pH 7.4 was 74.35% while at pH 5.2 was 94.59%. The DOX release was pH-dependent, being markedly faster in acidic conditions.

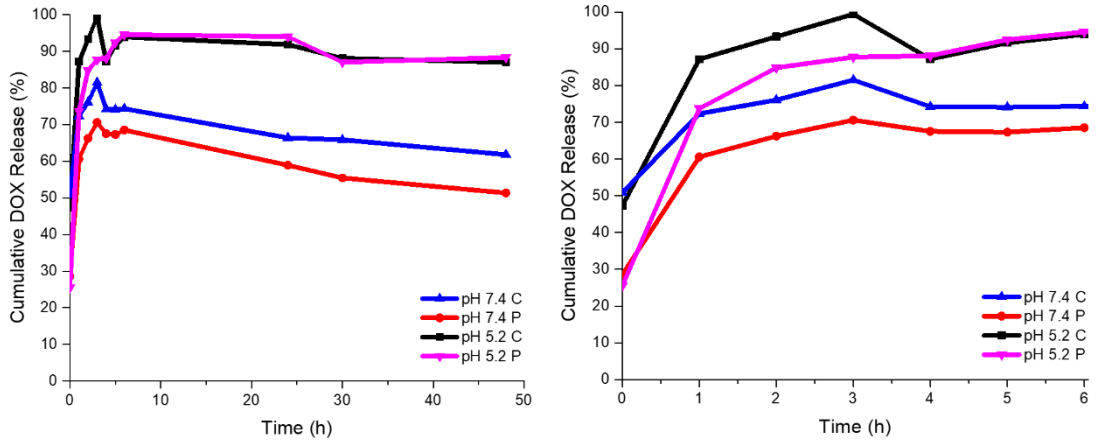

Figure 40: Doxorubicin release over time from loaded UCNPs@mSiO$_2$-PO$_4$ and UCNPs@mSiO$_2$-COOH nanoparticles at 37°C and pH 7.4 and 5.2. Full profile for 48h (left) and first 6h (right).

V – DISCUSSION

Combination therapy, a modality that combines two or more therapeutic agents, is the basis of cancer therapy (Mokhtari et al., 2017). What makes monotherapy ineffective in fighting cancer is related to drug resistance caused by long-term treatment with a single therapy and also to the occurrence of metastases (Tian et al., 2015). It is essential to improve diagnostic tools so that their detection is increasingly earlier. The detection of cancer in its early stages greatly increases the chances of survival (Islami et al., 2018; Ott et al., 2009).

In this work, the biocompatibility of different UCNPs was tested and the physicochemical characterization of two of the four tested nanoparticles was carried out. To explore photothermal therapy different assays were performed to optimize the conditions of laser irradiation. Two different melanoma cell lines were used in this work, namely, MNT-1 pigmented human melanoma cells and A375 amelanotic human melanoma cells.

The host matrix and dopants used in these UCNPs are $NaYF_4$:Lu,Yb,Er(47%,18%,2%) and $NaYF_4$:Yb,Er(20%,2%). The first nanoparticles mentioned were coated with silica shell while the second nanoparticles were coated with functionalized mesoporous silica shell. These coatings make UCNPs more dispersible in aqueous solution, provide functional groups, such as -COOH or -NH_2 that are used to attach functional biomolecules, and act as a protective barrier against chemical species that can damage the nanoparticle structure (Qian et al., 2009; Sedlmeier & Gorris, 2015; Wang et al., 2019; Zhang, Zheng et al., 2012).

The proper characterization of nanoparticles is extremely important for the development of well-defined nanoformulations with therapeutic relevance. The determination of the size and surface charge of nanoparticles are essential for the correct physicochemical characterization (Bhattacharjee, 2016). Surface charge and particle size are two factors responsible for various effects of nanoparticles, such as toxicity or dissolution (Axson et al., 2015; Bhattacharjee et al., 2013).

Dynamic Light Scattering (DLS) is a non-invasive technique that is used for the analysis of dispersed particles and colloidal nanoparticles. DLS measurements are based on the interference of light on nanoparticles based on the Brownian motion of suspended nanoparticles and the correlation between size and velocity of the Stokes-Einstein equation (Ball, 2015; Bhattacharjee, 2016; Bizheva et al., 1998; Kumar & Dixit, 2017).

Through the DLS, we were able to obtain characteristics such as the hydrodynamic diameter (D_h) and the polydispersity index (PdI). D_h depends on ionic strength, size, and shape. PdI indicates the particle size distribution in a range of 0 to 1 where 1 is the highly heterogeneous nanoparticle population (distribution is polydisperse) and 0 is the highly homogeneous nanoparticle population (distribution is monodisperse). The proteins, salts, and constituents present in the solvent contribute to the PdI. (Kumar & Dixit, 2017; Malvern Panalytical, 2013 ;Malvern Panalytical, 2017).

Analysing the obtained results, we conclude that the gold-functionalized nanoparticles have a much larger diameter (more than twice) compared to the non-conjugated nanoparticles. These higher values may be the result of greater agglomeration. One reason for this could be the fact that these nanoparticles spent less time in the ultrasonic bath to prevent possible disaggregation of the functionalized gold particles in UCNPs@SiO_2. They were only subjected to a 10-15 seconds of ultrasonic bath while the gold-free nanoparticles were dispersed in an ultrasonic bath for 5min. These values are corroborated by higher PdI values showing that there are large differences in nanoparticle sizes. Furthermore, as reported in Casals et al., (2010) and Maiorano et al., (2010), metal nanoparticles form a protein corona when suspended in DMEM culture medium, which increases their hydrodynamic diameter.

The zeta potential is a physical property exhibited by all suspended particles that can be quantified by measuring electrophoretic mobility. The zeta potential provides information about the surface charge of nanoparticles and is considered a good measure of the charge interaction between particles. Its measurement is used to assess the stability of colloidal systems (Connah, 2012). High zeta potential values mean high stability because the attraction forces between nanoparticles cannot overcome the electrical repulsion between particles with the same charge (Sedlmeier & Gorris, 2015).

Our zeta potential results show nanoparticle instability and aggregation tendency. This is true at both concentrations, 25µg/ml and 100µg/ml, and for the two nanoparticles since the highest measured zeta potential value is -10.93 ± 0.76mV and, according to Agrawal & Patel, (2011) and Kumar & Dixit, (2017), it is necessary a minimum zeta potential of ±30mV for electrostatically stabilized nanosuspensions.

Nowadays it is believed that UCNPs have low toxicity to cells and tissues (Bai et al., 2020; Cheng et al., 2011; Jiang et al., 2009; Xiong et al., 2010). According to ISO 10993-5:2009 for biological evaluation of medical devices, nanoparticles are considered non-cytotoxic if cell viability is above the 70% threshold, at the range of tested concentrations

(ISO 10993-5, 2009). Its use in biomedical applications has been growing and, therefore, it is necessary to study the potential risks *in vitro* and *in vivo* after its interaction with cells.

In the present work, we explore the biocompatibility of diverse UCNPs in two human melanoma cell lines: MNT-1 and A375. UCNPs@SiO_2 and UCNPs@SiO_2-Au nanoparticles were studied with the aim of being used in laser irradiation tests to determine the optimal conditions for the application of photothermal therapy, while UCNPs@mSiO_2-PO_4 and UCNPs@mSiO_2-COOH nanoparticles were used with the aim of studying the controlled delivery of drugs, in this case, doxorubicin. In terms of cell viability, evaluated through the MTT mitochondrial activity assay, gold-functionalized UCNPs caused a greater reduction in viability than non-functionalized ones. The A375 cell line also proves to be more sensitive than the MNT-1 cell line.

The viability of MNT-1 cells was poorly affected by UCNPs@SiO_2. In this cell line, there was only a statistically significant decrease in viability at the highest concentrations (100µg/ml and 200µg/ml) after 48h of exposure. Despite this decrease being significant ($p<0.05$), cell viability was not below the 70% threshold, and for that, these nanoparticles can be considered non-cytotoxic for this cell line.

The A375 cell line is less tolerant than MNT-1 cell line, as its viability significantly decreased after exposure to 50µg/ml and higher concentrations for both exposure times tested. This decrease caused a reduction in viability below the 70% threshold for all concentrations at 48h after exposure and only for the concentration of 200µg/ml after 24h. The obtained results demonstrate that, for this cell line, prolonged exposure to UCNPs@SiO_2 has a negative impact on viability. Results obtained by other studies with UCNPs applied on HeLa cells also showed biocompatibility for concentrations at and below 50µg/ml for both times of exposure, as it turns out for MNT-1 cell line (Kowalik et al., 2017).

To confirm the results obtained through the MTT assay, the Neutral Red Uptake assay was performed for the MNT-1 cell line exposed to UCNPs@SiO_2. As seen in the MTT assay, this assay also showed that there was no reduction in viability below the 70% threshold, and therefore both assays are in agreement.

After adding gold nanoparticles to UCNPs@SiO_2, the sensitivity of the A375 cell line became more evident. Through the results obtained, it can be seen that this cell line suffered a drastic reduction in viability in the entire range of concentrations tested after an exposure period of 48h. For the 24h of exposure, only the lowest concentration tested (12.5µg/ml) did not induced a decrease in viability below the 70% threshold. This addition also affected the viability of the MNT-1 cell line. For an exposure time of 48h, there was a reduction in cell viability below the 70% threshold for the highest concentrations, proving that these

nanoparticles are cytotoxic at high concentrations and at longer exposure times. To our knowledge, the biocompatibility measurement made with these nanoparticles in human melanoma cells has not been previously reported but, Ramírez-García et al., (2019) tested the cell viability of $NaYF_4$:Yb,Er covalently decorated with AuNPs in breast cancer MCF-7 cells. Results showed that there was no decrease below the 70% limit in viability, even at higher concentrations, contrary to what happened with our results. Vu et al. (2021) tested the biocompatibility of UCNPs coupled with gold nanorods for OML-1 oral cancer cells, and these also proved to be biocompatible. Differences in nanoparticles properties, as well as cell type-dependent characteristics, may account for the discrepancy in relation to our results.

Cell viability assay of MNT-1 melanoma cells exposed to UCNPs@$mSiO_2$-PO_4 nanoparticles showed a significant decrease in the viability ($p<0.05$) at all tested concentrations after 24h of exposure. For 48h of exposure, the viability decreased from the concentration of 25µg/ml. Despite this, this reduction is only below the 70% threshold at the concentration of 200µg/ml for 48h of exposure, showing that for this cell line, prolonged exposure to UCNPs@$mSiO_2$-PO_4 at the higher concentration has a negative impact on the viability.

The viability assay of UCNPs@$mSiO_2$-COOH nanoparticles on the MNT-1 cell line demonstrated a statistically significant decrease for all concentrations tested during 48h of exposure. Nevertheless, the results showed that this architecture is biocompatible with this cell line, and at a concentration of 200µg/ml, the cellular viability is greater than 70% indicating non-cytotoxicity of UCNPs@$mSiO_2$-COOH. The greater toxicity of UCNPs@$mSiO_2$-PO_4 was particularly relevant for high doses since a higher concentration (200µg/ml) of UCNPs@$mSiO_2$-PO_4 induced a decrease in cell viability (below the 70%) 48h post-exposure, that was not evident for UCNPs@$mSiO_2$-COOH. This difference in toxicity may be related to groups functionalized on the mesoporous silica shell.

Photothermal therapy is a minimally invasive and effective treatment that has attracted a lot of attention. This therapy uses photothermal agents to selectively kill cancer cells with the help of lasers (Yang et al., 2019).

In this work, we wanted to test what were the ideal conditions for irradiation so that, later, we could apply photothermal therapy in cells. We used a 980nm laser and tested various power densities.

The results obtained for irradiation with low power densities were not in agreement with what we found in the literature. Vu et al. (2021) described a temperature increase of

approximately 16°C after 12min of irradiation for a power density of 0.3W/cm^2. In our tests the maximum reached was 2,15°C for the same power density.

Through the obtained results, we can conclude that the temperature increase of the DMEM culture medium without nanoparticles is very similar to the increase that occurred in the presence of nanoparticles. This high-temperature rise in the culture medium may be because DMEM is mostly constituted by water. The samples were irradiated at 980nm since the sensitizer of the nanoparticles used is Yb^{3+} which absorbs light at this wavelength. Water molecules also absorb light at this wavelength. This fact may be the explanation for a large increase in temperature when DMEM is irradiated. This effect is undesirable as water present in many biological tissues will absorb excitation light, causing damage to cells and tissues. An alternative to this problem would be to use Nd^{3+} ions as a sensitizer because it absorbs light at 808nm, where the absorption coefficient of water is much smaller (Oliveira et al., 2019)

With these assays, we found that the measurements obtained were not always consistent. Measurements made under the same conditions but at distant times gave rise to quite different temperature increases. For example, for a power density of 3W/cm^2 using DMEM culture medium with phenol red and in the absence of nanoparticles, measurements were performed at two different times: the first three measurements were performed in the morning (having obtained results temperature increase of 33.61ºC, 30.10ºC and 26.63ºC) while the last two were only carried out at the end of the day (lower temperature increases were obtained, namely 18.72ºC and 16.75ºC). It should be noted that the measurements were carried out in the same well, with only the time between measurements being varied. Also, note that between the second and third measurements (33.61°C, 30.10°C, 26.63°C and, 18.72°C), at the power density of 0.7W/cm^2 in DMEM medium culture without phenol red, the plate was lowered and raised again to test if there was a change when moving the plate. Although the plate was again in the same position, every time the plate was moved, the results were not consistent with the previous ones. These considerable differences were only observed when there was a change in the position of the plate because, when measurements were made without changing the position of the plate, the results obtained were consistent. A possible explanation for these results may be the fact that there is a change in the position of the nanoparticles in relation to the thermocouple each time the plate moves, and the results will be different from those previously obtained. To overcome these differences, more measurements can be performed to understand the trend in measurements. Vortexing before each measurement could also be an alternative since this way, there is no deposition of nanoparticles in the waiting time between measurements.

The differences observed between the two irradiation schemes were also notable. The temperature increases obtained with the irradiation scheme that used the cuvette were greater than the increases seen in the irradiation scheme that used the 96-well plate. This fact may be due to the greater volume of solution used in the cuvette in relation to that used in the well, as a greater volume has a greater amount of nanoparticles, hence greater heating. More studies would have to be done to be able to determine which method provides the most accurate and consistent measurements.

Gold nanoparticles (AuNPs) are especially suited for the thermal destruction of cancer due to their photothermal heating ability (Ramírez-García et al., 2019). Thus, we were supposed to see a greater temperature rise for the gold-functionalized nanoparticles. Through the obtained results, we verified that this did not happen. For UCNPs–Au materials, there are two important influencing factors in obtaining a high photothermal efficiency: the distance between the UCNPs and the Au nanomaterials as well as the type and loading amount of Au nanomaterials (Li et al., 2011; Park et al., 2015; Yu et al., 2016). The shape or size of gold nanoparticles used or the distance they are from the UCNPs may be interfering with the efficiency of the process. Furthermore, Chen, Lee et al., (2015) demonstrated that Au nanorods could generate heat more efficiently than Au nanoparticles. A possible alternative would be to change the shape of Au nanoplatforms.

Doxorubicin is a first-line drug in the treatment of different types of cancer such as breast cancer, ovarian cancer, or lung cancer (Zhao et al., 2018). The action mechanisms of doxorubicin continue to be studied, but it is believed that it acts through intercalation into DNA disrupting gene expression, inhibition of topoisomerase II (important for DNA synthesis and replication), and through the generation of reactive oxygen species (Chatterjee et al., 2010).

Despite its wide use, this drug has a number of drawbacks. Only a small amount of the drug reaches the target site as about 40% of the drug and its metabolites are excreted (Tan et al., 2009). In addition, one of the most serious side effects of doxorubicin is irreversible cardiomyopathy (Chatterjee et al., 2010). Another problem is related to the development of drug resistance mechanisms, which contributes to a high failure rate of chemotherapy treatments (Luqmani, 2005).

In the specific case of melanoma, doxorubicin has yet another flaw because melanoma is not sensitive to this drug. Melanoma patients have a treatment response rate below 15% (Li et al., 2015; Tan et al., 2009). To overcome these problems, one of the ways is the use of nanoparticles as drug delivery systems, as their use will allow to increase the

concentration of DOX in the tumour environment, raising the response rate, and decreasing adverse effects (Gao et al., 2012; Tan et al., 2009).

In this work, the loading capacity and pH mediated release of two different types of nanoparticles (UCNPs@mSiO$_2$-PO$_4$ and UCNPs@mSiO$_2$-COOH) were tested using the drug doxorubicin. Nanoparticles were loaded with 209.56 µg DOX/ml. Through the obtained results, we can conclude that phosphonated nanoparticles adsorb more than carboxylated nanoparticles, since the average loading percentage is higher for these nanoparticles. Thus, the functionalization with the carboxyl group appears to decrease the loading efficiency.

The cumulative DOX release at pH 7.4 in UCNPs@mSiO$_2$-PO$_4$ was 68.53% at 6h, while at pH 5.2 was 93.93%. For UCNPs@mSiO$_2$-COOH nanoparticles, the cumulative DOX release at pH 7.4 was 74.35% at 6h, while at pH 5.2 was 94.59%. The DOX release was pH-dependent being faster in acidic conditions. This pH sensitive DOX release behaviour can be elucidated by the fact that with the decrease of the pH value, the potential of the particle surface becomes more positive and weakens the electrostatic adsorption force with positively charged DOX molecules, resulting in the faster drug release (Wang, Yang et al., 2013). Similar behaviour has been observed for other pH-responsive DOX nanocarriers (Dai et al., 2012; Li et al., 2013; Wang, Yang et al., 2013; Zhao et al., 2017). This pH-sensitive behaviour is of high interest since it may permit the controlled release of doxorubicin in tumour cells, as the intracellular pH is lower than in the healthy cells (Wang, Yang et al., 2013).

Our results showed that after 1h, a burst release occurs in all formulations. This can be due to a controlled diffusion process. Thus, at an early stage, sodium phosphate buffer penetrates the nanoparticle cavity, causing the release of DOX molecules. In the initial phase, the drug concentration inside the nanoparticles is high, thus there is a greater release of DOX. When concentration balance is reached, continuous drug release occurs in a diffusion-controlled manner, where the rate of diffusion depends exclusively on the dynamic balance between the drug concentration in the nanoparticles and the drug concentration in the solution. Thus, a sustained drug release stage is reached. The initial rapid release will allow an inhibition to occur in the growth of tumour cells because this initial dosage is strong enough for. For the cancer cells that survive in the initial stage of the drug release process, sustained DOX release is necessary to prevent their further proliferation (Wang, Yang et al., 2013).

Through the obtained results, we can conclude that phosphonated nanoparticles release faster than carboxylated nanoparticles and release at pH 5.2 is higher than 7.4, but at 7.4, the release is still very high.

VI – CONCLUSIONS

Cancer is a disease that affects more and more people all over the world. It represents a serious burden on human health and is urgent the development of new treatment strategies. Existing treatments are very aggressive, not differentiating tumour cells from normal cells. Photothermal therapy is a cancer treatment that induces cancer cell death by heat generated in tumour tissue exposed to near-infrared light. This new cancer-fighting strategy combines the use of nanomaterials with the irradiation of a laser. It aims to be a localized and effective treatment that only kills tumour cells. Considering the fact that there is great variation in pH values at various body sites and that cancer tissue is acidic, the pH-sensitive carrier could be used to control the release of drugs, which is beneficial to the targeting of cancerous cells, reducing the toxic side effects of chemotherapeutics for normal cells. Upconversion nanoparticles emerge as ideal candidates for use in this therapy. They can convert radiation with a wavelength in the near-infrared region (which does not cause damage to biological tissues) into radiation of a shorter wavelength which has more energy.

In this work, several UCNPs were tested to assess their biocompatibility. In summary, functionalization with gold nanoparticles causes a considerable increase in cytotoxicity to occur. On the other hand, the UCNPs@mSiO_2-COOH nanoparticles were the tested nanoparticles that conferred less toxicity on the cells.

Subsequently, tests were carried out to optimize the conditions of laser irradiation to determine the ideal conditions for applying photothermal therapy. Since the results were inconclusive, this could be a starting point for further assays. Changes in the architecture of the nanoparticles can be tested to be able to use another laser with a different wavelength of irradiation or change the thickness of the silica layer.

About the assays carried out to test the loading and release of DOX, we concluded that the phosphonated nanoparticles have a greater loading capacity and that they also have a faster release. The two different functionalizations tested presented a higher release at acidic pH, although the release at neutral pH was also considered high. In future work, the priority is to determine the biocompatibility of nanoparticles loaded with DOX in melanoma cells and non-tumour cells to understand if delivery is specific only to tumour cells and does not negatively affect healthy cells. It would also be interesting to study different coatings on the specific release of drugs at acidic pH, since in the ones we studied, the phosphorylated and carboxylated ones, there was considerable drug release at neutral

pH. To fully assess the cytotoxic mechanism induced by DOX delivery by UCNPs, it is also important to evaluate apoptosis and cell cycle dynamics.

In future work, it will also be interesting to test the combination of multiple therapies.

REFERENCES:

Abadeer, N. S., & Murphy, C. J. (2016). Recent Progress in Cancer Thermal Therapy Using Gold Nanoparticles. Journal of Physical Chemistry C, 120(9), 4691–4716. https://doi.org/10.1021/acs.jpcc.5b11232

Abdul Hakeem, D., Su, S., Mo, Z., & Wen, H. (2021). Upconversion luminescent nanomaterials: A promising new platform for food safety analysis. Critical Reviews in Food Science and Nutrition, 0(0), 1–42. https://doi.org/10.1080/10408398.2021.1937039

Adams, J. M., & Cory, S. (2007). The Bcl-2 apoptotic switch in cancer development and therapy. Oncogene, 26(9), 1324–1337. https://doi.org/10.1038/sj.onc.1210220

Agrawal, Y., & Patel, V. (2011). Nanosuspension: An approach to enhance solubility of drugs. Journal of Advanced Pharmaceutical Technology & Research, 2(2), 81. https://doi.org/10.4103/2231-4040.82950

AIM at melanoma Foundation. (n.d.). Stages of Melanoma. Retrieved October 8, 2021, from https://www.aimatmelanoma.org/stages-of-melanoma/

Albulet, D., Florea, D. A., Boarca, B., Ditu, L. M., Chifiriuc, M. C., Grumezescu, A. M., & Andronescu, E. (2017). Nanotechnology for personalized medicine: Cancer research, diagnosis, and therapy. In Nanostructures for Cancer Therapy. Elsevier Inc. https://doi.org/10.1016/B978-0-323-46144-3.00001-5

Amin, M. B., Greene, F. L., Edge, S. B., Compton, C. C., Gershenwald, J. E., Brookland, R. K., Meyer, L., Gress, D. M., Byrd, D. R., & Winchester, D. P. (2017). The Eighth Edition AJCC Cancer Staging Manual: Continuing to build a bridge from a population-based to a more “personalized” approach to cancer staging. CA: A Cancer Journal for Clinicians, 67(2), 93–99. https://doi.org/10.3322/caac.21388

Arnold, K. M., Opdenaker, L. M., Flynn, D., & Sims-Mourtada, J. (2015). Wound Healing and Cancer Stem Cells: Inflammation as a Driver of Treatment Resistance in Breast Cancer. Cancer Growth and Metastasis, 8, CGM.S11286. https://doi.org/10.4137/cgm.s11286

Auzel, F. (2004). Upconversion and Anti-Stokes Processes with f and d Ions in Solids. Chemical Reviews, 104(1), 139–173. https://doi.org/10.1021/cr020357g

Axson, J. L., Stark, D. I., Bondy, A. L., Capracotta, S. S., Maynard, A. D., Philbert, M. A., Bergin, I. L., & Ault, A. P. (2015). Rapid Kinetics of Size and pH-Dependent Dissolution and Aggregation of Silver Nanoparticles in Simulated Gastric Fluid. Journal of Physical Chemistry C, 119(35), 20632–20641. https://doi.org/10.1021/acs.jpcc.5b03634

Ayyub, P., Palkar, V. R., Chattopadhyay, S., & Multani, M. (1995). Effect of crystal size reduction on lattice symmetry and cooperative properties. Physical Review B, 51(9), 6135–6138. https://doi.org/10.1103/PhysRevB.51.6135

Bai, Y., Li, Y., Wang, R., & Li, Y. (2020). Low Toxicity, High Resolution, and Red Tissue Imaging in the Vivo of Yb/Tm/GZO@SiO2 Core-Shell Upconversion Nanoparticles. ACS Omega, 5(10), 5346–5355. https://doi.org/10.1021/acsomega.9b04381

Balch, C. M., Gershenwald, J. E., Soong, S. J., Thompson, J. F., Atkins, M. B., Byrd, D. R., Buzaid, A. C., Cochran, A. J., Coit, D. G., Ding, S., Eggermont, A. M., Flaherty, K. T., Gimotty, P. A., Kirkwood, J. M., McMasters, K. M., Mihm, M. C., Morton, D. L., Ross, M. I., Sober, A. J., & Sondak, V. K. (2009). Final version of 2009 AJCC melanoma staging and classification. Journal of Clinical Oncology, 27(36), 6199–6206. https://doi.org/10.1200/JCO.2009.23.4799

Ball, S. (2015). Dynamic Light Scatttering- Colloidal Gold: The Gold Standard for Drug Delivery? Drug Development & Delivery, 15(2), 32–35.

Barker, C. A., & Postow, M. A. (2014). Combinations of radiation therapy and immunotherapy for melanoma: A review of clinical outcomes. International Journal of Radiation Oncology Biology Physics, 88(5), 986–997. https://doi.org/10.1016/j.ijrobp.2013.08.035

Barnes, D. E., & Lindahl, T. (2004). Repair and genetic consequences of endogenous DNA base damage in mammalian cells. Annual Review of Genetics, 38, 445–476. https://doi.org/10.1146/annurev.genet.38.072902.092448

Benjamin, C. L., & Ananthaswamy, H. N. (2007). p53 and the Pathogenesis of Skin Cancer. Toxicol Appl Pharmacol, 241–248.

Bhatia, S., Tykodi, S. S., & Thompson, J. A. (2009). Treatment of metastatic melanoma: An overview. Oncology, 23(6), 488–496.

Bhattacharjee, S. (2016). DLS and zeta potential - What they are and what they are not? Journal of Controlled Release, 235, 337–351. https://doi.org/10.1016/j.jconrel.2016.06.017

Bhattacharjee, S., Rietjens, I. M. C. M., Singh, M. P., Atkins, T. M., Purkait, T. K., Xu, Z., Regli, S., Shukaliak, A., Clark, R. J., Mitchell, B. S., Alink, G. M., Marcelis, A. T. M., Fink, M. J., Veinot, J. G. C., Kauzlarich, S. M., & Zuilhof, H. (2013). Cytotoxicity of surface-functionalized silicon and germanium nanoparticles: The dominant role of surface charges. Nanoscale, 5(11), 4870–4883. https://doi.org/10.1039/c3nr34266b

Bhushan, B. (2010). Introduction to Nanotechnology. In Springer Handbook of Nanotechnology (pp. 1–6).

Bizheva, K. K., Siegel, A. M., & Boas, D. A. (1998). Path-length-resolved dynamic light scattering in highly scattering random media: The transition to diffusing wave spectroscopy. Physical Review E - Statistical Physics, Plasmas, Fluids, and Related Interdisciplinary Topics, 58(6), 7664–7667. https://doi.org/10.1103/PhysRevE.58.7664

Black, H. S., Gruijl, F. R., Forbes, P. D., Cleaver, J. E., Ananthaswamy, H. N., Fabo, E. C., Ulrich, S. E., & Tyrrel, R. M. (1997). Photocarcinogenesis: An overview. Journal of Investigative Dermatology, 29–47.

Blasco, M. A. (2005). Telomeres and human disease: Ageing, cancer and beyond. Nature Reviews Genetics, 6(8), 611–622. https://doi.org/10.1038/nrg1656

Boisseau, P., & Loubaton, B. (2011). Nanomedicine, nanotechnology in medicine. Comptes Rendus Physique, 12(7), 620–636. https://doi.org/10.1016/j.crhy.2011.06.001

Bourneuf, E. (2017). The MeLiM minipig: An original spontaneous model to explore cutaneous melanoma genetic basis. Frontiers in Genetics, 8(OCT), 1–12. https://doi.org/10.3389/fgene.2017.00146

Boya, P., Reggiori, F., & Codogno, P. (2013). Emerging regulation and functions of autophagy. Nature Cell Biology, 15(7), 713–720. https://doi.org/10.1038/ncb2788

Boyer, J.-C., Cuccia, L. A., & Capobianco, J. A. (2006). Synthesis of Colloidal Upconverting NaYF4: Er3+/Yb3+ and Tm3+/Yb3+ Monodisperse Nanocrystals. Nano Letters, 0(0), 0–0. https://doi.org/10.1021/nl0619958

Burkhart, D. L., & Sage, J. (2008). Cellular mechanisms of tumour suppression by the retinoblastoma gene. Nature Reviews Cancer, 8(9), 671–682. https://doi.org/10.1038/nrc2399

Candido, J., & Hagemann, T. (2013). Cancer-related inflammation. Journal of Clinical Immunology, 33(SUPPL.1). https://doi.org/10.1007/s10875-012-9847-0

Cao, T., Yang, Y., Gao, Y., Zhou, J., Li, Z., & Li, F. (2011). High-quality water-soluble and surface-functionalized upconversion nanocrystals as luminescent probes for bioimaging. Biomaterials, 32(11), 2959–2968. https://doi.org/10.1016/j.biomaterials.2010.12.050

Caramel, J., Papadogeorgakis, E., Hill, L., Browne, G. J., Richard, G., Wierinckx, A., Saldanha, G., sborne, J., Hutchinson, P., Tse, G., Lachuer, J., Puisieux, A., Pringle, J. H., Ansieau, S., & Tulchinsky, E. (2013). A Switch in the Expression of Embryonic EMT-Inducers Drives the Development of Malignant Melanoma. Cancer Cell, 24(4), 466–480. https://doi.org/10.1016/j.ccr.2013.08.018

Carbone, A. (2020). Cancer classification at the crossroads. Cancers, 12(4), 10–15. https://doi.org/10.3390/cancers12040980

Carmeliet, P. (2005a). Angiogenesis in life, disease and medicine. Nature, 438(7070), 932–936. https://doi.org/10.1038/nature04478

Carmeliet, P. (2005b). VEGF as a key mediator of angiogenesis in cancer. Oncology, 69(SUPPL. 3), 4–10. https://doi.org/10.1159/000088478

Carr, S., Smith, C., & Wernberg, J. (2020). Epidemiology and Risk Factors of Melanoma. Surgical Clinics of North America, 100(1), 1–12. https://doi.org/10.1016/j.suc.2019.09.005

Casals, E., Pfaller, T., Duschl, A., Oostingh, G. J., & Puntes, V. (2010). Time evolution of the nanoparticle protein corona. ACS Nano, 4(7), 3623–3632. https://doi.org/10.1021/nn901372t

Chatterjee, K., Zhang, J., Honbo, N., & Karliner, J. S. (2010). Doxorubicin cardiomyopathy. Cardiology, 115(2), 155–162. https://doi.org/10.1159/000265166

Chaturvedi, V. K., Singh, A., Singh, V. K., & Singh, M. P. (2018). Cancer Nanotechnology: A New Revolution for Cancer Diagnosis and Therapy. Current Drug Metabolism, 20(6), 416–429. https://doi.org/10.2174/1389200219666180918111528

Chávez-García, D., Juarez-Moreno, K., Campos, C. H., Tejeda, E. M., Alderete, J. B., & Hirata, G. A. (2018). Cytotoxicity, genotoxicity and uptake detection of folic acid-functionalized green upconversion nanoparticles Y2O3/Er3+, Yb3+ as biolabels for cancer cells. Journal of Materials Science, 53(9), 6665–6680. https://doi.org/10.1007/s10853-017-1946-0

Chen, C. W., Lee, P. H., Chan, Y. C., Hsiao, M., Chen, C. H., Wu, P. C., Wu, P. R., Tsai, D. P., Tu, D., Chen, X., & Liu, R. S. (2015). Plasmon-induced hyperthermia: hybrid upconversion NaYF4:Yb/Er and gold nanomaterials for oral cancer photothermal therapy. Journal of Materials Chemistry B, 3(42), 8293–8302. https://doi.org/10.1039/c5tb01393c

Chen, Cailing, Li, C., & Shi, Z. (2016). Current Advances in Lanthanide-Doped Upconversion Nanostructures for Detection and Bioapplication. Advanced Science, 3(10). https://doi.org/10.1002/advs.201600029

Chen, Chaohao, Wang, F., Wen, S., Su, Q. P., Wu, M. C. L., Liu, Y., Wang, B., Li, D., Shan, X., Kianinia, M., Aharonovich, I., Toth, M., Jackson, S. P., Xi, P., & Jin, D. (2018). Multi-photon near-infrared emission saturation nanoscopy using upconversion nanoparticles. Nature Communications, 9(1), 4–9. https://doi.org/10.1038/s41467-018-05842-w

Chen, D. S., & Mellman, I. (2013). Oncology meets immunology: The cancer-immunity cycle. Immunity, 39(1), 1–10. https://doi.org/10.1016/j.immuni.2013.07.012

Chen, G., Ågren, H., Ohulchanskyy, T. Y., & Prasad, P. N. (2015). Light upconverting core-shell nanostructures: Nanophotonic control for emerging applications. Chemical Society Reviews, 44(6), 1680–1713. https://doi.org/10.1039/c4cs00170b

Chen, G., Qiu, H., Prasad, P. N., & Chen, X. (2014). Upconversion nanoparticles: Design, nanochemistry, and applications in Theranostics. Chemical Reviews, 114(10), 5161–5214. https://doi.org/10.1021/cr400425h

Chen, G., Roy, I., Yang, C., & Prasad, P. N. (2016). Nanochemistry and Nanomedicine for Nanoparticle-based Diagnostics and Therapy. Chemical Reviews, 116(5), 2826–2885. https://doi.org/10.1021/acs.chemrev.5b00148

Chen, W., Chen, M., Zang, Q., Wang, L., Tang, F., Han, Y., Yang, C., Deng, L., & Liu, Y. N. (2015). NIR light controlled release of caged hydrogen sulfide based on upconversion nanoparticles. Chemical Communications, 51(44), 9193–9196. https://doi.org/10.1039/c5cc02508g

Chen, X., Peng, D., Ju, Q., & Wang, F. (2015). Photon upconversion in core-shell nanoparticles. Chemical Society Reviews, 44(6), 1318–1330. https://doi.org/10.1039/c4cs00151f

Cheng, L., Wang, C., Feng, L., Yang, K., & Liu, Z. (2014). Functional nanomaterials for phototherapies of cancer. Chemical Reviews, 114(21), 10869–10939. https://doi.org/10.1021/cr400532z

Cheng, L., Wang, C., & Liu, Z. (2013). Upconversion nanoparticles and their composite nanostructures for biomedical imaging and cancer therapy. Nanoscale, 5(1), 23–37. https://doi.org/10.1039/c2nr32311g

Cheng, L., Yang, K., Shao, M., Lu, X., & Liu, Z. (2011). and Toxicology Study of Functionalized Upconversion Nanoparticles in Mice. Nanomedicine, 6(8), 1327–1340.

Cheng, X., Ge, H., Wei, Y., Zhang, K., Su, W., Zhou, J., Yin, L., Zhan, Q., Jing, S., & Huang, L. (2018). Design for Brighter Photon Upconversion Emissions via Energy Level Overlap of Lanthanide Ions. ACS Nano, 12(11), 10992–10999. https://doi.org/10.1021/acsnano.8b04988

Chhetri, B. P., Karmakar, A., & Ghosh, A. (2019). Recent Advancements in Ln-Ion-Based Upconverting Nanomaterials and Their Biological Applications. Particle and Particle Systems Characterization, 36(8), 1–29. https://doi.org/10.1002/ppsc.201900153

Chien, Y. H., Chan, K. K., Yap, S. H. K., & Yong, K. T. (2018). NIR-responsive nanomaterials and their applications; upconversion nanoparticles and carbon dots: a perspective. Journal of Chemical Technology and Biotechnology, 93(6), 1519–1528. https://doi.org/10.1002/jctb.5581

Colebatch, A. J., & Scolyer, R. A. (2018). Trajectories of premalignancy during the journey from melanocyte to melanoma. Pathology, 50(1), 16–23. https://doi.org/10.1016/j.pathol.2017.09.002

Conde-Perez, A., & Larue, L. (2014). Human relevance of NRAS/BRAF mouse melanoma models. European Journal of Cell Biology, 93(1–2), 82–86. https://doi.org/10.1016/j.ejcb.2013.10.010

Connah, M. T. (2012). Measuring the stability of Nanoparticle Suspensions. 2878–2889.

Cryns, V., & Yuan, J. (1998). Proteases to die for. Genes and Development, 12(11), 1551–1570. https://doi.org/10.1101/gad.12.11.1551

D'Orazio, J., Jarrett, S., Amaro-Ortiz, A., & Scott, T. (2013). UV radiation and the skin. International Journal of Molecular Sciences, 14(6), 12222–12248. https://doi.org/10.3390/ijms140612222

Dai, Y., Ma, P., Cheng, Z., Kang, X., Zhang, X., Hou, Z., Li, C., Yang, D., Zhai, X., & Lin, J. (2012). Up-conversion cell imaging and ph-induced thermally controlled drug release from NaYF 4:Yb 3+/Er 3+@hydrogel core-shell hybrid microspheres. ACS Nano, 6(4), 3327–3338. https://doi.org/10.1021/nn300303q

De Gruijl, F. R. (2000). Photocarcinogenesis: UVA vs UVB. Methods in Enzymology, 319, 359–366. https://doi.org/10.1016/s0076-6879(00)19035-4

Debasu, M. L., Oliveira, H., Rocha, J., & Carlos, L. D. (2020). Colloidal (Gd0.98Nd0.02)2O3 nanothermometers operating in a cell culture medium within the first and second biological windows. Journal of Rare Earths, 38(5), 483–491. https://doi.org/10.1016/j.jre.2019.12.011

Debniak, T., Scott, R. J., Górski, B., Cybulski, C., van de Wetering, T., Serrano-Fernandez, P., Huzarski, T., Byrski, T., Nagay, L., Debniak, B., Kowalska, E., Jakubowska, A., Gronwald, J., Wokolorczyk, D., Maleszka, R., Kładny, J., & Lubinski, J. (2008). Common variants of DNA repair genes and malignant melanoma. European Journal of Cancer, 44(1), 110–114. https://doi.org/10.1016/j.ejca.2007.10.006

DeNardo, G. L., & DeNardo, S. J. (2008). Turning the heat on cancer. Cancer Biotherapy and Radiopharmaceuticals, 23(6), 671–679. https://doi.org/10.1089/cbr.2008.0591

DeSantis, C. E., Lin, C. C., Mariotto, A. B., Siegel, R. L., Stein, K. D., Kramer, J. L., Alteri, R., Robbins, A. S., & Jemal, A. (2014). Cancer treatment and survivorship statistics, 2014. CA: A Cancer Journal for Clinicians, 64(4), 252–271. https://doi.org/10.3322/caac.21235

Deshpande, A., Sicinski, P., & Hinds, P. W. (2005). Cyclins and cdks in development and cancer: A perspective. Oncogene, 24(17), 2909–2915. https://doi.org/10.1038/sj.onc.1208618

Ding, B., Shao, S., Yu, C., Teng, B., Wang, M., Cheng, Z., Wong, K. L., Ma, P., & Lin, J. (2018). Large-Pore Mesoporous-Silica-Coated Upconversion Nanoparticles as Multifunctional Immunoadjuvants with Ultrahigh Photosensitizer and Antigen Loading Efficiency for Improved Cancer Photodynamic Immunotherapy. Advanced Materials, 30(52), 1–10. https://doi.org/10.1002/adma.201802479

Dolmans, D. E. J. G. J., Fukumura, D., & Jain, R. K. (2003). Photodynamic therapy for cancer. Nature Reviews Cancer, 3(5), 375–380. https://doi.org/10.1038/nrc1071

Duan, C., Liang, L., Li, L., Zhang, R., & Xu, Z. P. (2018). Recent progress in upconversion luminescence nanomaterials for biomedical applications. Journal of Materials Chemistry B, 6(2), 192–209. https://doi.org/10.1039/c7tb02527k

Dukhno, O., Przybilla, F., Muhr, V., Buchner, M., Hirsch, T., & Mély, Y. (2018). Time-dependent luminescence loss for individual upconversion nanoparticles upon dilution in aqueous solution. Nanoscale, 10(34), 15904–15910. https://doi.org/10.1039/c8nr03892a

Egeblad, M., Nakasone, E. S., & Werb, Z. (2010). Tumors as organs: Complex tissues that interface with the entire organism. Developmental Cell, 18(6), 884–901. https://doi.org/10.1016/j.devcel.2010.05.012

Eggermont, A. M. M. (2010). Advances in systemic treatment of melanoma. Annals of Oncology, 21(SUPPL. 7), 339–344. https://doi.org/10.1093/annonc/mdq364

Ehlert, O., Thomann, R., Darbandi, M., & Nann, T. (2008). A four-color colloidal multiplexing nanoparticle system. ACS Nano, 2(1), 120–124. https://doi.org/10.1021/nn7002458

Eigentler, T. K., & Garbe, C. (2013). New landscape in the treatment of melanoma: A 2012 update. Oncologie, 15(2), 71–77. https://doi.org/10.1007/s10269-013-2258-x

Erlich, T. H., & Fisher, D. E. (2018). Pathways in melanoma development. Giornale Italiano Di Dermatologia e Venereologia, 153(1), 68–76. https://doi.org/10.23736/S0392-0488.17.05795-9

Faião-Flores, F., & Smalley, K. S. M. (2018). Get with the Program! Stemness and

Reprogramming in Melanoma Metastasis. Journal of Investigative Dermatology, 138(1), 10–13. https://doi.org/10.1016/j.jid.2017.07.001

Feng, W., Zhu, X., & Li, F. (2013). Recent advances in the optimization and functionalization of upconversion nanomaterials for in vivo bioapplications. NPG Asia Materials, 5(12). https://doi.org/10.1038/am.2013.63

Feron, O. (2009). Pyruvate into lactate and back: From the Warburg effect to symbiotic energy fuel exchange in cancer cells. Radiotherapy and Oncology, 92(3), 329–333. https://doi.org/10.1016/j.radonc.2009.06.025

Ferrara, N., Gerber, H.-P., & LeCouter, J. (2003). The biology of VEGF and its receptors Napoleone. Nature Medicine, 669–676. https://doi.org/10.1038/nm0603-669

Ferrara, N., & Kerbel, R. S. (2005). Angiogenesis as a therapeutic target. Nature, 438(7070), 967–974. https://doi.org/10.1038/nature04483

Fiandalo, M. V., & Kyprianou, N. (2012). CASPASE CONTROL: PROTAGONISTS OF CANCER CELL APOPTOSIS. Exp Oncol., 165–175.

Fisher, R., Pusztai, L., & Swanton, C. (2013). Cancer heterogeneity: Implications for targeted therapeutics. British Journal of Cancer, 108(3), 479–485. https://doi.org/10.1038/bjc.2012.581

Forman, S. B., Ferringer, T. C., Peckham, S. J., Dalton, S. R., Sasaki, G. T., Libow, L. F., & Elston, D. M. (2008). Is superficial spreading melanoma still the most common form of malignant melanoma? Journal of the American Academy of Dermatology, 58(6), 1013–1020. https://doi.org/10.1016/j.jaad.2007.10.650

Frändberg, P. A., Doufexis, M., Kapas, S., & Chhajlani, V. (1998). Human pigmentation phenotype: A point mutation generates nonfunctional MSH receptor. Biochemical and Biophysical Research Communications, 245(2), 490–492. https://doi.org/10.1006/bbrc.1998.8459

Gainkam, L. O. T., Huang, L., Caveliers, V., Keyaerts, M., Hernot, S., Vaneycken, I., Vanhove, C., Revets, H., De Baetselier, P., & Lahoutte, T. (2008). Comparison of the biodistribution and tumor targeting of two 99mTc-labeled anti-EGFR nanobodies in mice, using pinhole SPECT/micro-CT. Journal of Nuclear Medicine, 49(5), 788–795. https://doi.org/10.2967/jnumed.107.048538

Gao, Z., Zhang, L., & Sun, Y. (2012). Nanotechnology applied to overcome tumor drug resistance. Journal of Controlled Release, 162(1), 45–55. https://doi.org/10.1016/j.jconrel.2012.05.051

Garbe, C., Peris, K., Hauschild, A., Saiag, P., Middleton, M., Spatz, A., Grob, J. J., Malvehy, J., Newton-Bishop, J., Stratigos, A., Pehamberger, H., & Eggermont, A. (2010). Diagnosis and treatment of melanoma: European consensus-based interdisciplinary guideline. European Journal of Cancer, 46(2), 270–283. https://doi.org/10.1016/j.ejca.2009.10.032

García-Caballero, M., Medina, M. Á., & Quesada, A. R. (2015). Toluquinol, A Marine Fungus Metabolite, Inhibits Some of the Hallmarks of Cancer. In Handbook of Anticancer Drugs from Marine Origin (pp. 1–805). © Springer International Publishing. https://doi.org/10.1007/978-3-319-07145-9

Ge, W., Li, Z., Chen, T., Liu, M., & Lu, Y. (2018). Extended near-infrared photoactivity of Bi6Fe1.9Co0.1Ti3O18 by upconversion nanoparticles. Nanomaterials, 8(7), 1–12. https://doi.org/10.3390/nano8070534

George, J., Nihal, M., Singh, C. K., Zhong, W., Liu, X., & Ahmad, N. (2016). Pro-Proliferative Function of Mitochondrial Sirtuin Deacetylase SIRT3 in Human Melanoma. Journal of Investigative Dermatology, 136(4), 809–818. https://doi.org/10.1016/j.jid.2015.12.026

Ghoncheh, M., & Salehiniya, H. (2016). Inequality in the incidence and mortality of all cancers in the world. Iranian Journal of Public Health, 45(12), 1675–1677.

Gilchrest, B. A., Eller, M. S., Geller, A. C., & Yaar, M. (1999). The Pathogenesis os Melanoma induced by ultraviolet radiation. In F. H. Epstein (Ed.), Mechanisms of Disease F (Vol. 340, Issue 17, pp. 1341–1348).

Girotti, M. R., Salatino, M., Dalotto-Moreno, T., Rabinovich, G. A., & Rabinovich, G. A. (2020). Sweetening the hallmarks of cancer: Galectins as multifunctional mediators of tumor progression. Journal of Experimental Medicine, 217(2), 1–14. https://doi.org/10.1084/jem_20182041

Gogas, H. J., Kirkwood, J. M., & Sondak, V. K. (2007). Chemotherapy for metastatic melanoma: Time for a change? Cancer, 109(3), 455–464. https://doi.org/10.1002/cncr.22427

Gray-Schopfer, V., Wellbrock, C., & Marais, R. (2007). Melanoma biology and new targeted therapy. Nature, 445(7130), 851–857. https://doi.org/10.1038/nature05661

Grivennikov, S. I., Greten, F. R., & Karin, M. (2010). Immunity, Inflammation, and Cancer. Cell, 140(6), 883–899. https://doi.org/10.1016/j.cell.2010.01.025

Grzywa, T. M., Paskal, W., & Włodarski, P. K. (2017). Intratumor and Intertumor Heterogeneity in Melanoma. Translational Oncology, 10(6), 956–975. https://doi.org/10.1016/j.tranon.2017.09.007

Gulzar, A., Xu, J., Yang, P., He, F., & Xu, L. (2017). Upconversion processes: Versatile biological applications and biosafety. Nanoscale, 9(34), 12248–12282. https://doi.org/10.1039/c7nr01836c

Hammami, I., Alabdallah, N. M., jomaa, A. Al, & kamoun, M. (2021). Gold nanoparticles: Synthesis properties and applications. Journal of King Saud University - Science, 33(7). https://doi.org/10.1016/j.jksus.2021.101560

Hanahan, D., & Coussens, L. M. (2012). Accessories to the Crime: Functions of Cells Recruited to the Tumor Microenvironment. Cancer Cell, 21(3), 309–322. https://doi.org/10.1016/j.ccr.2012.02.022

Hanahan, D., & Folkman, J. (1996). Patterns and emerging mechanisms of the angiogenic switch during tumorigenesis. Cell, 86(3), 353–364. https://doi.org/10.1016/S0092-8674(00)80108-7

Hanahan, D., & Weinberg, R. A. (2011). Hallmarks of cancer: The next generation. Cell, 144(5), 646–674. https://doi.org/10.1016/j.cell.2011.02.013

Hanahan, D., & Weinberg, R. A. (2017). Biological Hallmarks of Cancer. Holland-Frei Cancer Medicine, 1–10. https://doi.org/10.1002/9781119000822.hfcm002

Haridas, P., McGovern, J. A., McElwain, S. D. L., & Simpson, M. J. (2017). Quantitative comparison of the spreading and invasion of radial growth phase and metastatic melanoma cells in a three-dimensional human skin equivalent model. PeerJ, 2017(9). https://doi.org/10.7717/peerj.3754

Harley, C. B., Kim, N. W., Prowse, K. R., Weinrich, S. L., Hirsch, K. S., West, M. D., Bacchetti, S., Hirte, H. W., Counter, C. M., Greider, C. W., Piatyszek, M. A., Wright, W. E., & Shay, J. W. (1994). Telomerase, cell immortality, and cancer. Cold Spring Harbor Symposia on Quantitative Biology, 59, 307–315. https://doi.org/10.1101/SQB.1994.059.01.035

Hassanpour, S. H., & Dehghani, M. (2017). Review of cancer from perspective of molecular. Journal of Cancer Research and Practice, 4(4), 127–129. https://doi.org/10.1016/j.jcrpr.2017.07.001

Heaphy, C. M., & Meeker, A. K. (2011). The potential utility of telomere-related markers for cancer diagnosis. Journal of Cellular and Molecular Medicine, 15(6), 1227–1238.

https://doi.org/10.1111/j.1582-4934.2011.01284.x
Heinke, J., Patterson, C., & Moser, M. (2012). Life is a pattern: vascular assembly within the embryo. Frontiers in Bioscience E4, 2269–2288.
Hofmann, U. B., Westphal, J. R., Van Muijen, G. N. P., & Ruiter, D. J. (2000). Matrix metalloproteinases in human melanoma. Journal of Investigative Dermatology, 115(3), 337–344. https://doi.org/10.1046/j.1523-1747.2000.00068.x
Honors, C. N., Kruger, C. A., & Abrahamse, H. (2018). Photodynamic therapy for metastatic melanoma treatment: A review. Technology in Cancer Research and Treatment, 17, 1–15. https://doi.org/10.1177/1533033818791795
Hossen, S., Hossain, M. K., Basher, M. K., Mia, M. N. H., Rahman, M. T., & Uddin, M. J. (2019). Smart nanocarrier-based drug delivery systems for cancer therapy and toxicity studies: A review. In Journal of Advanced Research (Vol. 15). Cairo University. https://doi.org/10.1016/j.jare.2018.06.005
Hynes, N. E., & MacDonald, G. (2009). ErbB receptors and signaling pathways in cancer. Current Opinion in Cell Biology, 21(2), 177–184. https://doi.org/10.1016/j.ceb.2008.12.010
Islami, F., Goding Sauer, A., Miller, K. D., Siegel, R. L., Fedewa, S. A., Jacobs, E. J., McCullough, M. L., Patel, A. V., Ma, J., Soerjomataram, I., Flanders, W. D., Brawley, O. W., Gapstur, S. M., & Jemal, A. (2018). Proportion and number of cancer cases and deaths attributable to potentially modifiable risk factors in the United States. CA: A Cancer Journal for Clinicians, 68(1), 31–54. https://doi.org/10.3322/caac.21440
ISO 10993-5. (2009). Biological evaluation of medical devices — Part 5: Tests for in vitro cytotoxicity.
Jackson, S. P., & Bartek, J. (2009). The DNA-damage response in human biology and disease. Nature, 461(7267), 1071–1078. https://doi.org/10.1038/nature08467
Jiang, S., Zhang, Y., Lim, K. M., Sim, E. K. W., & Ye, L. (2009). NIR-to-visible upconversion nanoparticles for fluorescent labeling and targeted delivery of siRNA. Nanotechnology, 20(15). https://doi.org/10.1088/0957-4484/20/15/155101
Kang, L., Gao, Z., Huang, W., Jin, M., & Wang, Q. (2015). Nanocarrier-mediated co-delivery of chemotherapeutic drugs and gene agents for cancer treatment. Acta Pharmaceutica Sinica B, 5(3), 169–175. https://doi.org/10.1016/j.apsb.2015.03.001
Kawai, T., Hiroi, S., Nakanishi, K., & Meeker, A. K. (2007). Telomere length and telomerase expression in atypical adenomatous hyperplasia and small bronchioloalveolar carcinoma of the lung. American Journal of Clinical Pathology, 127(2), 254–262. https://doi.org/10.1309/91PY0RBD9W8Y5GNX
Kawczyk-Krupka, A., Bugaj, A. M., Latos, W., Zaremba, K., & Sieroń, A. (2013). Photodynamic therapy in treatment of cutaneous and choroidal melanoma. Photodiagnosis and Photodynamic Therapy, 10(4), 503–509. https://doi.org/10.1016/j.pdpdt.2013.05.006
Kennedy, C., Ter Huurne, J., Berkhout, M., Gruis, N., Bastiaens, M., Bergman, W., Willemze, R., & Bouwes Bavinck, J. N. (2001). Melanocortin 1 receptor (MC1R) gene variants are associated with an increased risk for cutaneous melanoma which is largely independent of skin type and hair color. Journal of Investigative Dermatology, 117(2), 294–300. https://doi.org/10.1046/j.0022-202x.2001.01421.x
Khan, I., Saeed, K., & Khan, I. (2019). Nanoparticles: Properties, applications and toxicities. Arabian Journal of Chemistry, 12(7), 908–931. https://doi.org/10.1016/j.arabjc.2017.05.011
Khan, M. H., Alam, M., & Yoo, S. (2011). Epidermal growth factor receptor inhibitors in the treatment of nonmelanoma skin cancers. Dermatologic Surgery, 37(9), 1199–1209.

https://doi.org/10.1111/j.1524-4725.2011.02038.x
Klier, D. T., & Kumke, M. U. (2015). Upconversion luminescence properties of NaYF4:Yb:Er nanoparticles codoped with Gd3+. Journal of Physical Chemistry C, 119(6), 3363–3373. https://doi.org/10.1021/jp5103548
Kobayashi, H., Kosaka, N., Ogawa, M., Morgan, N. Y., Smith, P. D., Murray, C. B., Ye, X., Collins, J., Kumar, G. A., Bell, H., & Choyke, P. L. (2009). In vivo multiple color lymphatic imaging using upconverting nanocrystals. Journal of Materials Chemistry, 19(36), 6481–6484. https://doi.org/10.1039/b910512c
Koch, S. E., & Lange, J. R. (2000). Amelanotic melanoma: The great masquerader. Journal of the American Academy of Dermatology, 42(5 I), 731–734. https://doi.org/10.1067/mjd.2000.103981
Kong, Q., Zhang, L., Liu, J., Wu, M., Chen, Y., Feng, J., & Shi, J. (2014). Facile synthesis of hydrophilic multi-colour and upconversion photoluminescent mesoporous carbon nanoparticles for bioapplications. Chemical Communications, 50(99), 15772–15775. https://doi.org/10.1039/c4cc07121b
Kowalik, P., Elbaum, D., Mikulski, J., Fronc, K., Kamińska, I., Morais, P. C., Eduardo De Souza, P., Nunes, R. B., Veiga-Souza, F. H., Gruzeł, G., Minikayev, R., Wojciechowski, T., Mosiniewicz-Szablewska, E., Szewczyk, M., Pawlyta, M., Sienkiewicz, A., Łapiński, M., Zajdel, K., Stępień, P., … Sikora, B. (2017). Upconversion fluorescence imaging of HeLa cells using ROS generating SiO2-coated lanthanide-doped NaYF4 nanoconstructs. RSC Advances, 7(48), 30262–30273. https://doi.org/10.1039/c6ra25383k
Kumar, A., & Dixit, C. K. (2017). Methods for characterization of nanoparticles. Advances in Nanomedicine for the Delivery of Therapeutic Nucleic Acids, 44–58. https://doi.org/10.1016/B978-0-08-100557-6.00003-1
Kumar, P., Nagarajan, A., & Uchil, P. D. (2018). Analysis of cell viability by the MTT assay. Cold Spring Harbor Protocols, 2018(6), 469–471. https://doi.org/10.1101/pdb.prot095505
Lane, D. P. (1992). P53, Guardian of the Genome. In Nature (Vol. 358, Issue 6381, pp. 15–16). https://doi.org/10.1038/358015a0
Lee, G., & Park, Y. Il. (2018). Lanthanide-doped upconversion nanocarriers for drug and gene delivery. Nanomaterials, 8(7). https://doi.org/10.3390/nano8070511
Leonardi, G. C., Falzone, L., Salemi, R., Zanghì, A., Spandidos, D. A., Mccubrey, J. A., Candido, S., & Libra, M. (2018). Cutaneous melanoma: From pathogenesis to therapy (Review). International Journal of Oncology, 52(4), 1071–1080. https://doi.org/10.3892/ijo.2018.4287
Levine, B., & Kroemer, G. (2008). Autophagy in the Pathogenesis of Disease. Cell, 132(1), 27–42. https://doi.org/10.1016/j.cell.2007.12.018
Li, C., Hou, Z., Dai, Y., Yang, D., Cheng, Z., Ma, P., & Lin, J. (2013). A facile fabrication of upconversion luminescent and mesoporous core-shell structured β-NaYF4:Yb3+, Er3+@mSiO 2 nanocomposite spheres for anti-cancer drug delivery and cell imaging. Biomaterials Science, 1(2), 213–223. https://doi.org/10.1039/c2bm00087c
Li, H., Wang, X., Huang, D., & Chen, G. (2020). Recent advances of lanthanide-doped upconversion nanoparticles for biological applications. Nanotechnology, 31(7). https://doi.org/10.1088/1361-6528/ab4f36
Li, J., Wang, Y., Liang, R., An, X., Wang, K., Shen, G., Tu, Y., Zhu, J., & Tao, J. (2015). Recent advances in targeted nanoparticles drug delivery to melanoma. Nanomedicine: Nanotechnology, Biology, and Medicine, 11(3), 769–794. https://doi.org/10.1016/j.nano.2014.11.006

Li, Z., Wang, L., Wang, Z., Liu, X., & Xiong, Y. (2011). Modification of NaYF4:Yb,Er@SiO2 nanoparticles with gold nanocrystals for tunable green-to-red upconversion emissions. Journal of Physical Chemistry C, 115(8), 3291–3296. https://doi.org/10.1021/jp110603r

Li, Z., Zhang, Y., & Jiang, S. (2008). Multicolor core/shell-structured upconversion fluorescent nanoparticles. Advanced Materials, 20(24), 4765–4769. https://doi.org/10.1002/adma.200801056

Liang, G., Wang, H., Shi, H., Wang, H., Zhu, M., Jing, A., Li, J., & Li, G. (2020). Recent progress in the development of upconversion nanomaterials in bioimaging and disease treatment. Journal of Nanobiotechnology, 18(1), 1–22. https://doi.org/10.1186/s12951-020-00713-3

Lim, E. K., Kim, T., Paik, S., Haam, S., Huh, Y. M., & Lee, K. (2015). Nanomaterials for theranostics: Recent advances and future challenges. Chemical Reviews, 115(1), 327–394. https://doi.org/10.1021/cr300213b

Lim, M. E., Lee, Y. ling, Zhang, Y., & Chu, J. J. H. (2012). Photodynamic inactivation of viruses using upconversion nanoparticles. Biomaterials, 33(6), 1912–1920. https://doi.org/10.1016/j.biomaterials.2011.11.033

Lingeshwar Reddy, K., Balaji, R., Kumar, A., & Krishnan, V. (2018). Lanthanide Doped Near Infrared Active Upconversion Nanophosphors: Fundamental Concepts, Synthesis Strategies, and Technological Applications. Small, 14(37), 1–27. https://doi.org/10.1002/smll.201801304

Liniker, E., Menzies, A. M., Kong, B. Y., Cooper, A., Ramanujam, S., Lo, S., Kefford, R. F., Fogarty, G. B., Guminski, A., Wang, T. W., Carlino, M. S., Hong, A., & Long, G. V. (2016). Activity and safety of radiotherapy with anti-PD-1 drug therapy in patients with metastatic melanoma. OncoImmunology, 5(9). https://doi.org/10.1080/2162402X.2016.1214788

Liu-Smith, F., Farhat, A. M., Arce, A., Ziogas, A., Taylor, T., Wang, Z., Yourk, V., Liu, J., Wu, J., McEligot, A. J., Anton-Culver, H., & Meyskens, F. L. (2017). Sex differences in the association of cutaneous melanoma incidence rates and geographic ultraviolet light exposure. Journal of the American Academy of Dermatology, 76(3), 499-505.e3. https://doi.org/10.1016/j.jaad.2016.08.027

Liu, J., Fukunaga-Kalabis, M., Li, L., & Herlyn, M. (2014). Developmental pathways activated in melanocytes and melanoma. Archives of Biochemistry and Biophysics, 563(August), 13–21. https://doi.org/10.1016/j.abb.2014.07.023

Liu, Q., Das, M., Liu, Y., & Huang, L. (2018). Targeted drug delivery to melanoma. Advanced Drug Delivery Reviews, 127, 208–221. https://doi.org/10.1016/j.addr.2017.09.016

Liu, S. (2012). Epigenetics advancing personalized nanomedicine in cancer therapy. Advanced Drug Delivery Reviews, 64(13), 1532–1543. https://doi.org/10.1016/j.addr.2012.08.004

Liu, Y., Lu, Y., Yang, X., Zheng, X., Wen, S., Wang, F., Vidal, X., Zhao, J., Liu, D., Zhou, Z., Ma, C., Zhou, J., Piper, J. A., Xi, P., & Jin, D. (2017). Amplified stimulated emission in upconversion nanoparticles for super-resolution nanoscopy. Nature, 543(7644), 229–233. https://doi.org/10.1038/nature21366

Lowe, S. W., Cepero, E., & Evan, G. (2004). Intrinsic tumour suppression. Nature, 432(7015), 307–315. https://doi.org/10.1038/nature03098

Lu, Y., Zhao, J., Zhang, R., Liu, Y., Liu, D., Goldys, E. M., Yang, X., Xi, P., Sunna, A., Lu, J., Shi, Y., Leif, R. C., Huo, Y., Shen, J., Piper, J. A., Robinson, J. P., & Jin, D. (2014). Tunable lifetime multiplexing using luminescent nanocrystals. Nature

Photonics, 8(1), 32–36. https://doi.org/10.1038/nphoton.2013.322
Luqmani, Y. A. (2005). Mechanisms of drug resistance in cancer chemotherapy. Medical Principles and Practice, 14(SUPPL. 1), 35–48. https://doi.org/10.1159/000086183
Madsen, C. D., & Sahai, E. (2010). Cancer Dissemination-Lessons from Leukocytes. Developmental Cell, 19(1), 13–26. https://doi.org/10.1016/j.devcel.2010.06.013
Maeda, H., Wu, J., Sawa, T., Matsumura, Y., & Hori, K. (2000). Tumor vascular permeability and the EPR effect in macromolecular therapeutics: A review. Journal of Controlled Release, 65(1–2), 271–284. https://doi.org/10.1016/S0168-3659(99)00248-5
Maiorano, G., Sabella, S., Sorce, B., Brunetti, V., Malvindi, M. A., Cingolani, R., & Pompa, P. P. (2010). Effects of cell culture media on the dynamic formation of protein-nanoparticle complexes and influence on the cellular response. ACS Nano, 4(12), 7481–7491. https://doi.org/10.1021/nn101557e
Malvern Panalytical. (2013). Dynamic Light Sca ering (DLS) - Understanding the Basics. 1–8.
Malvern Panalytical. (2017). A basic introduction to Dynamic Light Scattering (DLS) for particle size analysis.
Marnett, L. J. (2000). Oxyradicals and DNA damage. Carcinogenesis, 21(3), 361–370. https://doi.org/10.1093/carcin/21.3.361
Martín-Gorgojo, A., & Nagore, E. (2018). Melanoma Arising in a Melanocytic Nevus. Actas Dermo-Sifiliográficas (English Edition), 109(2), 123–132. https://doi.org/10.1016/j.adengl.2017.12.006
McNeil, S. E. (2005). Nanotechnology for the biologist. Journal of Leukocyte Biology, 78(3), 585–594. https://doi.org/10.1189/jlb.0205074
Meacham, C. E., & Morrison, S. J. (2013). Tumour heterogeneity and cancer cell plasticity. Nature, 501(7467), 328–337. https://doi.org/10.1038/nature12624
Meeran, S. M., Punathil, T., & Katiyar, S. K. (2008). IL-12 deficiency exacerbates inflammatory responses in UV-irradiated skin and skin tumors. Journal of Investigative Dermatology, 128(11), 2716–2727. https://doi.org/10.1038/jid.2008.140
Megahed, A. I., & Koon, H. B. (2014). What is the role of chemotherapy in the treatment of melanoma? Current Treatment Options in Oncology, 15(2), 321–335. https://doi.org/10.1007/s11864-014-0277-5
Melle, S., Calderón, O. G., Laurenti, M., Mendez-Gonzalez, D., Egatz-Gómez, A., López-Cabarcos, E., Cabrera-Granado, E., Díaz, E., & Rubio-Retama, J. (2018). Förster Resonance Energy Transfer Distance Dependence from Upconverting Nanoparticles to Quantum Dots. Journal of Physical Chemistry C, 122(32), 18751–18758. https://doi.org/10.1021/acs.jpcc.8b04908
Mihajlovic, M., Vlajkovic, S., Jovanovic, P., & Stefanovic, V. (2012). Primary mucosal melanomas: A comprehensive review. International Journal of Clinical and Experimental Pathology, 5(8), 739–753.
Millikan, R. C., Hummer, A., Begg, C., Player, J., de Cotret, A. R., Winkel, S., Mohrenweiser, H., Thomas, N., Armstrong, B., Kricker, A., Marrett, L. D., Gruber, S. B., Culver, H. A., Zanetti, R., Gallagher, R. P., Dwyer, T., Rebbeck, T. R., Busam, K., From, L., … Setlow, R. (2006). Polymorphisms in nucleotide excision repair genes and risk of multiple primary melanoma: The Genes Environment and Melanoma Study. Carcinogenesis, 27(3), 610–618. https://doi.org/10.1093/carcin/bgi252
Mokhtari, R. B., Homayouni, T. S., Baluch, N., Morgatskaya, E., Kumar, S., Das, B., & Yeger, H. (2017). Combination therapy in combating cancer SYSTEMATIC REVIEW: COMBINATION THERAPY IN COMBATING CANCER BACKGROUND. Oncotarget,

8(23), 38022–38043. www.impactjournals.com/oncotarget
Monge-Fuentes, V., Muehlmann, L. A., & de Azevedo, R. B. (2014). Perspectives on the application of nanotechnology in photodynamic therapy for the treatment of melanoma. Nano Reviews, 5(1), 24381. https://doi.org/10.3402/nano.v5.24381
Murdoch, C., Muthana, M., Coffelt, S. B., & Lewis, C. E. (2008). The role of myeloid cells in the promotion of tumour angiogenesis. Nature Reviews Cancer, 8(8), 618–631. https://doi.org/10.1038/nrc2444
Narayanan, D. L., Saladi, R. N., & Fox, J. L. (2010). Ultraviolet radiation and skin cancer. International Journal of Dermatology, 49(9), 978–986. https://doi.org/10.1111/j.1365-4632.2010.04474.x
Naves, L. B., Dhand, C., Venugopal, J. R., Rajamani, L., Ramakrishna, S., & Almeida, L. (2017). Nanotechnology for the treatment of melanoma skin cancer. Progress in Biomaterials, 6(1–2), 13–26. https://doi.org/10.1007/s40204-017-0064-z
Naysmith, L., Waterston, K., Ha, T., Flanagan, N., Bisset, Y., Ray, A., Wakamatsu, K., Ito, S., & Rees, J. L. (2004). Quantitative Measures of the Effect of the Melanocortin 1 Receptor on Human Pigmentary Status. Journal of Investigative Dermatology, 122(2), 423–428. https://doi.org/10.1046/j.0022-202X.2004.22221.x
Negrini, S., Gorgoulis, V. G., & Halazonetis, T. D. (2010). Genomic instability an evolving hallmark of cancer. Nature Reviews Molecular Cell Biology, 11(3), 220–228. https://doi.org/10.1038/nrm2858
Nikolaou, V., & Stratigos, A. J. (2014). Emerging trends in the epidemiology of melanoma. British Journal of Dermatology, 170(1), 11–19. https://doi.org/10.1111/bjd.12492
Nikolaou, Vasiliki, Stratigos, A., Bafaloukos, D., & Katsambas, A. (2013). Antiangiogenic and antiapoptotic treatment in advanced melanoma. Clinics in Dermatology, 31(3), 257–263. https://doi.org/10.1016/j.clindermatol.2012.08.018
Noculak, A., & Podhorodecki, A. (2018). Size and shape effects in β-NaGdF4: Yb3+, Er3+ nanocrystals. December 2016, 11–14.
O. Warburg. (1956). On the Origin of Cancer Cells. Science, 123(3191), 309–314.
Okada, K., Takahashi, Y., Ohnishi, K., Ishikawa, O., & Miyachi, Y. (1994). Time-dependent effect of chronic UV irradiation on superoxide dismutase and catalase activity in hairless mice skin. Journal of Dermatological Science, 8(3), 183–186. https://doi.org/10.1016/0923-1811(94)90052-3
Oliveira, H., Bednarkiewicz, A., Falk, A., Fröhlich, E., Lisjak, D., Prina-Mello, A., Resch, S., Schimpel, C., Vrček, I. V., Wysokińska, E., & Gorris, H. H. (2019). Critical Considerations on the Clinical Translation of Upconversion Nanoparticles (UCNPs): Recommendations from the European Upconversion Network (COST Action CM1403). Advanced Healthcare Materials, 8(1). https://doi.org/10.1002/adhm.201801233
Orthaber, K., Pristovnik, M., Skok, K., Perić, B., & Maver, U. (2017). Skin Cancer and Its Treatment: Novel Treatment Approaches with Emphasis on Nanotechnology. Journal of Nanomaterials, 2017. https://doi.org/10.1155/2017/2606271
Ott, J. J., Ullrich, A., & Miller, A. B. (2009). The importance of early symptom recognition in the context of early detection and cancer survival. European Journal of Cancer, 45(16), 2743–2748. https://doi.org/10.1016/j.ejca.2009.08.009
Ouyang, L., Shi, Z., Zhao, S., Wang, F. T., Zhou, T. T., Liu, B., & Bao, J. K. (2012). Programmed cell death pathways in cancer: A review of apoptosis, autophagy and programmed necrosis. Cell Proliferation, 45(6), 487–498. https://doi.org/10.1111/j.1365-2184.2012.00845.x
Paluncic, J., Kovacevic, Z., Jansson, P. J., Kalinowski, D., Merlot, A. M., Huang, M. L. H.,

Lok, H. C., Sahni, S., Lane, D. J. R., & Richardson, D. R. (2016). Roads to melanoma: Key pathways and emerging players in melanoma progression and oncogenic signaling. Biochimica et Biophysica Acta - Molecular Cell Research, 1863(4), 770–784. https://doi.org/10.1016/j.bbamcr.2016.01.025

Park, W., Lu, D., & Ahn, S. (2015). Plasmon enhancement of luminescence upconversion. Chemical Society Reviews, 44(10), 2940–2962. https://doi.org/10.1039/c5cs00050e

Parkin, D. M. (2006). The global health burden of infection-associated cancers in the year 2002. International Journal of Cancer, 118(12), 3030–3044. https://doi.org/10.1002/ijc.21731

Pasqualini, R., Arap, W., & McDonald, D. M. (2002). Probing the structural and molecular diversity of tumor vasculature. Trends in Molecular Medicine, 8(12), 563–571. https://doi.org/10.1016/S1471-4914(02)02429-2

Pastila, R., & Leszczynski, D. (2007). Ultraviolet-A radiation induces changes in cyclin G gene expression in mouse melanoma B16-F1 cells. Cancer Cell International, 7, 11–13. https://doi.org/10.1186/1475-2867-7-7

Peters, G. (2008). Tumor suppression for ARFicionados: The relative contributions of p16 INK4a and p14ARF in melanoma. Journal of the National Cancer Institute, 100(11), 757–759. https://doi.org/10.1093/jnci/djn156

Pop, C., & Salvesen, G. S. (2009). Human caspases: Activation, specificity, and regulation. Journal of Biological Chemistry, 284(33), 21777–21781. https://doi.org/10.1074/jbc.R800084200

Potente, M., Gerhardt, H., & Carmeliet, P. (2011). Basic and therapeutic aspects of angiogenesis. Cell, 146(6), 873–887. https://doi.org/10.1016/j.cell.2011.08.039

Prokopiou, E. M., Ryder, S. A., & Walsh, J. J. (2013). Tumour vasculature targeting agents in hybrid/conjugate drugs. Angiogenesis, 16(3), 503–524. https://doi.org/10.1007/s10456-013-9347-8

Qian, B. Z., & Pollard, J. W. (2010). Macrophage Diversity Enhances Tumor Progression and Metastasis. Cell, 141(1), 39–51. https://doi.org/10.1016/j.cell.2010.03.014

Qian, H. S., Guo, H. C., Ho, P. C. L., Mahendran, R., & Zhang, Y. (2009). Mesoporous-silica-coated up-conversion fluorescent nanoparticles for photodynamic therapy. Small, 5(20), 2285–2290. https://doi.org/10.1002/smll.200900692

Rabinovich, G. A., Gabrilovich, D., & Sotomayor, E. M. (2007). Immunosuppressive strategies that are mediated by tumor cells. Annual Review of Immunology, 25, 267–296. https://doi.org/10.1146/annurev.immunol.25.022106.141609

Rafique, R., Gul, A. R., Lee, I. G., Baek, S. H., Kailasa, S. K., Iqbal, N., Cho, E. J., Lee, M., & Park, T. J. (2020). Photo-induced reactions for disassembling of coloaded photosensitizer and drug molecules from upconversion-mesoporous silica nanoparticles: An effective synergistic cancer therapy. Materials Science and Engineering C, 110(December 2019). https://doi.org/10.1016/j.msec.2019.110545

Ramasamy, P., & Kim, J. (2014). Combined plasmonic and upconversion rear reflectors for efficient dye-sensitized solar cells. Chemical Communications, 50(7), 879–881. https://doi.org/10.1039/c3cc47290f

Ramírez-García, G., Honorato-Colin, M. Á., De la Rosa, E., López-Luke, T., Panikar, S. S., Ibarra-Sánchez, J. de J., & Piazza, V. (2019). Theranostic nanocomplex of gold-decorated upconversion nanoparticles for optical imaging and temperature-controlled photothermal therapy. Journal of Photochemistry and Photobiology A: Chemistry, 384(August), 112053. https://doi.org/10.1016/j.jphotochem.2019.112053

Rastrelli, M., Tropea, S., Rossi, C. R., & Alaibac, M. (2016). Melanoma: Epidemiology, Risk Factors, Pathogenesis, Diagnosis and Classification. Melanoma, 1012, 10–30.

Repetto, G., del Peso, A., & Zurita, J. L. (2008). Neutral red uptake assay for the estimation of cell viability/ cytotoxicity. Nature Protocols, 3(7), 1125–1131. https://doi.org/10.1038/nprot.2008.75

Ribero, S., Argenziano, G., Lallas, A., Moscarella, E., Benati, E., Raucci, M., Piana, S., & Longo, C. (2017). Dermoscopic features predicting the presence of mitoses in thin melanoma. Journal of Dermatological Science, 86(2), 158–161. https://doi.org/10.1016/j.jdermsci.2017.01.013

Rigon, R. B., Oyafuso, M. H., Fujimura, A. T., Gonçalez, M. L., Do Prado, A. H., Gremião, M. P. D., & Chorilli, M. (2015). Nanotechnology-based drug delivery systems for melanoma antitumoral therapy: A review. BioMed Research International, 2015, 16–20. https://doi.org/10.1155/2015/841817

Roh, M. R., Eliades, P., Gupta, S., Grant-Kels, J. M., & Tsao, H. (2017). Cutaneous melanoma in women. International Journal of Women's Dermatology, 3(1), S11–S15. https://doi.org/10.1016/j.ijwd.2017.02.003

Roh, M. R., Eliades, P., Gupta, S., & Tsao, H. (2015). Genetics of melanocytic nevi. Pigment Cell and Melanoma Research, 28(6), 661–672. https://doi.org/10.1111/pcmr.12412

Safdar, M., Ghazy, A., Lastusaari, M., & Karppinen, M. (2020). Lanthanide-based inorganic-organic hybrid materials for photon-upconversion. Journal of Materials Chemistry C, 8(21), 6946–6965. https://doi.org/10.1039/d0tc01216e

Saldanha, G., Potter, L., DaForno, P., & Pringle, J. H. (2006). Cutaneous melanoma subtypes show different BRAF and NRAS mutation frequencies. Clinical Cancer Research, 12(15), 4499–4505. https://doi.org/10.1158/1078-0432.CCR-05-2447

Sanchez-Vega, F., Mina, M., Armenia, J., Chatila, W. K., Luna, A., La, K. C., Dimitriadoy, S., Liu, D. L., Kantheti, H. S., Saghafinia, S., Chakravarty, D., Daian, F., Gao, Q., Bailey, M. H., Liang, W. W., Foltz, S. M., Shmulevich, I., Ding, L., Heins, Z., … Schultz, N. (2018). Oncogenic Signaling Pathways in The Cancer Genome Atlas. Cell, 173(2), 321-337.e10. https://doi.org/10.1016/j.cell.2018.03.035

Sander, C. S., Hamm, F., Elsner, P., & Thiele, J. J. (2003). Oxidative stress in malignant melanoma and non-melanoma skin cancer. British Journal of Dermatology, 148(5), 913–922. https://doi.org/10.1046/j.1365-2133.2003.05303.x

Sander, Christina S., Chang, H., Salzmann, S., Müller, C. S. L., Ekanayake-Mudiyanselage, S., Elsner, P., & Thiele, J. J. (2002). Photoaging is associated with protein oxidation in human skin In Vivo. Journal of Investigative Dermatology, 118(4), 618–625. https://doi.org/10.1046/j.1523-1747.2002.01708.x

Sasaki, H., Akamatsu, H., & Horio, T. (1997). Effects of a single exposure to UVB radiation on the activities and protein levels of copper-zinc and manganese superoxide dismutase in cultured human keratinocytes. Photochemistry and Photobiology, 65(4), 707–713. https://doi.org/10.1111/j.1751-1097.1997.tb01914.x

Sedlmeier, A., & Gorris, H. H. (2015). Surface modification and characterization of photon-upconverting nanoparticles for bioanalytical applications. Chemical Society Reviews, 44(6), 1526–1560. https://doi.org/10.1039/c4cs00186a

Seto, M., Honma, K., & Nakagawa, M. (2010). Diversity of genome profiles in malignant lymphoma. Cancer Science, 101(3), 573–578. https://doi.org/10.1111/j.1349-7006.2009.01452.x

Shanmugam, V., Selvakumar, S., & Yeh, C. S. (2014). Near-infrared light-responsive nanomaterials in cancer therapeutics. Chemical Society Reviews, 43(17), 6254–6287. https://doi.org/10.1039/c4cs00011k

Sherr, C. J., & McCormick, F. (2002). The RB and p53 pathways in cancer. Cancer Cell,

2(2), 103–112. https://doi.org/10.1016/S1535-6108(02)00102-2
Shin, W. K., Cho, J., Kannan, A. G., Lee, Y. S., & Kim, D. W. (2016). Cross-linked Composite Gel Polymer Electrolyte using Mesoporous Methacrylate-Functionalized SiO2 Nanoparticles for Lithium-Ion Polymer Batteries. Scientific Reports, 6(April), 1–10. https://doi.org/10.1038/srep26332
Shtivelman, E., Lifshitz, B., Gale, R. P., & Canaani, E. (1985). Used Transcript of Abl and Bcr Genes in Chronic Myelogenous Leukaemia. Nature, 315(6020), 550–554. https://doi.org/10.1038/315550a0
Simões, M. C. F., Sousa, J. J. S., & Pais, A. A. C. C. (2015). Skin cancer and new treatment perspectives: A review. Cancer Letters, 357(1), 8–42. https://doi.org/10.1016/j.canlet.2014.11.001
Soehnge, H., Ouhtit, A., & Ananthaswamy, O. N. (1997). Mechanisms of induction of skin cancer by UV radiation. Frontiers in Bioscience : A Journal and Virtual Library, 2(1). https://doi.org/10.2741/a211
Song, S., Qin, Y., He, Y., Huang, Q., Fan, C., & Chen, H. Y. (2010). Functional nanoprobes for ultrasensitive detection of biomolecules. Chemical Society Reviews, 39(11), 4234–4243. https://doi.org/10.1039/c000682n
Stylios, G. K., Giannoudis, P. V., & Wan, T. (2005). Applications of nanotechnologies in medical practice. Injury, 36(SUPPL. 4), S6. https://doi.org/10.1016/j.injury.2005.10.011
Sui, M., Kunwar, S., Pandey, P., & Lee, J. (2019). Strongly confined localized surface plasmon resonance (LSPR) bands of Pt, AgPt, AgAuPt nanoparticles. Scientific Reports, 9(1), 1–14. https://doi.org/10.1038/s41598-019-53292-1
Sung, H., Ferlay, J., Siegel, R. L., Laversanne, M., Soerjomataram, I., Jemal, A., & Bray, F. (2021). Global Cancer Statistics 2020: GLOBOCAN Estimates of Incidence and Mortality Worldwide for 36 Cancers in 185 Countries. CA: A Cancer Journal for Clinicians, 71(3), 209–249. https://doi.org/10.3322/caac.21660
Swavey, S., & Tr, M. (2013). Porphyrin and Phthalocyanine Photosensitizers as PDT Agents: A New Modality for the Treatment of Melanoma. Recent Advances in the Biology, Therapy and Management of Melanoma. https://doi.org/10.5772/54940
Tan, M. L., Choong, P. F. M., & Dass, C. R. (2009). Review: doxorubicin delivery systems based on chitosan for cancer therapy. Journal of Pharmacy and Pharmacology, 61(2), 131–142. https://doi.org/10.1211/jpp/61.02.0001
Tang, J., Yang, C., & Li, Y. (2017). Recent developments in nanomedicine for melanoma treatment Running title : Nanomedicine for melanoma treatment , Xiao-Yang Hou Department of Dermatology , Affiliated Hospital of Xuzhou Medical Department of Dermatology , Affiliated Huai ' an Hospital of X.
Thompson, J. F., Scolyer, R. A., & Kefford, R. F. (2005). Cutaneous melanoma (Vol. 365, pp. 687–701).
Tian, G., Zhang, X., Gu, Z., & Zhao, Y. (2015). Recent Advances in Upconversion Nanoparticles-Based Multifunctional Nanocomposites for Combined Cancer Therapy. Advanced Materials, 27(47), 7692–7712. https://doi.org/10.1002/adma.201503280
Tian, T., Olson, S., Whitacre, J. M., & Harding, A. (2011). The origins of cancer robustness and evolvability. Integrative Biology, 3(1), 17–30. https://doi.org/10.1039/c0ib00046a
Tiwari, J. N., Tiwari, R. N., & Kim, K. S. (2012). Zero-dimensional, one-dimensional, two-dimensional and three-dimensional nanostructured materials for advanced electrochemical energy devices. Progress in Materials Science, 57(4), 724–803. https://doi.org/10.1016/j.pmatsci.2011.08.003

Trubini, S., Ubiali, A., Paties, C., & Cavanna, L. (2018). Novel BRAF mutation in melanoma: A case report. Molecular and Clinical Oncology, 460–462. https://doi.org/10.3892/mco.2018.1555

Tsao, H., Chin, L., Garraway, L. A., & Fisher, D. E. (2012). Melanoma: From mutations to medicine. Genes and Development, 26(11), 1131–1155. https://doi.org/10.1101/gad.191999.112

Tu, L., Liu, X., Wu, F., & Zhang, H. (2015). Excitation energy migration dynamics in upconversion nanomaterials. Chemical Society Reviews, 44(6), 1331–1345. https://doi.org/10.1039/c4cs00168k

Unsoy, G., Khodadust, R., Yalcin, S., Mutlu, P., & Gunduz, U. (2014). Synthesis of Doxorubicin loaded magnetic chitosan nanoparticles for pH responsive targeted drug delivery. European Journal of Pharmaceutical Sciences, 62, 243–250. https://doi.org/10.1016/j.ejps.2014.05.021

Vajdic, C. M., & Van Leeuwen, M. T. (2009). Cancer incidence and risk factors after solid organ transplantation. International Journal of Cancer, 125(8), 1747–1754. https://doi.org/10.1002/ijc.24439

Valverde, P., Healy, E., Jackson, I., Rees, J. L., & Thody, A. J. (1995). Variants of the melanocyte–stimulating hormone receptor gene are associated with red hair and fair skin in humans. Nature Genetics, 11(3), 328–330. https://doi.org/10.1038/ng1195-328

Vetrone, F., Naccache, R., Mahalingam, V., Morgan, C. G., & Capobianco, J. A. (2009). The active-core/active-shell approach: A strategy to enhance the upconversion luminescence in lanthanide-doped nanoparticles. Advanced Functional Materials, 19(18), 2924–2929. https://doi.org/10.1002/adfm.200900234

Vu, D. T., Vu-Le, T. T., Nguyen, V. N., Le, Q. M., Wang, C. R. C., Chau, L. K., Yang, T. S., Chan, M. W. Y., Lee, C. I., Ting, C. C., Lin, J. Y., Kan, H. C., & Hsu, C. C. (2021). Gold nanorods conjugated upconversion nanoparticles nanocomposites for simultaneous bioimaging, local temperature sensing and photothermal therapy of OML-1 oral cancer cells. International Journal of Smart and Nano Materials, 12(1), 49–71. https://doi.org/10.1080/19475411.2020.1839595

Walker, G. J., & Hayward, N. K. (2002). Pathways to melanoma development: Lessons from the mouse. Journal of Investigative Dermatology, 119(4), 783–792. https://doi.org/10.1046/j.1523-1747.2002.00217.x

Wang, C., Tao, H., Cheng, L., & Liu, Z. (2011). Near-infrared light induced in vivo photodynamic therapy of cancer based on upconversion nanoparticles. Biomaterials, 32(26), 6145–6154. https://doi.org/10.1016/j.biomaterials.2011.05.007

Wang, D., Liu, B., Quan, Z., Li, C., Hou, Z., Xing, B., & Lin, J. (2017). New advances on the marrying of UCNPs and photothermal agents for imaging-guided diagnosis and the therapy of tumors. Journal of Materials Chemistry B, 5(12), 2209–2230. https://doi.org/10.1039/c6tb03117j

Wang, F., Han, Y., Lim, C. S., Lu, Y., Wang, J., Xu, J., Chen, H., Zhang, C., Hong, M., & Liu, X. (2010). Simultaneous phase and size control of upconversion nanocrystals through lanthanide doping. Nature, 463(7284), 1061–1065. https://doi.org/10.1038/nature08777

Wang, F., & Liu, X. (2009). Recent advances in the chemistry of lanthanide-doped upconversion nanocrystals. Chemical Society Reviews, 38(4), 976–989. https://doi.org/10.1039/b809132n

Wang, F., Wang, J., & Liu, X. (2010). Direct evidence of a surface quenching effect on size-dependent luminescence of upconversion nanoparticles. Angewandte Chemie -

International Edition, 49(41), 7456–7460. https://doi.org/10.1002/anie.201003959
Wang, M., Mi, C., Wang, W., Liu, C., Wu, Y., Xu, Z., Mao, B., & Xu, S. (2009). Immunolabeling and NIR-Excited (Vol. 3, Issue 6).
Wang, P., Tang, H., & Zhang, P. (2016). Plasmonic Nanoparticle-based Hybrid Photosensitizers with Broadened Excitation Profile for Photodynamic Therapy of Cancer Cells. Scientific Reports, 6(May), 2–9. https://doi.org/10.1038/srep34981
Wang, R., Yang, H., Fu, R., Su, Y., Lin, X., Jin, X., Du, W., Shan, X., & Huang, G. (2020). Biomimetic Upconversion Nanoparticles and Gold Nanoparticles for Novel Simultaneous Dual-Modal Imaging-Guided Photothermal Therapy of Cancer. Cancers. https://doi.org/10.3390/cancers12113136
Wang, Y. F., Liu, G. Y., Sun, L. D., Xiao, J. W., Zhou, J. C., & Yan, C. H. (2013). Nd3+-sensitized upconversion nanophosphors: Efficient in vivo bioimaging probes with minimized heating effect. ACS Nano, 7(8), 7200–7206. https://doi.org/10.1021/nn402601d
Wang, Yan, Yang, P., Ma, P., Qu, F., Gai, S., Niu, N., He, F., & Lin, J. (2013). Hollow structured SrMoO4:Yb3+, Ln3+ (Ln = Tm, Ho, Tm/Ho) microspheres: Tunable up-conversion emissions and application as drug carriers. Journal of Materials Chemistry B, 1(15), 2056–2065. https://doi.org/10.1039/c3tb00377a
Wang, Yinghui, Song, S., Zhang, S., & Zhang, H. (2019). Stimuli-responsive nanotheranostics based on lanthanide-doped upconversion nanoparticles for cancer imaging and therapy: current advances and future challenges. Nano Today, 25, 38–67. https://doi.org/10.1016/j.nantod.2019.02.007
Wang, Z., Thang, D. C., Han, Q., Zhao, X., Xie, X., Wang, Z., Lin, J., & Xing, B. (2020). Near-infrared photocontrolled therapeutic release via upconversion nanocomposites. Journal of Controlled Release, 324(April), 104–123. https://doi.org/10.1016/j.jconrel.2020.05.011
Wicki, A., Witzigmann, D., Balasubramanian, V., & Huwyler, J. (2015). Nanomedicine in cancer therapy: Challenges, opportunities, and clinical applications. Journal of Controlled Release, 200, 138–157. https://doi.org/10.1016/j.jconrel.2014.12.030
Willis, S. N., & Adams, J. M. (2005). Life in the balance: How BH3-only proteins induce apoptosis. Current Opinion in Cell Biology, 17(6), 617–625. https://doi.org/10.1016/j.ceb.2005.10.001
Witsch, E., Sela, M., & Yarden, Y. (2010). Roles for Growth Factors in Cancer Progression. Physiology, 25(2), 85–101. https://doi.org/10.1152/physiol.00045.2009
Wu, J., Zuo, F., Du, J., Wong, P. F., Qin, H., & Xu, J. (2013). Icariside II induces apoptosis via inhibition of the EGFR pathways in A431 human epidermoid carcinoma cells. Molecular Medicine Reports, 8(2), 597–602. https://doi.org/10.3892/mmr.2013.1557
Wu, Shiwei, Han, G., Milliron, D. J., Aloni, S., Altoe, V., Talapin, D. V., Cohen, B. E., & Schuck, P. J. (2009). Non-blinking and photostable upconverted luminescence from single lanthanide-doped nanocrystals. Proceedings of the National Academy of Sciences of the United States of America, 106(27), 10917–10921. https://doi.org/10.1073/pnas.0904792106
Wu, Si, & Butt, H. J. (2016). Near-Infrared-Sensitive Materials Based on Upconverting Nanoparticles. Advanced Materials, 28(6), 1208–1226. https://doi.org/10.1002/adma.201502843
Xie, J., Lee, S., & Chen, X. (2010). Nanoparticle-based theranostic agents. Advanced Drug Delivery Reviews, 62(11), 1064–1079. https://doi.org/10.1016/j.addr.2010.07.009
Xie, X., Gao, N., Deng, R., Sun, Q., Xu, Q., & Liu, X. (2013). Mechanistic Investigation of

Photon Upconversion in Nd 3 + -Sensitized. Journal of the American Chemical Society, 135(34), 12608–12611.
Xiong, L., Yang, T., Yang, Y., Xu, C., & Li, F. (2010). Long-term in vivo biodistribution imaging and toxicity of polyacrylic acid-coated upconversion nanophosphors. Biomaterials, 31(27), 7078–7085. https://doi.org/10.1016/j.biomaterials.2010.05.065
Yang, S., Li, N., Liu, Z., Sha, W., Chen, D., Xu, Q., & Lu, J. (2014). Amphiphilic copolymer coated upconversion nanoparticles for near-infrared light-triggered dual anticancer treatment. Nanoscale, 6(24), 14903–14910. https://doi.org/10.1039/c4nr05305b
Yang, W., Liang, H., Ma, S., Wang, D., & Huang, J. (2019). Gold nanoparticle based photothermal therapy: Development and application for effective cancer treatment. Sustainable Materials and Technologies, 22, e00109. https://doi.org/10.1016/j.susmat.2019.e00109
Yeh, Y. C., Creran, B., & Rotello, V. M. (2012). Gold nanoparticles: Preparation, properties, and applications in bionanotechnology. Nanoscale, 4(6), 1871–1880. https://doi.org/10.1039/c1nr11188d
Yu, X., Bi, J., Yang, G., Tao, H., & Yang, S. (2016). Synergistic effect induced high photothermal performance of Au Nanorod@Cu7S4 Yolk-shell nanooctahedron particles. Journal of Physical Chemistry C, 120(43), 24533–24541. https://doi.org/10.1021/acs.jpcc.6b06213
Zaidi, M. R., Day, C. P., & Merlino, G. (2008). From UVs to metastases: Modeling melanoma initiation and progression in the mouse. Journal of Investigative Dermatology, 128(10), 2381–2391. https://doi.org/10.1038/jid.2008.177
Zhang, D., Chen, C., Fu, X., Gu, S., Mao, Y., Xie, Y., Huang, Y., & Li, Y. (2008). A meta-analysis of DNA repair gene XPC polymorphisms and cancer risk. Journal of Human Genetics, 53(1), 18–33. https://doi.org/10.1007/s10038-007-0215-5
Zhang, P., Steelant, W., Kumar, M., & Scholfield, M. (2007). Versatile photosensitizers for photodynamic therapy at infrared excitation. Journal of the American Chemical Society, 129(15), 4526–4527. https://doi.org/10.1021/ja0700707
Zhang, Q. wen, Liu, L., Gong, C. yang, Shi, H. shan, Zeng, Y. hui, Wang, X. ze, Zhao, Y. wei, & Wei, Y. quan. (2012). Prognostic Significance of Tumor-Associated Macrophages in Solid Tumor: A Meta-Analysis of the Literature. PLoS ONE, 7(12). https://doi.org/10.1371/journal.pone.0050946
Zhang, T., Lin, H., Cui, L., An, N., Tong, R., Chen, Y., Yang, C., Li, X., Liu, J., & Qu, F. (2016). Near Infrared Light Triggered Reactive Oxygen Species Responsive Upconversion Nanoplatform for Drug Delivery and Photodynamic Therapy. European Journal of Inorganic Chemistry, 2016(8), 1206–1213. https://doi.org/10.1002/ejic.201501320
Zhang, X., Yang, P., Dai, Y., Ma, P., Li, X., Cheng, Z., Hou, Z., Kang, X., Li, C., & Lin, J. (2013). Multifunctional up-converting nanocomposites with smart polymer brushes gated mesopores for cell imaging and thermo/pH dual-responsive drug controlled release. Advanced Functional Materials, 23(33), 4067–4078. https://doi.org/10.1002/adfm.201300136
Zhang, Yanqiu, Xu, S., Li, X., Zhang, J., Sun, J., Xia, H., Hua, R., & Chen, B. (2019). Fabrication, photothermal conversion and temperature sensing of novel nanoplatform-hybrid nanocomposite of NaYF 4 :Er 3+ ,Yb 3+ @NaYF 4 and Au nanorods for photothermal therapy. Materials Research Bulletin, 114(December 2018), 148–155. https://doi.org/10.1016/j.materresbull.2019.03.003
Zhang, Ye, Li, M., Gao, X., Chen, Y., & Liu, T. (2019). Nanotechnology in cancer diagnosis: Progress, challenges and opportunities. Journal of Hematology and

Oncology, 12(1), 1–13. https://doi.org/10.1186/s13045-019-0833-3

Zhang, Yunjiao, Zheng, F., Yang, T., Zhou, W., Liu, Y., Man, N., Zhang, L., Jin, N., Dou, Q., Zhang, Y., Li, Z., & Wen, L. P. (2012). Tuning the autophagy-inducing activity of lanthanide-based nanocrystals through specific surface-coating peptides. Nature Materials, 11(9), 817–826. https://doi.org/10.1038/nmat3363

Zhao, J., Yang, H., Li, J., Wang, Y., & Wang, X. (2017). Fabrication of pH-responsive PLGA(UCNPs/DOX) nanocapsules with upconversion luminescence for drug delivery. Scientific Reports, 7(1), 1–11. https://doi.org/10.1038/s41598-017-16948-4

Zhao, N., C Woodle, M., & Mixson, A. J. (2018). Advances in Delivery Systems for Doxorubicin. Journal of Nanomedicine & Nanotechnology, 09(05), 1–9. https://doi.org/10.4172/2157-7439.1000519

Zhou, B., Shi, B., Jin, D., & Liu, X. (2015). Controlling upconversion nanocrystals for emerging applications. Nature Nanotechnology, 10(11), 924–936. https://doi.org/10.1038/nnano.2015.251

Zhou, J., Liu, Z., & Li, F. (2012). Upconversion nanophosphors for small-animal imaging. Chemical Society Reviews, 41(3), 1323–1349. https://doi.org/10.1039/c1cs15187h

Zuo, L., Weger, J., Yang, Q., Goldstein, A. M., Tucker, M. A., Walker, G. J., Hayward, N., & Dracopoli, N. C. (1996). Germline mutations in the p16(INK4a) binding domain of CDK4 in familial melanoma. Nature Genetics, 12(1), 97–99. https://doi.org/10.1038/ng0196-97